

PERPUSTAKAAN UMP



0000117826

NUMERICAL INVESTIGATION OF COMBUSTION PERFORMANCE AND
EMISSIONS CHARACTERISTICS IN HOMOGENEOUS CHARGE
COMPRESSION IGNITION ENGINE

MOHAMMAD MEHEDI HASAN

Thesis submitted in fulfillment of the requirements
for the award of the degree of
Master of Engineering in Mechanical Engineering

Faculty of Mechanical Engineering
UNIVERSITI MALAYSIA PAHANG

NOVEMBER 2016

PERPUSTAKAAN 040517 UNIVERSITI MALAYSIA PAHANG p	
No. Perolehan 117826	No. Panggilan PCM 437
Tarikh 17 APR 2017	2016 Thesis

ABSTRAK

Homogen caj pencucuhan mampatan (HCCI) enjin telah menjadi bidang penyelidikan yang aktif kerana potensinya untuk penggunaan bahan api yang bercekapan tinggi dan pelepasan zarah dan oksida nitrogen (NO_x) yang amat rendah. Walau bagaimanapun, lingkungan operasi menggunakan pembakaran HCCI dari segi kelajuan dan beban adalah terhad kerana permulaan pembakaran (SOC) dan kadar pembebasan haba tidak boleh dikawal secara langsung. Bergantung hanya pada sejarah haba dan tingkah laku kimia yang terkandung dalam silinder, SOC dimanipulasi oleh manipulasi tepat pembolehubah ini melalui kaedah seperti; suhu pengambilan dan penyaman tekanan, campuran bahan api, silinder geometri boleh ubah, dan pengaturan masa injap berubah-ubah. Dalam usaha untuk mereka bentuk enjin untuk pelbagai operasi lanjutan serta pelbagai bahan api dan campuran bahan api, model yang tepat diperlukan bagi membolehkan pemodelan kedua-dua pembakaran dan prestasi. Objektif kajian ini adalah untuk memodelkan enjin HCCI secara numerikal menggunakan pengurangan mekanisme kimia dan untuk menyiasat pengaruh perbezaan parameter enjin, perbezaan bahan api dan campuran bahan api ke atas pembakaran, prestasi dan ciri-ciri asap dalam enjin HCCI. Dalam kajian ini, satu simulasi numerical sifar dimensi zon tunggal dengan pengurangan kimia bahan api pelbagai bahan api dan campuran bahan api telah dibangunkan dan disahkan. Bagi penyelidikan enjin, model sifar dimensi dikenali dengan kelebihan dalam mengurangkan masa pengiraan berbanding dengan pendekatan pelbagai dimensi Computational Fluid Dynamics. Fokus utama kajian ini adalah untuk mendapatkan hasil yang lebih baik untuk model sifar dimensi, manakala keputusan eksperimen akan digunakan untuk tujuan pengesahan. Keputusan yang diperolehi menunjukkan persamaan yang baik dengan keputusan eksperimen yang diterbitkan dan menyamai trend fasa pembakaran yang penting apabila parameter enjin berubah dengan maksimum peratusan kesilapan yang kurang daripada 6% untuk HCCI diesel dan 4% untuk HCCI petrol. Kemajuan fasa pembakaran, dan pemendekan tempoh pembakaran diperolehi dengan peningkatan pengambilan suhu caj dan penurunan kelajuan enjin untuk kedua-dua diesel dan petrol HCCI. Beban maksimum berjaya ditingkatkan dengan peningkatan tekanan pengambilan. Beban tertinggi dalam kajian ini adalah 11.27 bar di IMEPg pada keadaan 200 kPa tekanan udara pengambilan dan 333 K dalam suhu udara pengambilan untuk HCCI diesel dan 10.86 bar di IMEPg pada keadaan 200 kPa tekanan udara pengambilan dan 393 K dalam suhu udara pengambilan untuk HCCI petrol. Ia didapati bahawa tekanan udara pengambilan memberikan pengaruh yang paling sensitif pada ciri-ciri pembakaran dan prestasi HCCI. Untuk pelbagai campuran bahan api, kecekapan haba telah meningkat kira-kira 17.71% dengan Bu30 berbanding n-heptana pada suhu pengambilan 393 K. IMEP menurun pada semua suhu pengambilan dengan n-heptana. Jumlah pelepasan NO_x yang sangat rendah pada kadar 2.5 ppm telah ditemui dengan bahan api ujian. Pelepasan NO_x telah meningkat dengan peningkatan suhu pengambilan. Pelepasan karbon monoksida (CO) telah didapati meningkat dengan peningkatan alkohol dalam bahan api ujian. Pelepasan maksimum CO telah didapati sebanyak 0.47% dengan E30 pada suhu pengambilan 313 K. Selain itu, pelepasan hidrokarbon (HC) telah diperolehi lebih tinggi terutamanya pada suhu pengambilan yang lebih rendah apabila etanol digunakan sebagai pemangkin bahan api. Pelepasan HC maksimum telah didapati sebanyak 159.6 ppm dengan bahan api ujian E30 pada suhu pengambilan 313 K. Hasilnya didapati bahawa julat operasi HCCI boleh dipanjangkan menggunakan alkohol yang mempunyai nombor oktana tinggi dan penyalaan sendiri yang boleh dikawal.

ABSTRACT

Homogeneous charge compression ignition (HCCI) engine has been an active research area due to its potential for high fuel conversion efficiency and extremely low emissions of particulate matter and oxides of nitrogen (NO_x). However, the operational range using HCCI combustion in terms of speed and load is restricted because the start of combustion (SOC) and the heat release rate cannot be controlled directly. Depending only on the thermal history and chemical behavior of the cylinder contents, SOC is manipulated by precise manipulation of these variables through methods such as intake temperature and pressure conditioning, fuel blending, variable cylinder geometry, and variable valve timings. In order to design an engine for extended operational range as well as various fuels and blends of fuels, accurate models are needed which are able to model both combustion and performance. The objectives of this study are to model a HCCI engine numerically using reduced chemical mechanism and to investigate the influence of different engine parameters, different fuels and blend of fuels on combustion, performance and emissions characteristics in HCCI engines. In this study, a zero dimensional single-zone numerical simulation with reduced fuel chemistry of various fuels and blends of fuels was developed and validated. It is known for its advantage in reducing computational time compared with a multi-dimensional Computational Fluid Dynamics approach. The main focus of the study is to obtain an improved result for the zero-dimensional model, while the experimental results were used for the purpose of validation. The obtained results show good agreement with the experimental published results and capture important combustion phase trends as engine parameters are varied with maximum percentage of error which is less than 6% for diesel HCCI and 4% for gasoline HCCI. The combustion phase advances, and the combustion duration shorten with the increase of intake charge temperature and the decrease of the engine speed for both diesel and gasoline HCCI. The maximum load successfully increased with increasing the intake pressure. The highest load in this study was 11.27 bar in IMEPg at the condition of 200 kPa in intake air pressure and 333 K in intake air temperature for diesel HCCI and 10.86 bar in IMEPg at the condition of 200 kPa in intake air pressure and 393 K in intake air temperature for gasoline HCCI. It is found that the intake air pressure gives the most sensitive influence on the HCCI combustion and performance characteristics. For various fuel blends thermal efficiency was increased by about 17.71% with Bu30 compared to n-heptane at 393 K intake temperature. IMEP decreased at all intake temperatures with n-heptane. Very low amount of NO_x emissions were found with test fuels which is less than 2.5 ppm. NO_x emissions were increased with the increase of intake temperature. It is also seen that carbon monoxide (CO) emissions were increased with the increase of alcohol in the test fuels. Maximum CO emissions were found as 0.47% with E30 at 313 K intake temperature. Moreover, higher hydrocarbon (HC) emissions were obtained especially at lower intake temperature when ethanol was used as an additive fuel. Maximum HC emissions were found as 159.6 ppm with E30 test fuel at 313 K intake temperature. As a result it is found that this numerical investigation can contribute to the determination of proper fuel mixture and intake temperature for the problems such as extending the HCCI operation range, controlling the combustion, preventing knocking combustion and reduction of CO and HC emissions in HCCI combustion. Therefore, future work is recommended to improve the zero-dimensional model by combining it with conditional moment closure model and also experimental test rig develop for the HCCI engine.

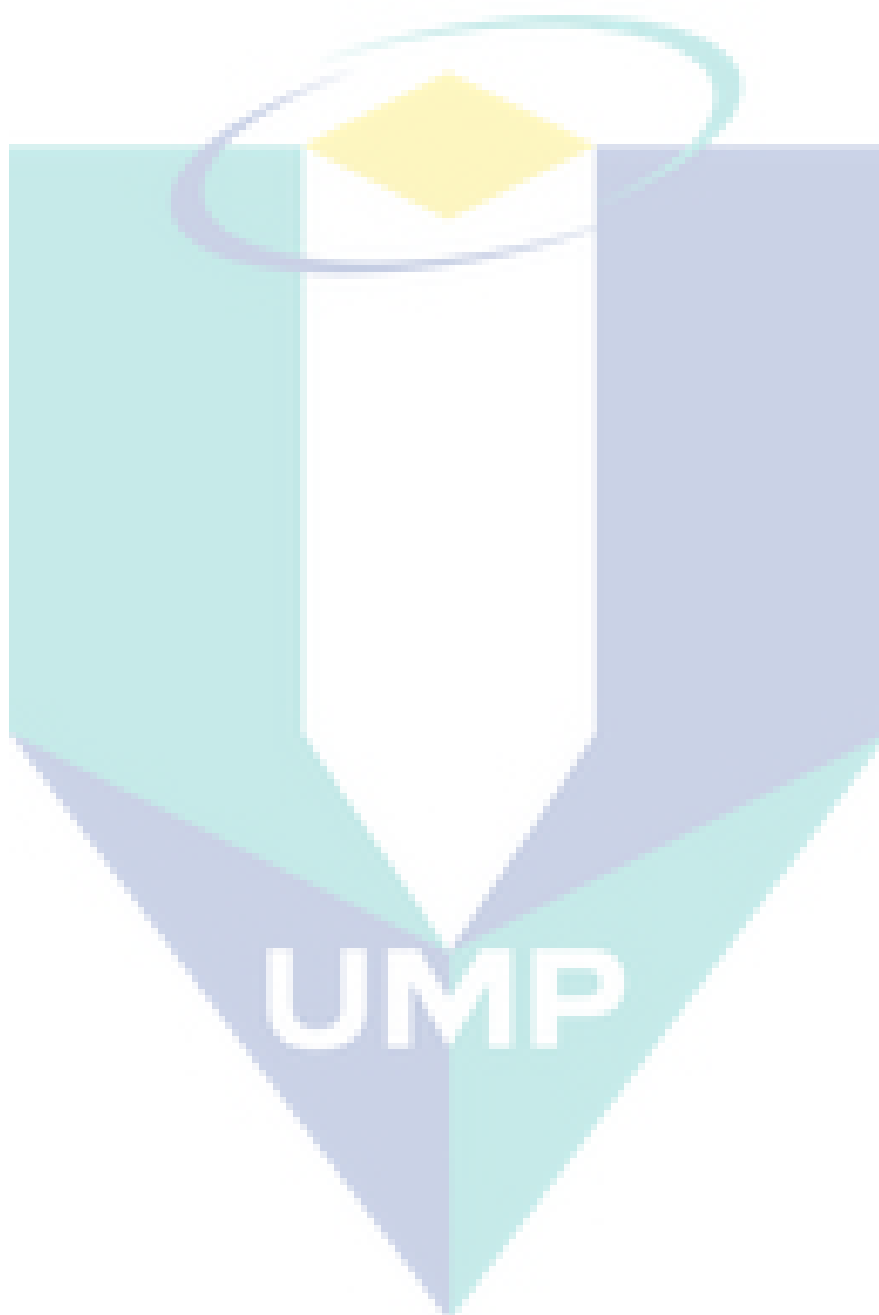
TABLE OF CONTENTS

	Page
DECLARATION	
TITLE PAGE	i
DEDICATION	ii
ACKNOWLEDGEMENTS	iii
ABSTRAK	iv
ABSTRACT	v
TABLE OF CONTENTS	vi
LIST OF TABLES	x
LIST OF FIGURES	xi
LIST OF SYMBOLS	xv
LIST OF ABBREVIATIONS	xviii
 CHAPTER 1 INTRODUCTION	
1.1 Introduction	1
1.1.1 Homogeneous Charge Compression Ignition	2
1.1.2 HCCI Diesel Combustion	4
1.1.3 HCCI Gasoline Combustion	5
1.1.4 Formation of NO _x and Soot	7
1.2 Problem Statements	9
1.3 Objectives of study	10
1.4 Scope of Study	10
1.5 Organization of Thesis	11
 CHAPTER 2 LITERATURE REVIEW	
2.1 Introduction	13
2.2 Performance Comparison	13
2.2.1 HCCI Diesel Combustion	16
2.2.2 HCCI Gasoline Combustion	18
2.3 Emissions Comparison	20

2.3.1	HCCI Diesel Combustion	21
2.3.2	HCCI Gasoline Combustion	25
2.4	Effects of Engine Parameters	26
2.4.1	Intake Temperature	26
2.4.2	Intake Pressure	27
2.4.3	Compression Ratio	28
2.5	Effects of Fuels and Additives	29
2.5.1	Effects of Fuels	29
2.5.2	Effects of Additives	32
2.6	Numerical Study of HCCI Engines	33
2.6.1	Chemical Kinetics	33
2.6.2	Single Zone Model	34
2.6.3	Multi Zone Models	36
2.7	Summary	37
 CHAPTER 3 NUMERICAL MODELING		
4.1	Introduction	38
4.2	Chemical Kinetics Mechanisms	39
3.2.1	Diesel Mechanism	39
3.2.2	Gasoline Mechanism	40
3.2.3	Mechanisms for Different Fuels and Blends of Fuels	41
3.2.4	Mechanisms of Emissions Formation	41
4.3	Engine Parameters	45
4.4	Valve Geometry	49
4.5	Combustion Process Model	53
3.5.1	Conservation of Mass	53
3.5.2	Conservation of Species	54
3.5.3	Conservation of Energy	54
4.6	Heat Release Model	55
4.7	Numerical Solutions	57
4.8	Combustion Parameters	59
4.9	Performance Parameters	60
4.10	Chemical Properties of Fuels	62

4.11	Summary	63
CHAPTER 4 RESULTS AND DISCUSSION		
4.1	Introduction	65
4.2	Model Validation	65
4.2.1	Diesel HCCI	65
4.2.2	Gasoline HCCI	69
4.2.3	Comparison of Different Models	72
4.3	Comparison of HCCI with CI	74
4.3.1	Engine Performance	74
4.3.2	Engine Emissions	78
4.4	Comparison of HCCI with SI	82
4.4.1	Engine Performance	82
4.4.2	Engine Emissions	87
4.5	Influence of Engine Parameters	90
4.5.1	Diesel HCCI	90
4.5.2	Gasoline HCCI	95
4.6	Different Fueled HCCI	100
4.6.1	Combustion Characteristics	101
4.6.2	Performance Characteristics	106
4.6.3	Emissions Characteristics	108
4.7	Summary	111
CHAPTER 5 CONCLUSIONS AND RECOMMENDATIONS		
5.1	Introduction	112
5.2	Summary of Findings	112
5.3	Recommendations for Future Research	115
REFERENCES		116
APPENDICES		135
A	Derivation of temperature equation	135

B	Computer software summary	139
C	Zero-dimensional single zone numerical model code	141
D	List of Publications	146



LIST OF TABLES

Table 1.1	Comparison of parameters influencing in SI, CI, and HCCI combustion engines	4
Table 2.1	Different experimental engine performance results using various fuels in HCCI engines compared to CI engines	14
Table 2.2	Different experimental engine performance results using various fuels in HCCI engines compared to SI engines	15
Table 2.3	Different experimental engine emissions results using various fuels in HCCI engines compared to CI engines	22
Table 2.4	Different experimental engine emissions results using various fuels in HCCI engines compared to SI engines	23
Table 3.1	Gasoline surrogate composition	40
Table 3.2	NO _x kinetic mechanism reaction rates parameters for A , b , and E_A	44
Table 3.3	The properties of diesel fuel	63
Table 3.4	The properties of gasoline fuel	63
Table 3.5	The chemical properties of the test fuels	63
Table 4.1	Engine model specifications	66
Table 4.2	Engine model specifications	70
Table 4.3	Engine model specifications	75
Table 4.4	Engine model specifications	82

LIST OF FIGURES

Figure 1.1	The differences between SI, CI, and HCCI engines	3
Figure 1.2	Combustion timing map in HCCI engine (10% burn), ($^{\circ}\text{CA}$)	6
Figure 1.3	Combustion duration map in HCCI engine (10-90% burn), ($^{\circ}\text{CA}$)	7
Figure 1.4	Equivalence ratios versus temperature	8
Figure 2.1	Intake temperature required for fuels to operate under HCCI mode with varying compression ratios.	29
Figure 3.1	Engine geometry of the piston and crank mechanisms	46
Figure 3.2	Instantaneous piston speed: zero at TDC and BDC, maximum at the middle of the stroke	48
Figure 3.3	Valve geometry for most engines with parameters defining the valve	49
Figure 3.4	Valve lift profile for typical poppet valves with mechanical lifters	51
Figure 3.5	Discharge coefficient for one valve event	53
Figure 3.6	An algorithm flow chart for zero-dimensional single-zone model simulation	58
Figure 3.7	Process of determining SOC and combustion duration (CA_{10-90})	60
Figure 3.8	Process of determining CA_{50}	61
Figure 4.1	Schematic diagram of the HCCI engine set up	67
Figure 4.2	Comparison between zero-dimensional single zone model with experimental data from Guo et al. (2010). $\text{CR}=10.0$, $N=900$ rpm, $T_{\text{in}}=333$ K, $P_{\text{in}}=100$ kPa, $\text{AFR}=50$	68
Figure 4.3	Schematic diagram of the HCCI engine set up	70
Figure 4.4	Comparison between zero-dimensional single zone model with experimental data from Gotoh et al. (2013). $\text{CR}=12.0$, $N=1500$ rpm, $T_{\text{in}}=393$ K, $P_{\text{in}}=100$ kPa, $\text{AFR}=40$	72

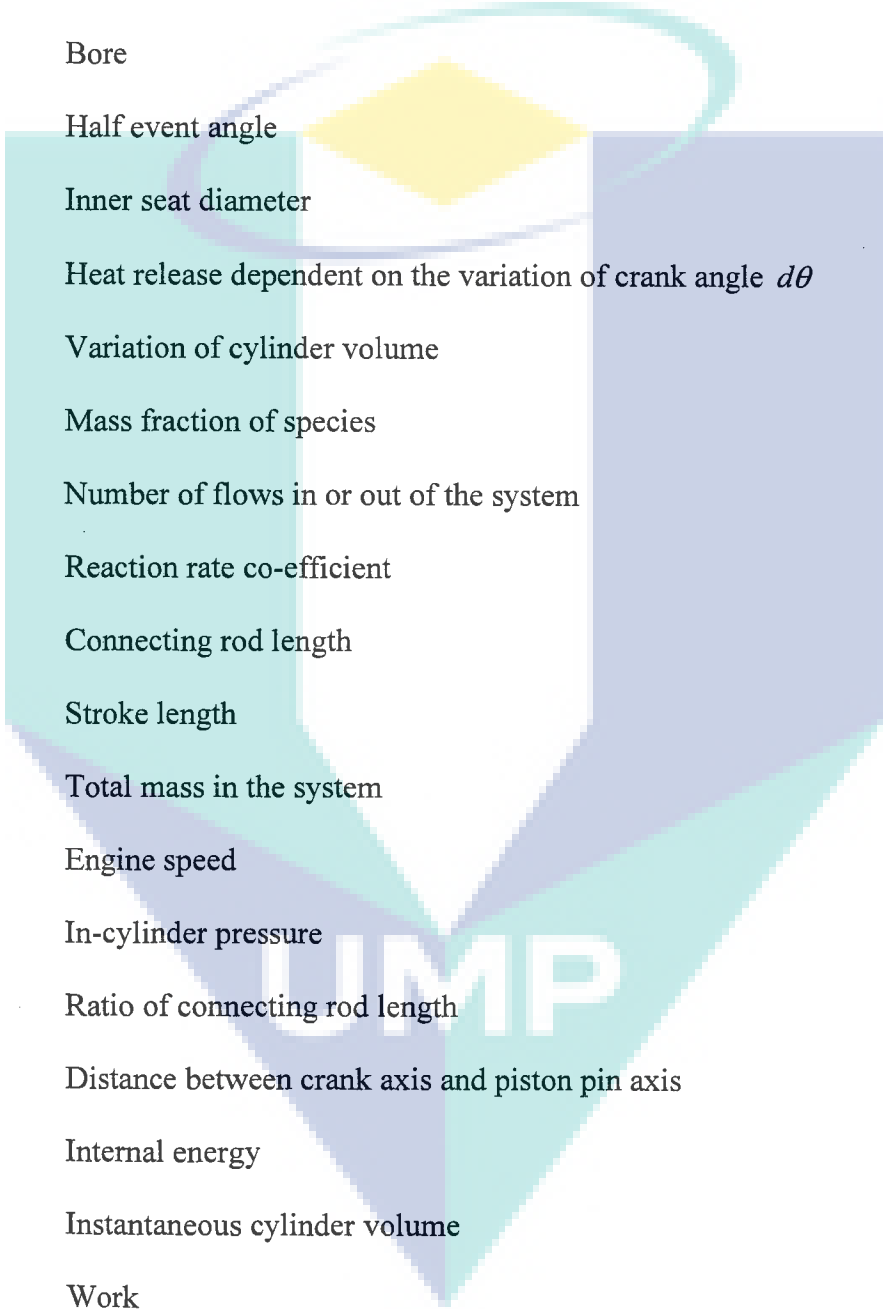
Figure 4.5	Comparison between zero-dimensional single zone model with experimental data and another zero-dimensional model from Maurya et al. (2016). CR=21, N=1000 rpm, T_{in} =365 K, P_{in} =100 kPa, $\lambda = 3$	73
Figure 4.6	Comparison between zero-dimensional single zone model with experimental data and one-dimensional model from Mo (2008). CR=12, N=1995.7 rpm, T_{in} =388.96 K, P_{in} =93.99 kPa, $\lambda = 1.5$	74
Figure 4.7	The variation of in-cylinder pressure between diesel engine and HCCI engine at a constant speed of 2400 rpm and full load condition	75
Figure 4.8	The variation of engine power between diesel engine and HCCI engine at variable speed and full load condition	77
Figure 4.9	The variation of BSFC between diesel engine and HCCI engine at variable speed and full load condition	77
Figure 4.10	The variation of BTE between diesel engine and HCCI engine at variable speed and full load condition	78
Figure 4.11	The variation of HC emission between diesel engine and HCCI engine at variable speed and full load condition	79
Figure 4.12	The variation of CO emission between diesel engine and HCCI engine at variable speed and full load condition	81
Figure 4.13	The variation of NO _x emission between diesel engine and HCCI engine at variable speed and full load condition	83
Figure 4.14	The variation of in-cylinder pressure between gasoline engine and HCCI engine at a constant speed of 3000 rpm and full load condition	83
Figure 4.15	The variation of engine power between gasoline engine and HCCI engine at variable speed and full load condition	84
Figure 4.16	The variation of BSFC between gasoline engine and HCCI engine at variable speed and full load condition	85
Figure 4.17	The variation of BTE between gasoline engine and HCCI engine at variable speed and full load condition	86
Figure 4.18	The variation of HC emission between gasoline engine and HCCI engine at variable speed and full load condition	87
Figure 4.19	The variation of CO emission between gasoline engine and HCCI engine at variable speed and full load condition	88

Figure 4.20	The variation of NO _x emission between gasoline engine and HCCI engine at variable speed and full load condition	89
Figure 4.21	Influence of speed on combustion and performance characteristics in HCCI engine. CR=10.0, T _{in} =360 K, P _{in} =100 kPa, AFR=50	91
Figure 4.22	Influence of intake air temperature on combustion and performance characteristics in HCCI engine. CR=10.0, N=900 rpm, P _{in} =100 kPa, AFR=50	93
Figure 4.23	Influence of intake air pressure on combustion and performance characteristics in HCCI engine. CR=10.0, N=900 rpm, T _{in} =360 K, AFR=50	94
Figure 4.24	Influence of Compression Ratio on combustion and performance characteristics in HCCI engine. N=900 rpm, T _{in} =360 K, P _{in} =100 kPa, AFR=50	95
Figure 4.25	Influence of speed on combustion and performance characteristics in HCCI engine. CR=12.0, T _{in} =310 K, P _{in} =100 kPa, AFR=40	96
Figure 4.26	Influence of intake air temperature on combustion and performance characteristics in HCCI engine. CR=12.0, N=1500 rpm, P _{in} =100 kPa, AFR=40	97
Figure 4.27	Influence of intake air pressure on combustion and performance characteristics in HCCI engine. CR=12.0, N=1500 rpm, T _{in} =310 K, AFR=40	99
Figure 4.28	Influence of Compression Ratio on combustion and performance characteristics in HCCI engine. N=1500 rpm, T _{in} =310 K, P _{in} =100 kPa, AFR=40	100
Figure 4.29	The variation of in-cylinder pressure of HCCI combustion at constant lambda $\lambda = 2$ and 900 rpm engine speed with different intake temperatures and test fuels	102
Figure 4.30	The variation of heat release rate of HCCI combustion at constant lambda, $\lambda = 2$ and 900 rpm engine speed with different intake temperatures and test fuels	103
Figure 4.31	The variation of SOC of HCCI combustion at constant lambda, $\lambda = 2$ and 900 rpm engine speed with different intake temperatures and test fuels	104
Figure 4.32	The variation of combustion duration (CA50 and CA10-90) of HCCI combustion at constant lambda, $\lambda = 2$ and 900 rpm engine speed with different intake temperatures and test fuels	105


Figure 4.33	The variation of indicated mean effective pressure on HCCI combustion at constant lambda, $\lambda = 2$ and 900 rpm engine speed with different intake temperatures and test fuels	107
Figure 4.34	The variation of indicated thermal efficiency of HCCI combustion at constant lambda, $\lambda = 2$ and 900 rpm engine speed with different intake temperatures and test fuels	107
Figure 4.35	The variation of CO emissions on HCCI combustion at constant lambda, $\lambda = 2$ and 900 rpm engine speed with different intake temperatures and test fuels	109
Figure 4.36	The variation of HC emissions on HCCI combustion at constant lambda, $\lambda = 2$ and 900 rpm engine speed with different intake temperatures and test fuels	109
Figure 4.37	The variation of NO _x emissions on HCCI combustion at constant lambda, $\lambda = 2$ and 900 rpm engine speed with different intake temperatures and test fuels	110

UMP

LIST OF SYMBOLS

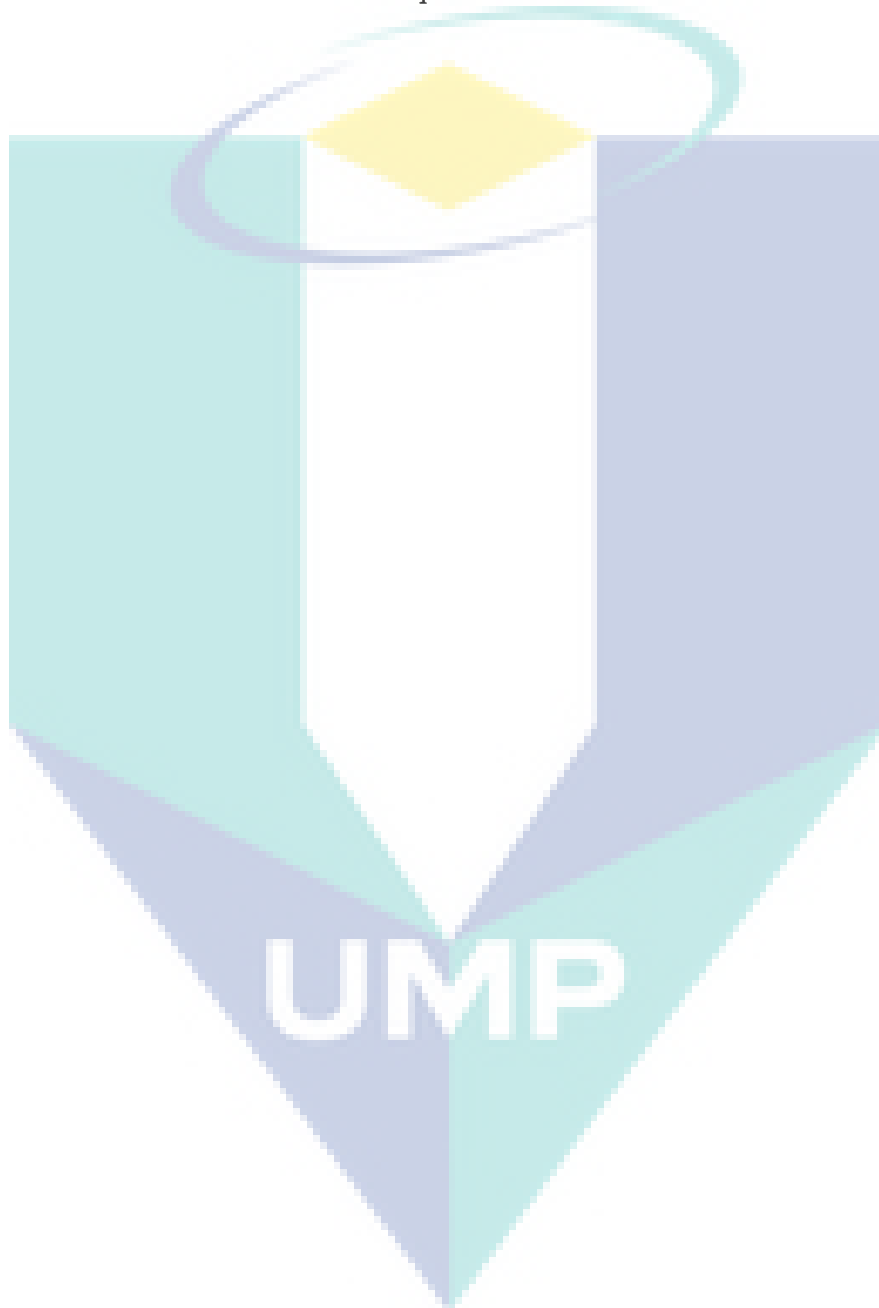


a	Crank radius
A	Pre-exponential term
b	Temperature dependent exponent
B	Bore
c	Half event angle
D	Inner seat diameter
dQ	Heat release dependent on the variation of crank angle $d\theta$
dV	Variation of cylinder volume
i	Mass fraction of species
j	Number of flows in or out of the system
k	Reaction rate co-efficient
l	Connecting rod length
L	Stroke length
m	Total mass in the system
N	Engine speed
p	In-cylinder pressure
R	Ratio of connecting rod length
s	Distance between crank axis and piston pin axis
U	Internal energy
V	Instantaneous cylinder volume
W	Work
y	Valve profile
γ	Ratio of specific heats
k	Ratio of specific heat values




τ	Indicated torque
ϕ	Equivalence ratio
ω	Rotational speed
A_c	Effective valve open area
A_p	Piston area
A_w	Wall area
C_d	Discharge co-efficient
D_s	Valve stem diameter
D_v	Valve head diameter
E_A	Activation energy
h_c	Heat transfer coefficient
H_j	Enthalpy of flows entering or leaving the system
L_v	Valve lift
p_0	Upstream stagnation pressure
p_T	Downstream static pressure
Q_h	Heat transfer
R_c	Compression ratio
R_u	Universal gas constant
S_p	Instantaneous piston speed
S_w	Valve seat width
t_0	Upstream stagnation temperature
T_w	Wall temperature
V_c	Clearance volume
V_d	Displacement volume
W_{mv}	Mean molecular weight of the mixture

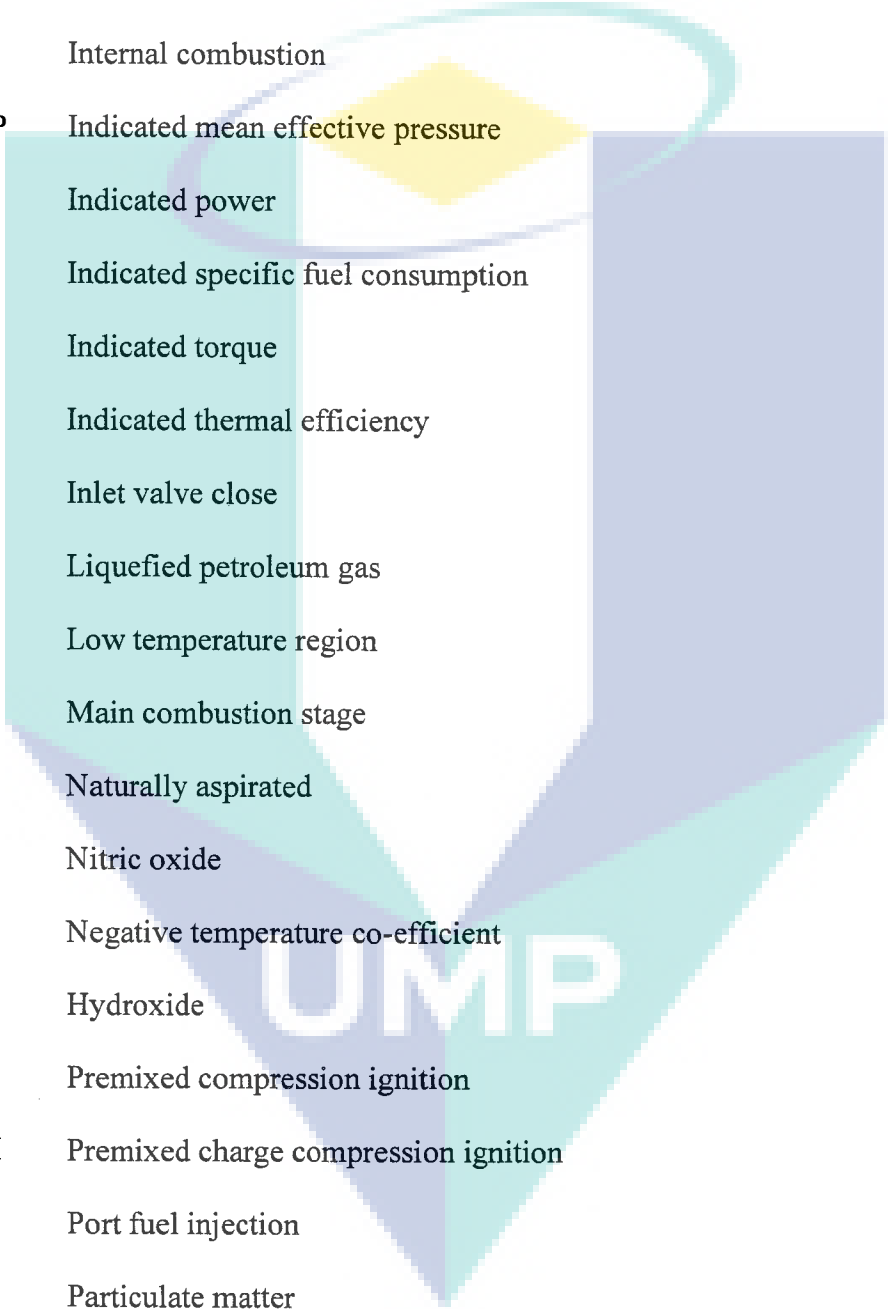
W_{net}	Net work done
Y_{in}	Inlet mass fraction
η_{ith}	Ratio of energy
ω_i	Mass reaction rate of the species i



LIST OF ABBREVIATIONS



AC	Air cooled
AFR	Air fuel ratio
ASTM	American society for testing and materials
ATDC	After top dead center
BDC	Bottom dead center
BSFC	Brake specific fuel consumption
BTDC	Before top dead center
BTE	Brake thermal efficiency
CA	Crank angle
CFD	Computational fluid dynamics
CFR	Co-operative fuel research
CI	Compression ignition
CO	Carbon monoxide
CPU	Central processing unit
CR	Compression ratio
DEE	Diethyl ether
DI	Direct injection
EGR	Exhaust gas recirculation
EPA	Environmental protection agency
EVO	Exhaust valve open
GDI	Gasoline direct injection
HC	Hydrocarbon
HCCI	Homogeneous charge compression ignition
HCT	Hydrodynamics chemistry and transport



HRD	Heat release duration
HRR	Heat release rate
HSDI	High speed direct injection
HTR	High temperature region
IC	Internal combustion
IMEP	Indicated mean effective pressure
IP	Indicated power
ISFC	Indicated specific fuel consumption
IT	Indicated torque
ITE	Indicated thermal efficiency
IVC	Inlet valve close
LPG	Liquefied petroleum gas
LTR	Low temperature region
MCS	Main combustion stage
NA	Naturally aspirated
NO	Nitric oxide
NTC	Negative temperature co-efficient
OH	Hydroxide
PCI	Premixed compression ignition
PCCI	Premixed charge compression ignition
PFI	Port fuel injection
PM	Particulate matter
RP	Rated power
RPM	Revolution per minute
RS	Rated speed

SACI	Spark-assisted compression ignition
SFC	Specific fuel consumption
SI	Spark ignition
SOC	Start of combustion
SOI	Start of ignition
TDC	Top dead center
TRG	Trapped residual gas
UHC	Unburned hydrocarbon
VCR	Variable compression ratio
VGR	Variable geometry turbocharger
WC	Water cooled
CO ₂	Carbon dioxide
NO ₂	Nitrogen dioxide
4S	Four stroke

UMP

CHAPTER 1

INTRODUCTION

1.1 Introduction

The concern about fuel economy and emissions is increasing day by day because these are the basic issues for internal combustion (IC) engine industry. The primary emissions from IC engines are nitrogen oxides (NO_x), particulate matter (PM), unburned hydrocarbon (HC) and carbon monoxide (CO). Temperature is the main factor for the formation of NO_x . In conventional compression ignition (CI) and spark ignition (SI) engines high temperature is produced during combustion because of the stoichiometric air-fuel mixture. Thus, NO_x cannot be averted in conventional IC engines. The reason for the formation of PM is similar to NO_x . When high temperature and rich mixture exists together in the combustion process, certainly PM produces. Especially, PM emissions cannot be averted at high load condition. The incomplete combustion is the main reason for the production of UHC and CO in IC engines. In the exhaust stroke, the temperature remains comparatively low. Due to this, unburned fuel and combustion intermediate species cannot be consumed properly in this low-temperature zone. As a result, unburned HC and CO are produced which is very common phenomena for conventional IC engines. A great attention has been paid to the fuel consumption and thermal efficiency of IC engines. Reduction of fuel consumption diminishes the fuel supply and lessens the dependency on foreign sources of fuel and ultimately cost of fuel is positively affected (Ball et al., 2009).

The thermal efficiency of conventional IC engines is very low which is another concern for automotive industry. It has been seen from research that higher compression ratio can provide higher thermal efficiency (Celik, 2008; Olsson et al., 2002a). Therefore, future combustion systems should incorporate high efficiency, high

compression ratio engines. However, the compression ratio of SI engines cannot be increased so much because high compression ratio creates abnormal combustion with knock in SI engines (Zhen et al., 2012).

To improve the performance of IC engines a number of initiatives have been taken out. Some modifications have been incorporated with IC engine to make it more energy efficient such as electric, fuel-cell or hybrid engines. The purpose of these technologies is to improve engine thermal efficiency as well as reduce engine emissions and fuel consumption throughout the lifespan of a vehicle. However, the implementation and commercialization of these technologies require a high cost which is the main obstacle of these new initiatives. Thus, an alternative solving is necessary to improve the current IC engines with comparatively low development cost. One of the solutions is Homogeneous Charge Compression Ignition (HCCI). HCCI offers the potential of nearly undetectable NO_x and PM emissions while operating at a high efficiency.

1.1.1 Homogeneous Charge Compression Ignition

HCCI combustion is defined as a process by which a homogeneous mixture of air and fuel is compressed until auto-ignition occurs near the end of the compression stroke (Hasan et al., 2016). SI engines have a spark plug to initiate the combustion with a flame front propagating across the combustion chamber. CI engines have a fuel injector to inject the diesel and the combustion takes place in a compressed hot air region. HCCI engines have no spark plug or fuel injector and the combustion starts spontaneously in multiple locations. High engine efficiency can be achieved with low NO_x and PM emissions. Figure 1.1 shows the differences between SI, CI, and HCCI engines. HCCI combustion is noticeably faster than either CI or SI combustion (Raitanapaibule et al., 2005). The comparison of different parameters influencing the combustion processes in SI, CI, and HCCI is given in Table 1.1. HCCI combustion can improve the thermal efficiency and maintain low emissions as well as can be implemented by modifying either SI or CI engines (Epping et al., 2002). A wide variety of fuels, a combination of fuels and alternative fuels can be used. Usually, a lean air-fuel mixture is used in HCCI engines. It ignites automatically in several locations and is then burned volumetrically without visible flame propagation (Kong et al., 2002). Once

ignited combustion occurs very quickly and it is fully controlled by chemical kinetics rather than spark or ignition timing (Najt et al., 1983).

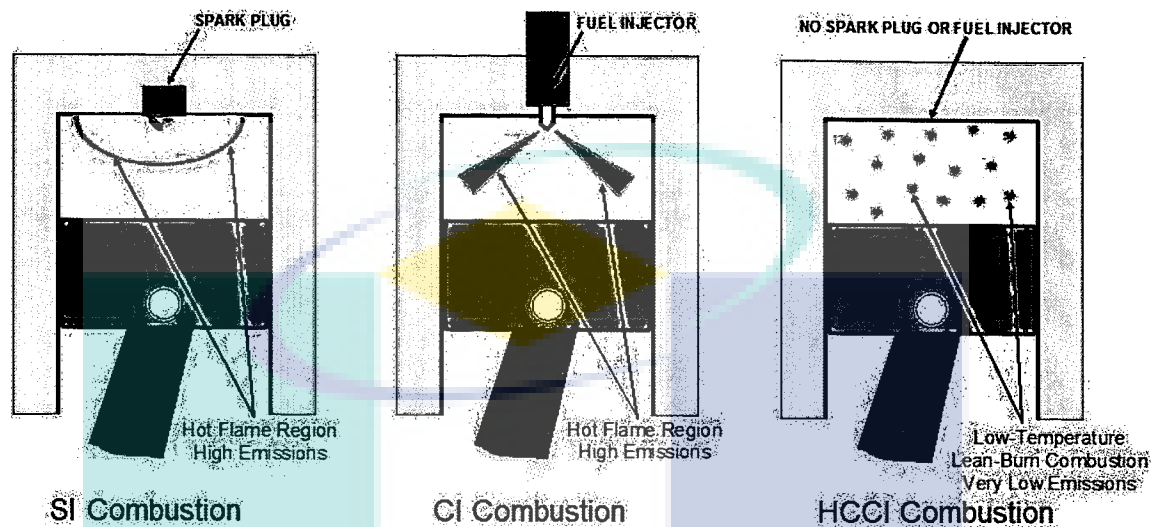


Figure 1.1 The differences between SI, CI, and HCCI engines

Source: Lin et al. (2011)

The advantages of HCCI technology are: i) as HCCI engines are fuel-lean that can operate at diesel-like compression ratios (>15), thus achieving higher efficiencies than conventional SI gasoline engines (Killingsworth et al., 2006); ii) it can operate on a wide range of fuels (Mack et al., 2009); iii) it can produce a cleaner combustion and lower emissions especially NO_x levels are almost negligible (Warnatz et al., 2006). Alternatively, HCCI technology has some disadvantages such as high levels of UHC and CO as well as knocking under certain operating conditions (Kong et al., 2003a). In terms of emissions, diesel engines produce higher NO_x and PM or soot which require proper control strategies because of having negative health and environmental effect, which can be solved by using HCCI combustion engines (Gan et al., 2011). As HCCI operates on lean mixtures, the peak temperatures are much lower than SI and CI. The low peak temperatures reduce the formation of NO_x . However, the low peak temperatures also lead to incomplete burning of fuel, especially near combustion chamber walls. This leads to high CO and HC emissions. An oxidizing catalyst can remove the regulated species because the exhaust is still oxygen-rich.

Table 1.1 Comparison of parameters influencing in SI, CI, and HCCI combustion engines

Engine type	SI	HCCI	CI
Ignition method	Spark ignition	Auto-ignition	Compression ignition
Charge	Premixed homogeneous before ignition	Premixed homogeneous before ignition	In-cylinder heterogeneous
Ignition point	Single	Multiple	Single
Throttle loss	Yes	No	-----
Compression ratio	Low	High	-----
Speed	High	Low	-----
Combustion flame	Flame propagation	Multi-point auto-ignition	Diffusive flame
Fuel economy	Good	Best	Better
Max. efficiency	30%	>40%	40%
Major emissions	HC, CO, and NO _x	HC and CO	NO _x , PM, and HC
Injection type	Port injection	Port and direct injection	Direct injection
Equivalence ratio	1	<1	-----

Source: Bendu et al. (2014)

1.1.2 HCCI Diesel Combustion

The HCCI diesel combustion is characterized by a set of several hundreds of species and complex reactions. This process consists of a two-stage heat release. The first stage of heat release occurs due to low-temperature reactions (LTR) and during this stage a small portion of total energy (7–10%) is released, while the second stage of heat release occurs due to high temperature reactions (Dang et al., 2011). During this stage, a huge amount of energy (approximately 90% of total energy) is released (Zheng et al., 2001). During LTR, fuel is consumed through an initial breakdown of HC fuel molecule which leads to form a HC radical. This radical reacts with oxygen and form an alkylperoxy radical. The alkylperoxy radical is then changed into a hydroperoxy alkyl radical through an isomerization process. After that, a second oxygen molecule addition reaction occurs where an oxohydroperoxide radical is formed. This radical is further isomerized and decomposed into ketohydroperoxide species and OH radicals. A time

delay exists between the LTR stage and the HTR stage which is known as the “negative temperature coefficient (NTC) regime” (Pucher et al., 1996). The alkylperoxy radicals decompose back into initial reactants, which help to form olefins and hydroperoxyl radicals. All the mentioned reactions are initiated at approximately 700 K and occur at modest reaction rates. Due to the heat release in this stage, the mixture temperature rises and when the temperature reaches at 900 K the HTR starts. In the HTR regime, mixture temperature rises rapidly and oxygen, as well as fuel molecules, are fully consumed to form carbon dioxide (CO_2), water, CO and hydrogen.

1.1.3 HCCI Gasoline Combustion

When HCCI is applied in a gasoline engine it shows a visible improvement in case of fuel consumption and emissions like NO_x and soot as compared to SI combustion (Kuboyama et al., 2011a; Kuboyama et al., 2011b; Lawler et al., 2011; Polovina et al., 2013; Yap et al., 2005). However, the combustion characteristic of HCCI from the gasoline engine is slightly different from HCCI from a diesel engine. HCCI gasoline combustion starts at the point of crank angle position where 10% of charge has burned. Figure 1.2 shows the timing map in HCCI gasoline combustion for 10% burn crank angle. It is found that exhaust gas recirculation (EGR) dilution has more effect than air dilution on the SOC when EGR rate remains 0-40%. SOC gradually becomes dependent on relative air-fuel ratio when EGR rate exceeds 40%. Figure 1.3 shows the combustion duration map in HCCI gasoline combustion for 10-90% burn crank angle. It is observed that combustion duration depends on lambda when EGR rate remains 0-30%. When EGR rate exceeds 30% combustion duration gradually becomes dependent on EGR rate rather than lambda. Among many reasons it can be one reason is that due to the dilution effect of EGR it can slow the reaction for auto ignition.

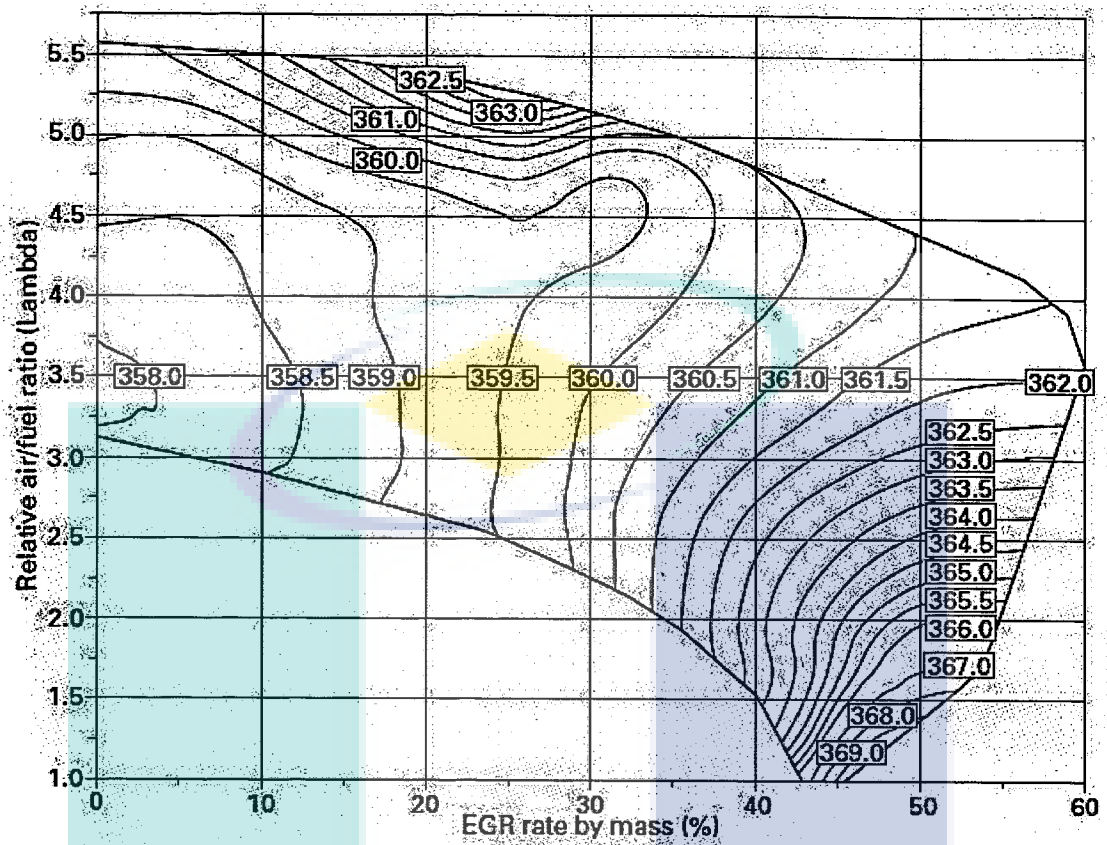


Figure 1.2 Combustion timing map in HCCI engine (10% burn), (°CA)

Source: Zhao (2007)

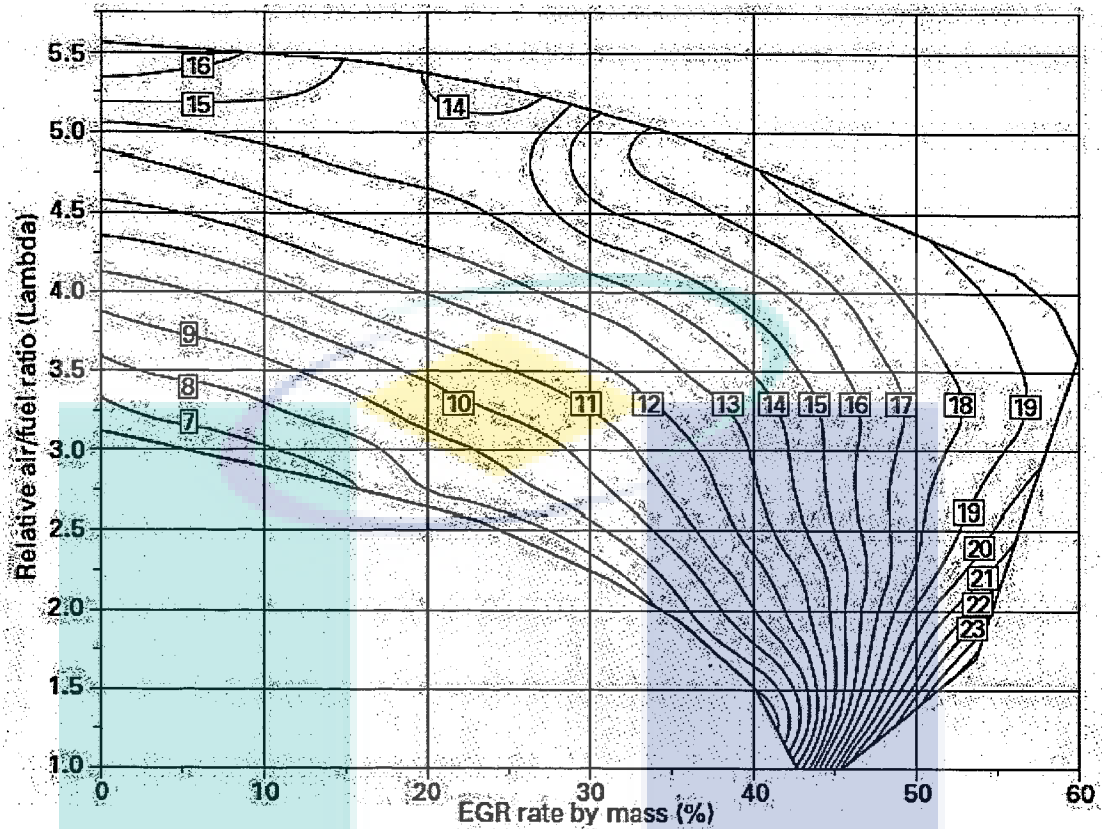


Figure 1.3 Combustion duration map in HCCI engine (10-90% burn), (°CA)

Source: Zhao (2007)

1.1.4 Formation of NO_x and Soot

The formation of NO_x and soot plays a significant role to understand the fundamentals of HCCI combustion. The regions of formation of NO_x and soot have been illustrated in Figure 1.4. The formation of NO_x is a complex process that involves the reactive combination of nitrogen found within the combustion air and organically bound nitrogen within the fuel itself. NO_x is a thermally produced gas and therefore its formation is largely dependent on the control of the combustion temperature (Zhao, 2007). It is seen that at low equivalence ratios and high flame temperatures usually NO_x formation occurs. The formation of NO_x can be reduced by keeping the flame temperature below 2200 K (Ericson et al., 2006). On the other hand, soot formation occurs in regions of high equivalence ratios or fuel rich mixtures and moderate temperatures. Net soot emission is a balance between formation and oxidation can be

reduced either increasing mixing or increasing oxidation (Gan et al., 2011). In conventional diesel engines, a representative fuel element would follow a path leading to both formations of both NO_x and soot emissions. Strategies to reduce NO_x formation during standard diesel operation normally lead to a penalty in soot emissions and vice versa.

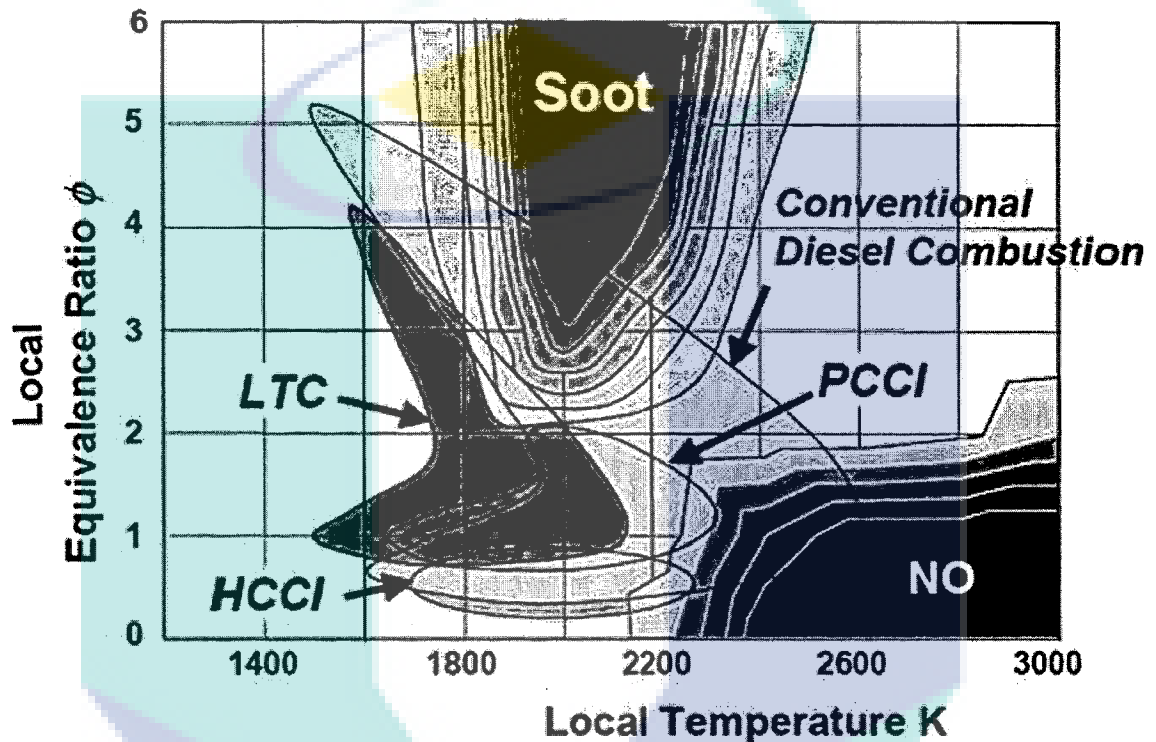


Figure 1.4 Equivalence ratios versus temperature

Source: Soloiu et al. (2013)

As both NO_x and soot emissions are strong functions of temperature and equivalence ratio, the most direct approach to reducing these emissions simultaneously is to carefully control the flame temperature and equivalence ratio (Miller et al., 1989). In line with this approach, the main purposes of HCCI combustion are to concurrently lower the flame temperature and allow sufficient air and fuel mixing to increase the homogeneity of charge. From a conceptual point of view, when a thoroughly homogeneous in-cylinder mixture is formed, the pressure and temperature rise during the compression stroke resulted in simultaneous auto ignition across the whole cylinder. Local temperatures are maintained at low levels with the absence of a high-temperature flame front and NO_x formation is thus avoided (Ishii et al., 1997). Soot formation is also

avoided due to the homogenized lean mixture which lowers local equivalence ratios (Tree et al., 2007).

1.2 Problem Statements

HCCI represents an evolutionary step in case of thermal efficiency, fuel economy and emissions especially NO_x and PM compared to diesel and gasoline engines. However, differing from both of these traditional engines, HCCI engines lack a physical event which controls the ignition timing. It is the main challenge which ultimately influences the power and efficiency (Izadi Najafabadi et al., 2013). Unlike SI engines and CI engines, HCCI engines have no direct mechanism to control the SOC. Its SOC is fully dependent on auto-ignition. According to Yao et al. (2009), this auto-ignition is affected by several factors like fuel auto-ignition chemistry and thermodynamic properties, combustion duration, wall temperatures, intake temperature and pressure, compression ratio, amount of EGR, engine speed, engine temperature, convective heat transfer to the engine, and other engine parameters. Higher intake temperatures and intake pressures cause earlier combustion timing due to the faster chemical kinetics (Saxena et al., 2013). For equivalence ratio sensitive fuels, higher equivalence ratios (up to stoichiometric) have a tendency to propel ignition timing due to the improvement of charge reactivity. The fuels without equivalence ratio sensitivity demonstrate an inverse pattern, where higher equivalence ratios have a tendency to bring about more delayed combustion timing. The lower specific heat ratio from higher equivalence ratios causes the prerequisite of more compression heating to achieve ignition temperatures. Nonetheless, in real operation, for both sorts of fuels the utilization of higher equivalence ratios likewise increases the in-cylinder wall and residuals temperatures, along these lines bringing on advanced combustion timing (Mangus et al., 2014). For fuels with little to no equivalence ratio sensitivity, there are contending impacts where lower specific heat ratios have a tendency to delay combustion while higher in-cylinder wall and residual temperatures have a tendency to propel combustion. To understand the effect of engine parameters on combustion, performance and emissions characteristics of HCCI engine, a fruitful study is needed which can be done by developing a more accurate simulation model based on zero-dimension and single zone rather than experiments or multidimensional modeling. Experimental work is costly and requires more time. Modeling is a way of exploring

engine behavior in ways that might otherwise impossible in a true experimental approach. A multi-dimensional model requires substantial computational time as compared to zero-dimensional and quasi-dimensional models, which are a simplified version of a multi-dimensional model (Komninos et al., 2012). Thus, the use of simplified model becomes increasingly important because of its advantages in computational time and resources. A zero-dimensional simulation would be an interim solution until the cost and time of running a multi-dimensional model is comparable with the current cost of the zero-dimensional model. The use of chemical kinetics mechanisms also helps in investigating the combustion behavior of an HCCI engine.

1.3 Objectives of Study

The objectives of this research are as follows:

1. To model a HCCI engine numerically using reduced chemical mechanism.
2. To investigate the influence of different engine parameters on combustion, performance and emissions characteristics in HCCI engines.
3. To analyze the influence of different fuels and blends of fuels on combustion, performance and emissions characteristics in HCCI engines.

1.4 Scope of Study

The scope of this research includes the following:

1. Develop a zero-dimensional single zone model for HCCI engine using detailed chemical kinetics. The air-fuel mixture inside the cylinder is considered to be homogeneous and the accumulated gas is assumed to be an ideal gas. Validation of model using previously published experimental results for both diesel HCCI and gasoline HCCI engines.
2. The use of different fuels in HCCI engines, including diesel, gasoline, *n*-heptane and blends of *n*-heptane and ethanol as well as blends of *n*-heptane and butanol using 15% and 30% of both ethanol and butanol in blends. Collection of chemical properties of different fuels and blends of fuels from previously published literature.
3. A study of the effects of engine speed, intake temperature and pressure and compression ratio by running simulation at engine speed ranging from 600 rpm

to 1200 rpm, intake temperature ranging from 313 K to 393 K, intake pressure ranging from 100 kPa to 200 kPa and compression ratio ranging from 10 to 16 for diesel HCCI engine and at engine speed ranging from 600 rpm to 1800 rpm, intake temperature ranging from 373 K to 453 K, intake pressure ranging from 100 kPa to 200 kPa and compression ratio ranging from 12 to 16 for gasoline HCCI engine.

4. A study of different combustion characteristics like in-cylinder pressure, heat release rate (HRR) and SOC and performance characteristics like indicated mean effective pressure (IMEP) and indicated thermal efficiency (ITE) emissions characteristics like HC, CO and NO_x using *n*-heptane as well as blends of *n*-heptane with ethanol and butanol at different intake temperatures ranging from 313 K to 393 K.

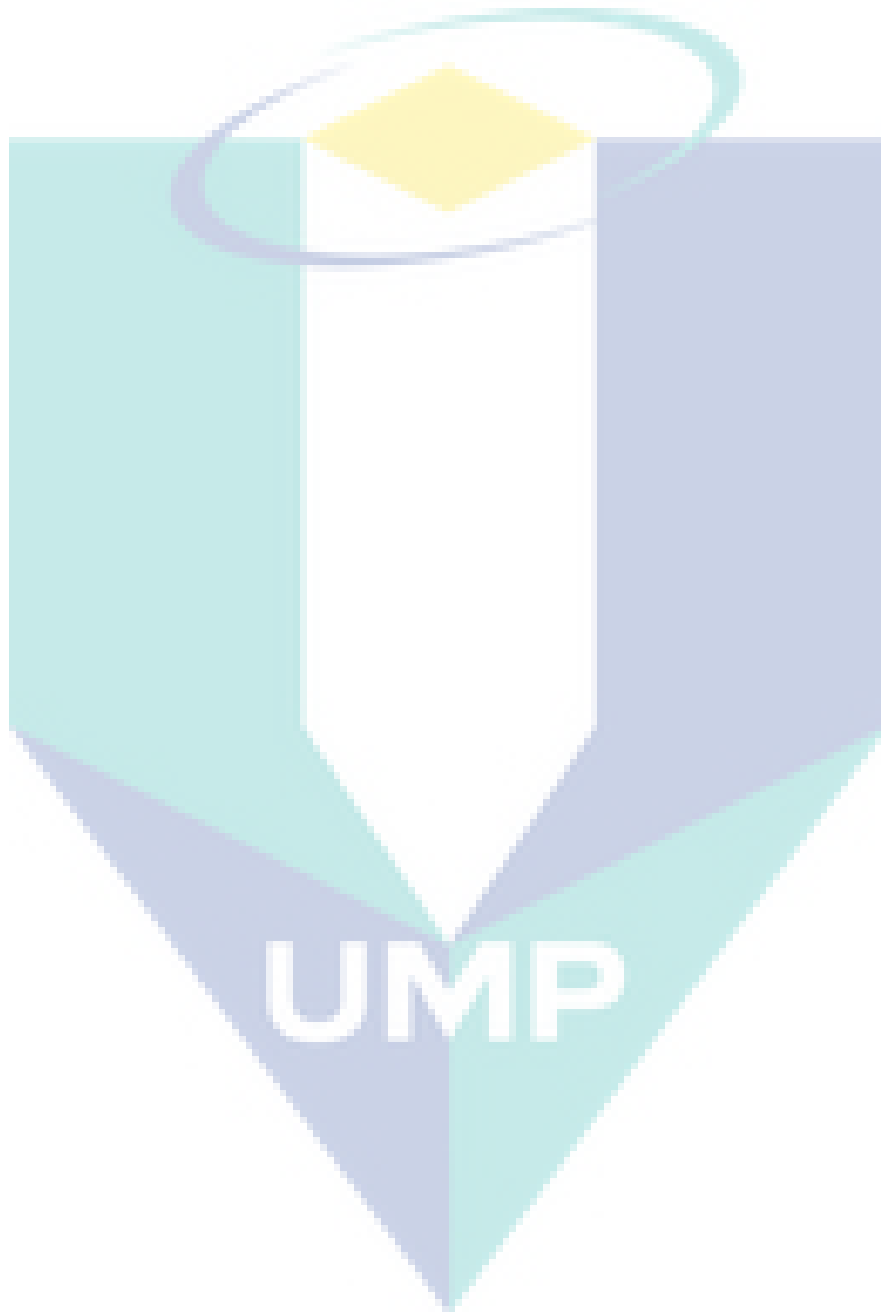
1.5 Organization of Thesis

The thesis consists of five chapters. Chapter 2 contains the literature review, which describes HCCI engines in general, and also covers the experimental and numerical studies on engine performance and emission characteristics of HCCI engines and compare with CI engines and SI engines. Effects of different engine parameters, as well as fuels and additives on HCCI engines, are discussed.

Chapter 3 presents the zero-dimensional single zone modeling and all the equations involved in zero-dimensional single zone modeling. The conservation equations including mass, momentum, species, and energy are described. The chemical reactions are also discussed. Some combustion and performance parameters, as well as the validation of the model, are presented in this chapter.

Chapter 4 presents the results obtained from the simulation study at different engine operating conditions. This chapter consists of diesel and gasoline HCCI engine. The experimental results from published literature for diesel and gasoline engines are compared and discussed. The effect of engine speed, intake air temperature, intake air pressure and compression ratio on combustion and performance characteristics in an HCCI engine fueled with diesel and gasoline using numerical simulations is investigated and described. The effect of intake temperature on combustion,

performance and emissions characteristics of HCCI engine fueled with diesel as well as diesel-ethanol and diesel-butanol blends in different ratios is also presented. The Chapter 5 summarizes the important findings and also gives suggestions for future work.



CHAPTER 2

LITERATURE REVIEW

2.1 Introduction

The following sections are included as a broad overview of HCCI and a more detailed look at engine performance and emission characteristics of HCCI engines, effects of engine parameters and fuels and additives on HCCI engines as well as relevant numerical studies of HCCI engines. There is a need to report the recent advancement of HCCI combustion due to the significance development of technology and which can be a replacement for conventional CI or SI engines. This chapter discusses the current issues for this technology where engine performance and emission characteristics of HCCI engines will be presented and compared with CI engines and SI engines. The performance of HCCI engine is strongly dependent on the engine parameters and fuel type, and these affect the emission levels as well. Due to this, effects of engine parameters as well as fuels and additives on HCCI engines will be described in next section. Another section will focus on relevant numerical studies of HCCI engines, concluding with summary of this chapter.

2.2 Performance Comparison

Engine performance is a parameter on which the acceptability of an engine is strongly dependent. Fuel properties, fuel injection pressure and timing, air-fuel mixture, amount of injected fuel, fuel spray pattern etc. have noticeable effect on engine performance. The review of performance comparison between HCCI engines and CI engines using different types of fuel in terms of cylinder pressure, HRR, specific fuel consumption (SFC) and thermal efficiency has been presented. The comparative results

related to the performance characteristics of HCCI engines using various fuels with CI and SI engines are summarized in Table 2.1 and Table 2.2 respectively.

Table 2.1 Different experimental engine performance results using various fuels in HCCI engines compared to CI engines

Engine	Test condition	Fuel	Performance	Reference
2-cylinder, 4S, AC, CI, DI, CR: 16.5:1, RP: 4.85 kW, RS: 1500 rpm	Constant speed, different loads and different percentages of EGR (0%, 10% and 20%)	Diesel	↑: HRR, combustion duration ↓: EGT	(Singh et al., 2012)
1-cylinder, 4S, AC, CI, DI, CR: 17.5:1, RP: 4.4 kW, RS: 1500 rpm	Constant speed, different loads and different percentages of EGR (0%, 10%, 20% and 30%)	Diesel	↓: Thermal efficiency, cylinder pressure	(Ganesh et al., 2010)
1-cylinder, 4S, NA, CI, DI, CR: 18.5:1, RS: 1800 rpm	Constant speed and different loads	Diesel	↓: Thermal efficiency ↑: Cylinder pressure, HRR	(Ma et al., 2008)
2-cylinder, 4S, AC, CI, DI, CR: 16.5:1, RP: 5.85 kW, RS: 1500 rpm	Constant speed, different loads and different percentages of EGR (0%, 15% and 30%)	Biodiesel-diesel blend	↓: Thermal efficiency, SFC, HRR ↑: Cylinder pressure	(Singh et al., 2014)
1-cylinder, 4S, NA, CI, DI, CR: 18.4:1	Constant speed, different loads and different percentages of EGR (0%, 11.5%, 16.6% and 24.3%)	Biodiesel-diesel blend	↓: Cylinder pressure ↑: HRR	(Jiménez-Espadafor et al., 2012)
1-cylinder, 4S, CI, DI, CR: 17.5:1 RS: 1500 rpm	Constant speed and fixed load	Biodiesel-diesel blend	—: Cylinder pressure, HRR	(Mancaruso et al., 2010)
4-cylinder, 4S, CI, IDI, CR: 16.5:1	Constant speed and different loads	Biodiesel-diesel blend	↑: SFC, Thermal efficiency	(Mohanamugan et al., 2011)
1-cylinder, 4S, CI, DI, CR: 17.5:1 RP: 4.4 kW RS: 1500 rpm	Constant speed, different loads and different percentages of EGR (0%, 10%, 20% and 30%)	Biodiesel-diesel blend	↓: HRR ↑: Cylinder pressure	(Ganesh et al., 2014)

Table 2.2 Different experimental engine performance results using various fuels in HCCI engines compared to SI engines

Engine	Test condition	Fuel	Performance	Reference
4-cylinder, 4S, AC, PFI, CR: 12:1, RS: 1500 rpm	Constant speed and different loads	Gasoline	↑: Cylinder pressure ↓: BSFC	(Kuboyama et al., 2011a)
1-cylinder, 4S, AC, PFI, CR: 12:1, RS: 2500 rpm	Variable speed , different loads and different percentages of EGR	Gasoline	↑: Cylinder pressure, BSFC	(Yun et al., 2010)
4-cylinder, 4S, AC, PFI, CR: 12:1, RS: 1500 rpm	Constant speed , different loads and different percentages of EGR	Gasoline	↑: Cylinder pressure, BTE	(Gotoh et al., 2013)
1-cylinder, 4S, AC, GDI, CR: 12:1, RS: 1500 rpm	Variable speed and fixed load	Gasoline	↑: Cylinder pressure, BTE ↓: BSFC	(Aceves et al., 2000)
1-cylinder, 4S, AC, DI, CR: 11.85:1	Constant speed , different loads and different percentages of EGR	Gasoline -ethanol blend	↑: Cylinder pressure, BSFC, BTE	(Szybist et al., 2013)
1-cylinder, 4S, AC, GDI, CR: 14:1	Constant speed , different loads and different percentages of EGR	Gasoline -ethanol blend	↑: Cylinder pressure, BTE	(Ji et al., 2014)
4-cylinder, 4S, AC, PFI, CR: 10.8:1, RS: 2000 rpm	Variable speed ,different loads and different percentages of EGR	Gasoline and ethanol	↑: Cylinder pressure →: BSFC ↓: BTE	(Polovina et al., 2013)
1& 4-cylinder, 4S, AC, PFI, CR: 17:1, 19:1 & 21:1 RS: 1500 rpm	Constant speed and variable compression ratio	Gasoline and CNG	↑: Cylinder pressure, BSFC, BTE	(Kobayashi et al., 2011)
4-cylinder, 4S, AC, GDI, CR: 4-16:1, RS: 600 rpm	Constant speed and variable compression ratio	n-heptane and iso-octane	↑: BTE	(Machrafi et al., 2008)
1-cylinder, 4S, AC, PFI, CR: 8;1:1, RS: 9000 rpm	Variable speed and fixed load	Diethyl ether	↑: Cylinder pressure, BTE ↓: BSFC	(Lemberger et al., 2009)

2.2.1 HCCI Diesel Combustion

The investigation on cylinder pressure in HCCI engines has been reported by many researchers (Canakci, 2012; Ganesh et al., 2014; Jiménez-Espadafor et al., 2012; Singh et al., 2014; Turkcan et al., 2013). Gajendra Singh et al. (2014) investigated experimentally the combustion, performance and emission characteristics of HCCI engines using diesel and different percentages of biodiesel-diesel blend and compared the results with conventional diesel engines. The authors modified a double cylinder, four stroke and air cooled diesel engine for HCCI operation and used different percentages of EGR (0%, 15% and 30%). They reported that the cylinder pressure is higher in HCCI engines than conventional CI engines. However, by increasing the percentage of EGR, it can be lower and suitable for engine performance. Ganesh et al. (2014) have also found similar results. Ramesh et al. (2014) used hydrogen as a fuel to investigate the combustion characteristics of HCCI engines. They also observed the higher cylinder pressure and used CO₂ as additive to keep the cylinder pressure in a reasonable level. Applying different techniques some researchers have found lower cylinder pressure in HCCI engines than CI engines. Lei Shi et al. (2006) applied internal and external exhaust gas recirculation technique to reduce the cylinder pressure. Recirculation of cooled external exhaust gas was very helpful in this case. Francisco et al. (2012) modified the cylinder used in their experiment to get a positive cylinder pressure. Turkcan et al. (2013) also found similar results.

From the investigations done by many researchers on HCCI combustion mode, it can be reported that HRR of HCCI combustion is completely different from both CI and SI combustion (García et al., 2009b). Most of the researchers (Canakci, 2012; Jiménez-Espadafor et al., 2012; Singh et al., 2012; Swami Nathan et al., 2010a; Turkcan et al., 2013) found HRR is higher in HCCI engines than diesel engines. Jimenez et al. (2012) investigated experimentally the combustion, performance and emission characteristics of HCCI engines using diesel and different percentages of biodiesel-diesel blend as well as compared the results with conventional diesel engines. From the investigation, the authors reported that HRR is higher in HCCI engines than conventional CI engines. Imperfect air-fuel mixture was the reason for this occurrence. Swami Nathan et al. (2010a) and Gomes et al. (2008) used different fuels i. e. acetylene and hydrogen to investigate the combustion characteristics of HCCI engines. In case of HRR, they also

found similar results like Jiménez-Espadafor et al. (2012). Some researchers (Ganesh et al., 2014; Kulzer et al., 2010; Singh et al., 2014; Zhang et al., 2012) found opposite results i.e. lower HRR than diesel engines because of their initiatives. Ganesh et al. (2014) modified a single cylinder, four stroke and direct injection diesel engine for HCCI operation. They also made a biodiesel vaporizer to vaporize the fuel perfectly so that it can mix with air to prepare a homogeneous charge. Due to this reason, they observed lower HRR than diesel engines. Singh et al. (2014) observed similar results while applying same technique like Ganesh et al. (2014) in a double cylinder, four stroke, air cooled and direct injection diesel engine. Zhang et al. (2012) and Kulzer et al. (2010) also found identical results in case of HRR. To reduce HRR in HCCI engines, the suitable mixture formation and appropriate auto-ignition chemistry play a vital role (Dec et al., 2004; Sjöberg et al., 2006; Yang et al., 2011). In addition, air-fuel equivalence ratio, engine speed and EGR have also effect on HRR in HCCI engines (García et al., 2009b; Garcia et al., 2011). Controlling this perfectly can provide a suitable HRR from HCCI engines.

According to the review on Table 2.1, most of the researchers (Canakci, 2012; Kulzer et al., 2010; Swami Nathan et al., 2010a, 2010b) observed that HCCI engines provide higher thermal efficiency than diesel engines. Swami et al. (2010b) have performed a study to measure the thermal efficiency of HCCI engine and compare with conventional diesel engine while using biogas as fuel. The authors used different intake temperatures i. e. 80 °C, 100 °C and 135 °C. The main component of fuel was methane (>60%) and produced anaerobic fermentation of cellulose biomass materials (Duc et al., 2007). It was reported that when the intake temperature was 135 °C, then thermal efficiency was higher than diesel engine. Gomes et al. (2008) found that HCCI engines can provide 45% higher thermal efficiency than diesel engines when hydrogen is used as a fuel. Canakci (2008) investigated combustion characteristics of HCCI engine using different boost pressures and gasoline as fuel. He also found similar results. Some of the researchers found opposite results i.e. lower thermal efficiency than conventional diesel engines due to inappropriate mixture, low fuel quality etc (Ganesh et al., 2010; Ganesh et al., 2008; Ma et al., 2008; Singh et al., 2014). Ganesh et al. in their two experiments (Ganesh et al., 2010; Ganesh et al., 2008) found a negative results in case of thermal efficiency while investigating the combustion characteristics of HCCI engines in a single cylinder, four stroke, air cooled and direct injection diesel engine when used

diesel as fuel. It was very difficult task to vaporize the diesel and mix it properly with air. Due to this reason, the mixture was not homogeneous and ultimately provided a lower thermal efficiency than diesel engine. However, same research team observed a higher thermal efficiency than diesel engine when biodiesel-diesel blend was used as a fuel (Ganesh et al., 2014). They used a vaporizer to vaporize the fuel perfectly and were able to prepare a homogeneous mixture.

2.2.2 HCCI Gasoline Combustion

The in-cylinder pressure measurement is considered to be very important because it provides valuable information such as the peak pressure, P–V diagram, IMEP, fuel supply effective pressure, HRR, combustion duration, ignition delay and so on (Payri et al., 2010). It is the predominant view that HCCI engines provide higher cylinder pressure than SI engines (Gotoh et al., 2013; Ji et al., 2014; Polovina et al., 2013; Szybist et al., 2013; Zhang et al., 2014b). Polovina et al. (2013) investigated experimentally the combustion, performance and emission characteristics of HCCI engines using gasoline and different percentages of gasoline–ethanol blend, and compared with conventional SI and spark-assisted compression ignition engines under various conditions such as naturally aspirated, boosted, lean and stoichiometric. The authors modified a four-cylinder, four-stroke, naturally aspirated, air-cooled and port fuel-injected gasoline engine for HCCI combustion. The authors reported that at partial load, the cylinder pressure of HCCI is quite similar to that of conventional SI engines. However, at higher load the cylinder pressure exceeds the SI engine. Yap et al. (2005) used hydrogen as a fuel to investigate the combustion and emission characteristics of HCCI engines. Their experiment was done in a modified single-cylinder, four-stroke and port fuel-injected gasoline engine and the authors also observed higher cylinder pressure than SI engines. The high cylinder pressure was at a reasonable level. Kobayashi et al. (2011) investigated the combustion, performance and emission characteristics of HCCI engines. Their experiment was conducted on both single- and four-cylinder gasoline engines using gasoline as fuel. But they observed higher cylinder pressure. To mitigate it, they used a blend of natural gas with gasoline. Milovanovic et al. (2005) investigated the combustion characteristics of an HCCI engine in a modified gasoline engine under constant speed and different load. The authors concluded that by varying the amount of trapped residual gas in the fresh air/fuel mixture (inside the

cylinder), the cylinder pressure can be controlled and hence also the auto-ignition timing and HRR.

Brake-specific fuel consumption (BSFC) is a measure of the fuel efficiency of any prime mover that burns fuel and produces rotational, or shaft, power (Ghazikhani et al., 2010). It is typically used for comparing the efficiency of IC engines with a shaft output (Zhuang et al., 2013). The investigations on BSFC in HCCI engines have been reported by researchers (Al-Khairi et al., 2011; Polovina et al., 2013; Szybist et al., 2013; Yun et al., 2010; Zhang et al., 2014b). Szybist et al. (2013) modified a boosted single-cylinder research engine for HCCI combustion which was equipped with a direct injection fuelling system. Their purpose was to apply different control systems to achieve an HCCI high load limit. They found that to increase the load, it is also necessary to increase the manifold pressure and external EGR, and that the BSFC was at a reasonable level at part load, but at high load operation the difference with SI combustion becomes greater. Similarly, Yun et al. (2010) investigated a spark-assisted HCCI combustion and double injection strategy to extend the higher operating load limit of an HCCI engine to maximize the fuel economy benefit of HCCI. The authors found that spark-assisted HCCI combustion was a key factor to reduce combustion noise and improve fuel economy at the high load condition. Alternatively, the double injection strategy could reduce combustion noise slightly, but the BSFC was increased due to incomplete combustion. Kobayashi et al. (2011) and Al-khairi et al. (2011) investigated the performance of an HCCI engine by modifying a gasoline engine and using natural gas as fuel. They found similar results in the case of the BSFC. Some of the researchers found the opposite results due to appropriate mixture homogeneity as well as complete combustion (Kuboyama et al., 2011a; Lemberger et al., 2009; Zhang et al., 2014b). Hyvonen et al. (2005) investigated the spark-assisted HCCI combustion in a five-cylinder variable compression ratio HCCI engine using gasoline. The authors found a lower BSFC than in the SI engine. Another experiment was done by Lemberger and Floweday (2009) on a single-cylinder 25cc, air-cooled, 4-stroke SI engine converted to run in HCCI mode with the aid of various combustion control systems and using diethyl ether as fuel. Later, the authors compared the performance result with an SI engine and found a lower BSFC than for SI.

The brake thermal efficiency (BTE) of an engine can be defined as the ratio of brake output power to input power and describes the brake power produced by an engine with respect to the energy supplied by the fuel. According to the review, most of the researchers observed that HCCI engines provide higher thermal efficiency than diesel engines (Gotoh et al., 2013; He et al., 2014a; Ji et al., 2014; Szybist et al., 2013; Zhang et al., 2014b). When an HCCI engine is modified from an SI engine it provides higher BTE than conventional SI engines. A study was performed by Gotoh et al. (2013) to measure the BTE of an HCCI engine and compare the value with a conventional gasoline engine while using gasoline as fuel. They applied a blow-down supercharging system and varied the intake temperature and pressure. Ultimately, they came to the conclusion that by imposing the blow-down charging system the operating load limit of the HCCI engine can be increased along with the BTE. An investigation and comparison of combustion, performance and emission characteristics of two-stroke and four-stroke SI and HCCI operations in a direct ignition gasoline engine was conducted by Zhang and Zhao (2014b). They observed that, among all the experiments, when the engine was run in HCCI mode it provided the highest BTE. Similar experiments were done by Machrafi et al. (2008) and He et al. (2013), but the authors used different types of fuels, i.e. blends of iso-octane and n-heptane as well as gasoline and n-butanol. In all these cases the authors found higher BTE.

Aceves et al. (2000) proposed a multi-zone model for predicting the combustion, performance and emissions characteristics of an HCCI combustion engine. From their prediction it was found that BTE was always higher than conventional SI engines in any load condition. Polovina et al. (2013) investigated the combustion characteristics of an HCCI engine in a modified gasoline engine under various conditions, including naturally aspirated, boosted, lean and stoichiometric. The authors reported that at partial load, the BTE of HCCI is quite similar to that of conventional SI engines. However, at higher load the BTE was less than for SI engines.

2.3 Emissions Comparison

The United States, Europe, Japan and Singapore are imposing various standards on emissions from vehicles (EPA-Gasoline, 1999; Popp, 2006; Wesselink et al., 2006). Emissions in HCCI engines consist of HC, CO, NO_x and PM. Various fuels used in

HCCI engines have been proved to have low emissions levels of NO_x and PM (Swami Nathan et al., 2010b) and high levels of UHC and CO (Kong et al., 2003b; Swami Nathan et al., 2010b). However, the emissions levels vary from one engine to another and are dependent on the operating conditions of the engine, fuel quality and the engine design (Rizvi, 2009). This section presents a review of emission characteristics in terms of HC, CO and NO_x of HCCI engines using various fuels and illustrates an emission comparison among HCCI, CI and SI engines at Table 2.3 and Table 2.4.

2.3.1 HCCI Diesel Combustion

CO is mainly produced due to incomplete combustion of the fuel. Incomplete combustion occurs when flame temperature cools down and progression to CO_2 remains incomplete (Sanjid et al., 2013). It is reported that CO emission is higher in HCCI engines than diesel engines in the literatures (Canakci, 2012; Ganesh et al., 2014; Jiménez-Espadafor et al., 2012; Singh et al., 2014; Turkcan et al., 2013) and still a challenge for HCCI engines which should be solved very soon to get the full benefit from HCCI engines. Ganesh et al. (Ganesh et al., 2014) reported that CO is higher in HCCI engines due to the nature of this type of combustion. The authors used different fuels but observed the similar results in case of CO emission. The amount of CO_2 and CO are dependent on the combustion efficiency, where the combustion efficiency can be defined as the ratio of CO_2 to the total of fuel carbon present in the exhaust including CO, CO_2 and UHC (Li et al., 2007). CO is formed by following $\text{RH-R-RO}_2\text{-RCHO-RCO-CO}$ equation, where R is the HC radical (Heywood, 1988). CO is mainly formed in the crevices of the cylinder which are so cold for complete combustion (Aceves et al., 2001a). That's why this problem needs to be solved for producing lower CO emission. In addition, for complete reaction of the conversion from CO to CO_2 needs temperature above 1500 K (Dec, 2002). However, CO formation occurs in case of HCCI combustion at low load peak burned gas temperature remains below that required level.

HCs in the exhaust exist for one of two reasons either from fuel that avoids combustion or from intermediate species of HCs that are formed during combustion and not completely combusted. The formation of HCs is typically due to local flame extinction, either by misfire or gaps in the cylinder geometry (Warnatz et al., 2006).

Table 2.3 Different experimental engine emissions results using various fuels in HCCI engines compared to CI engines

Engine	Test condition	Fuel	Emissions	Reference
1-cylinder, 4S, AC, CI, DI, CR: 17.5:1, RP: 4.4 kW, RS: 1500 rpm	Constant speed, different loads and different percentages of EGR (0% and 10%)	Diesel	↓: NO _x , Smoke ↑: HC, CO	(Ganesh et al., 2008)
1-cylinder, 4S, CI, DI, CR: 15:1, RS: 1500 rpm	Constant speed and different loads	Diesel	↓: NO _x , HC	(Guo et al., 2011)
1-cylinder, 4S, WC, NA, CI, CR: 14.8:1	Variable speed and different percentages of EGR (0%, 29%, 42% and 50%)	Diesel	↓: NO _x , Smoke ↑: HC, CO	(Shi et al., 2006)
1-cylinder, 4S, CI, CR: 19:1, RP: 11 kW, RS: 3000 rpm	Variable speed and different loads	Diesel	↓: NO _x , Smoke ↑: HC, CO	(Kim et al., 2007)
4-cylinder, High pressure common rail, CR: 18.5:1, RP: 87 kW, RS: 4000 rpm	Variable speed and different loads	Diesel	↓: NO _x , soot	(Yang et al., 2013)
1-cylinder, 4S, NA, CI, DI, CR: 16.1:1, RP: 62 kW, RS: 1800 rpm	Variable speed and different loads	Gasoline	↓: NO _x ↑: HC, CO	(Canakci, 2008)
1-cylinder, 4S, NA, CI, DI, CR: 16.1:1, RP: 62 kW, RS: 1800 rpm	Variable speed and different loads	Gasoline	↓: NO _x ↑: HC, CO	(Canakci, 2012)
1-cylinder, 4S, WC, NA, CI, DI, CR: 17:1	Variable speed and different loads	Gasoline -Alcohol	↓: NO _x ↑: HC, CO	(Turkcan et al., 2013)

Table 2.4 Different experimental engine emissions results using various fuels in HCCI engines compared to SI engine

Engine	Test condition	Fuel	Emissions	Reference
1-cylinder, 4S, AC, GDI, CR: 11.3:1, RS: 2500 rpm	Variable speed and fixed load	Gasoline	↑: HC, CO ↓: NO _x , PM	(Elghawi et al., 2010)
1-cylinder, 4S, AC, PFI, CR: 12:1, RS: 1500 rpm	Constant speed , different loads and different percentages of EGR	Gasoline	↓: NO _x	(Zhao, 2007)
1-cylinder, 4S, AC, GDI, CR: 11.78:1, RS: 1500 rpm	Constant speed , different loads and different percentages of EGR	Gasoline	↑: HC, CO ↓: NO _x	(Zhang et al., 2014b)
1-cylinder, 4S, WC, PFI, CR: 10.5:1, RS: 2000 rpm	Constant speed and different loads	Gasoline	↓: HC, CO, NO _x	(Milovanovic et al., 2005)
5-cylinder, 4S, AC, PFI, CR: 10-30:1	Constant speed and different loads	Gasoline	↑: HC, CO ↓: NO _x	(Hyvönen et al., 2005)
1-cylinder, 4S, AC, GDI, CR: 11.85:1, RS: 2000 rpm	Constant speed and different loads	Gasoline -ethanol blend	↑: NO _x	(Weall et al., 2012)
1-cylinder, 4S, AC, PFI, CR: 14:1, RS: 2100 rpm	Constant speed and different loads	Gasoline and CNG	↑: CO ↓: HC, NO _x	(Al-Khairi et al., 2011)
1-cylinder, 4S, AC, PFI, CR: 10.66:1, RS: 1500 rpm	Variable speed and fixed load	Gasoline and n-butanol	↓: NO _x	(He et al., 2013)
1-cylinder, 4S, AC, PFI, CR: 10.66:1, RS: 1500 rpm	Variable speed and fixed load	n-butanol	↓: NO _x	(He et al., 2014a)
1-cylinder, 4S, AC, PFI, CR: 12.5:1 & 15:1, RS: 1500 rpm	Constant speed and variable compression ratio	Propane	↑: HC, CO ↓: NO _x	(Yap et al., 2005)

HCs in the exhaust exist for one of two reasons either from fuel that avoids combustion or from intermediate species of HCs that are formed during combustion and not completely combusted. The formation of HCs is typically due to local flame extinction, either by misfire or gaps in the cylinder geometry (Warnatz et al., 2006). It is

predominant viewpoint that HC emissions increases when HCCI combustion is applied (Canakci, 2012; Ganesh et al., 2014; Jiménez-Espadafor et al., 2012; Singh et al., 2014; Turkcan et al., 2013) and like CO emission, it is another challenge of HCCI engines. Ganesh et al. (Ganesh et al., 2010) reported that HC is higher in HCCI engines due to the nature of this type of combustion. The authors used different fuels but observed the similar results in case of HC emission. For low combustion temperature, incomplete combustion is occurred and ultimately HC emissions is produced (Bression et al., 2008; Ganesh et al., 2008). HC is mainly formed in the crevices of the cylinder which are so cold for complete consumption (Aceves et al., 2001a). Higher concentrations of hydrogen and natural gas in diesel engines have the ability to reduce UHC and CO emission levels, because the gaseous state of hydrogen and natural gas will reduce the wall wetting effect on the cylinder liner (Cho et al., 2007). Since HCCI engines typically operate fuel lean, the final flame temperature is usually well below 2000 K (Gan et al., 2011). At this low post-combustion temperature chemical reactions that produce NO_x are essentially inactive (Mack, 2007a).

NO_x is generally formed in a high temperature reaction, where the nitrogen in air dissociates into nitrogen radicals to form NO when reacting with oxygen. NO is converted to NO_2 when further reactions occur in the chamber. From the review, it is common conclusion that NO_x emission is negligible in HCCI engines compared to CI engines (Canakci, 2012; Ganesh et al., 2014; Singh et al., 2012; Singh et al., 2014; Turkcan et al., 2013). Gajendra Singh et al. (2014) investigated experimentally the combustion, performance and emission characteristics of HCCI engines using diesel and different percentages of biodiesel-diesel blend as well as compared the results with conventional diesel engines. The authors modified a double cylinder, four stroke and air cooled diesel engine for HCCI operation and used different percentages of EGR (0%, 15% and 30%). From the investigation, the authors reported that NO_x emission is very low in HCCI engines compared to conventional CI engines. NO_x formation is dependent on equivalence ratio. Tanaka et al. (2003) found that equivalence ratio more than 0.33 is the possible reason for substantial increase in NO_x . Authors in literatures (Komninos, 2009; Miller et al., 1989) used high compression ratio engines in their experiment and observed a very low amount of NO_x . NO_x emission can also be reduced by applying EGR technique which was proved by Bression et al. (2008).

2.3.2 HCCI Gasoline Combustion

It is reported that CO emission is higher in HCCI engines than gasoline engines (Al-Khairi et al., 2011; Elghawi et al., 2010; Kobayashi et al., 2011; Zhang et al., 2014b). Kobayashi et al. (2011) investigated the combustion, performance and emission characteristics of HCCI engines. Their experiment was conducted on both single- and four-cylinder gasoline engines using gasoline as fuel. However, they observed higher CO than in SI engines. Aceves et al. (2000) proposed a multi-zone model for predicting the combustion, performance and emissions characteristics of an HCCI combustion engine. From their prediction it was found that CO was always higher than in conventional SI engines in any load condition. It is the predominant viewpoint that HC emissions increase when HCCI combustion is applied (Hyvönen et al., 2005; Kobayashi et al., 2011; Lemberger et al., 2009) and, like CO emission, this is another challenge with HCCI engines. Kobayashi et al. (2011) investigated the emissions characteristics of an HCCI engine by modifying a gasoline engine and using natural gas as fuel. They found higher HC than in SI engines. A similar experiment was done by Lemberger and Floweday (2009) on a single-cylinder 25cc, air-cooled, 4-stroke SI engine converted to run in HCCI mode with the aid of various combustion control systems and using diethyl ether as fuel. Later they compared the emission result with an SI engine and found higher HC than for SI.

NO_x emission is negligible in HCCI engines compared to SI engines (He et al., 2013; He et al., 2014a; Polovina et al., 2013; Szybist et al., 2013; Zhang et al., 2014b). Polovina et al. (2013) investigated experimentally the combustion, performance and emission characteristics of HCCI engines using gasoline and different percentages of gasoline–ethanol blend as well as comparing with conventional SI and spark-assisted compression ignition engines under various conditions including naturally aspirated, boosted, lean and stoichiometric. The authors modified a four-cylinder, four-stroke, naturally aspirated, air-cooled and port fuel-injected gasoline engine for HCCI combustion. The authors reported that NO_x emission is very low for every load condition. Kobayashi et al. (2011) investigated the combustion, performance and emission characteristics of HCCI engines. Their experiment was conducted on both single- and four- cylinder gasoline engines by using gasoline. The authors also observed lower NO_x than in SI engines. Similarly, Lemberger and Floweday (2009) modified a

single-cylinder 25cc, air-cooled, 4-stroke SI engine for HCCI combustion. Their observations were also similar to those of others. Aceves et al. (2000) proposed a multi-zone model for predicting the combustion, performance and emissions characteristics of an HCCI combustion engine. From their prediction it was found that NO_x was always lower than conventional SI engines in any load condition.

2.4 Effects of Engine Parameters

In order to develop an appreciable control method to optimize ignition timing and smooth HRR, it is very important to understand the effects of engine parameters on the ignition timing, combustion rate, performance and emissions (Lu et al., 2005). This section presents a review of the effects of different engine parameters such as intake temperature, intake pressure and compression ratio on HCCI engines using various fuels, with some brief discussion.

2.4.1 Intake Temperature

One of the main parameters to control HCCI combustion is the intake air temperature, which affects the time-temperature history of the mixture. High intake temperature advances the SOC but causes a reduction in the volumetric efficiency (Machrafi et al., 2010). Intake charge temperature affects the combustion and formation of emissions through two distinct pathways. When temperature is lowered, ignition delay is extended leading to enhanced air/fuel premixing. Additionally, the adiabatic flame temperature of a fuel parcel is decreased when it is mixed to a particular equivalence ratio. This means that fuel element is steered away from the NO_x -soot formation region on the equivalence ratios-temperature map. Lu et al. (2005) found that the intake temperature plays the most sensitive influence on the HCCI combustion characteristics. They showed that the combustion phase was advanced, and the combustion duration was shortened with the increase of intake charge temperature. They also showed that increasing intake charge temperature from 31°C to 54°C increased NO_x emissions linearly from approximately 10 ppm to 50 ppm when n-heptane fuel was combusted at fixed fuel delivery rate, engine speed and 30% EGR. This is in agreement with another HCCI work whereby NO_x increased when inlet air temperature increased from 35°C to 80°C (Akagawa et al., 1999). Both unburned HC

and CO were observed to be unaffected by intake temperature (Lu et al., 2005). Experiments conducted on a HSDI diesel engine revealed that peak soot luminosity were markedly reduced when intake temperature decreased from 110°C to 30°C under a load condition of 3 bar IMEP (Choi et al., 2005). This was attributed to both lower soot temperatures and reduced soot formation. Nonetheless, in-cylinder soot luminosity was clearly observed even at 30°C which indicated that complete eradication of soot formation was difficult with typical fuel injection system parameters.

2.4.2 Intake Pressure

Turbocharging is used in HCCI operation to extend the operating load range (Christensen et al., 2000; Christensen et al., 1998a; Hyvönen et al., 2003). This is particularly relevant in HCCI operations whereby reasonably high EGR rates are typically employed to control combustion and limit NO_x formation. The resulting dilution limits the amount of fuel that can be added for a fixed charge mass leading to a loss in engine power. To counter this for a given engine size, more mass needs to be forced through the engine through turbocharging. By supercharging to 86 kPa and increasing the fuel quantity at a lowered compression ratio of 12.5, the power output could be increased to nearly the full load of conventional, naturally aspirated diesel combustion. Similarly, in the premixed compression ignition combustion system, a boost pressure of 80 kPa produced an output which was comparable to that of the full load of conventional, naturally aspirated diesel combustion (Iwabuchi et al., 1999). Tests with n-heptane in a Cooperative Fuels Research engine operated in HCCI mode showed that raising the intake pressure from approximately 117.5 kPa to 152.5 kPa resulted in a directly proportional increase in IMEP when all influential parameters such as compression ratio, intake charge temperature, EGR rate and equivalence ratio were kept constant (Hosseini et al., 2007). In another study, turbocharging on a six-cylinder diesel engine achieved high loads of up to 16 bar BMEP with ultra-low specific NO_x emissions (0.1 g/kW-hr) (Olsson et al., 2001). This compares to 21 bar BMEP for the same engine under standard diesel operation. Evaluation of boosting strategies for HCCI applications have been carried out by Olsson et al. (2004). The dilution required to limit NO_x necessitates the use of much more boost compared to conventional engines for the same load. When high boost is required, turbocharger efficiency was presented to be very important for HCCI in order to reduce pumping losses. For high load

applications, two stages turbocharging with inter-cooling is recommended. Better control of the turbocharger such as using variable geometry turbocharger avoids unnecessary pumping work through 'over boost'.

2.4.3 Compression Ratio

By lowering the compression ratio, ignition delay is prolonged which allows complete injection of all fuels prior to ignition, a prerequisite for premixed combustion and a reduction in the gas temperature of the combustion field at TDC of the compression stroke (Gan et al., 2011). Reducing compression ratio from 18:1 to 16:1 was part of the strategy used in the second generation of modulated kinetics diesel engines to extend low temperature, premixed combustion to higher load conditions (Raheman et al., 2004). It has been demonstrated by Olsson et al. (2002a) that knock in HCCI diesel combustion can be prevented by reducing the compression ratio. When compression ratio is reduced, the accompanying reduction in temperature rise of the end gas prevents explosive self-ignition from occurring. Peng et al. (2005) conducted experiments on a four-stroke, single cylinder, variable compression ratio engine using n-heptane which verified the effects of compression ratio on HCCI combustion. The results showed that the possibility of knocking decreased, with the knock limit pulled to lower air fuel ratio region (richer mixture) when compression ratio was reduced from 18:1 to 12:1. The maximum IMEP attainable on this engine thus increased from 2.7 bar to 3.5 bar. Experiments carried out on a PCCI engine demonstrated that under premixed combustion, NO_x emissions were only mildly reduced when compression ratio was reduced from 18.4:1 to 16.0:1 within the SOI timing range of 5°BTDC to 3°ATDC (Laguitton et al., 2007). Soot emissions, unlike NO_x , were reduced more markedly when compression ratio reduced. The reductions in NO_x and soot emissions can be explained by the retardation in ignition delay which leads to a reduction in the gas temperature at TDC of the compression stroke and more complete mixing of air and fuel mixture.

2.5 Effects of Fuels and Additives

2.5.1 Effects of Fuels

Because of the restriction brought on by the combustion mode and engine set-up, conventional IC engines must utilize particular fuels. For spark-ignition engines, gasoline is more appropriate due to having good volatility and anti-knock characteristics. On the other hand, for CI engines, diesel is more appropriate due to having higher viscosity and lower resistance to auto-ignition (Valentino et al., 2012). Nonetheless, the HCCI combustion methodology can accommodate an assortment of fuel types as long as the fuel can be vaporized and mixed with air before ignition (Aceves et al., 2004). Since ignition happens in an HCCI engine through auto-ignition of the air–fuel mixture, the selection of fuel will have a huge effect on both the engine outline and the control procedures. Both fuel volatility and auto-ignition qualities are essential. Different fuels have different auto-ignition points. Figure 2.1 shows the intake temperature required for different fuels to auto-ignite at different compression ratios while operating in HCCI mode.

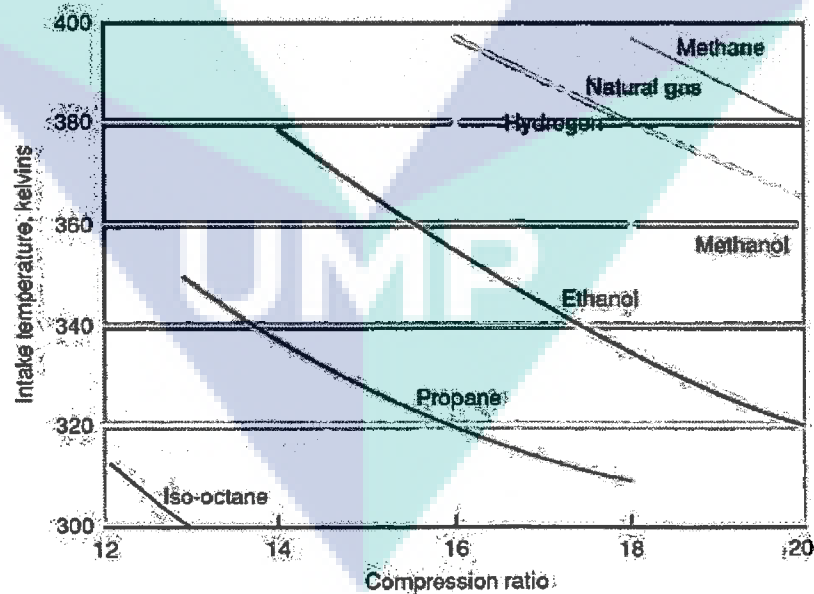


Figure 2.1 Intake temperature required for fuels to operate under HCCI mode with varying compression ratios

Source: Aceves et al. (2004)

It is seemingly singular digress that the auto-ignition point decreases when the amid of carbon atoms in the HC increases. According to Epping et al. (2002), to form a homogeneous charge easily the fuel must have a high volatility property. Chemically, fuels which have single-stage ignition react less with the change in load and speed. This helps the HCCI engine to run over a wide range of operating conditions. Christensen et al. (1999a) concentrated on the relationship between the fuel's octane number, the inlet air temperature and the compression ratio expected to get auto-ignition near to TDC by blending iso-octane with octane number 100 and n-heptane with octane number 0. The test outcomes demonstrate that any fluid fuel can be utilized as a part of an HCCI engine utilizing a variable compression ratio. Diesel fuel auto-ignites more readily than gasoline. However, the non-premixed diesel engine is becoming a less suitable power production device due to the high NO_x and soot emissions. Due to these challenges faced by the traditional diesel engine, diesel HCCI combustion gained lot of attention in the 1990s. Three different approaches were followed to achieve HCCI combustion with diesel fuel: premixed HCCI, early direct-injection HCCI, and late direct-injection HCCI. Ryan and Callahan (1996), followed by Gray and Ryan (1997), used the premixed HCCI approach in a single-cylinder, four-stroke, variable compression ratio engine. Fuel injectors introduced diesel fuel into the intake air stream and the mixture temperature was increased using an intake air heater. Compression ratio variation along with exhaust gas recirculation (EGR) was used to achieve HCCI. The study highlighted three issues with premixed diesel HCCI. First, premature ignition and knocking occurred if diesel compression ratios were used. Second, high intake temperatures were required to avoid the accumulation of liquid fuel on the surfaces of the intake system. Third, reduced combustion efficiency resulted in high HC emissions relative to traditional diesel operation. Several others (Christensen et al., 1999a; Kaneko et al., 2002; Kelly-Zion et al., 2000; Suzuki et al., 1997) worked with premixed diesel HCCI and their results indicate that substantial reductions of NO_x and soot emissions were achieved using this approach. However, it was also clear from these publications that premixed diesel HCCI is not the best strategy for diesel-fuelled HCCI and alternative fuel-delivery or mixing techniques have to be developed. Early direct-injection (i.e. direct fuel injection well before TDC) is a favored diesel HCCI technique for two reasons. First, easy vaporization and better mixing is achieved when fuel is injected in hot compressed air during the compression stroke. Second, with an appropriately designed injector, fuel wall wetting can be minimized, which increases the

combustion efficiency and reduces emissions. Several publications (Nakagome et al., 1997; Takeda et al., 1996; Walter et al., 2002; Yokota et al., 1997) reported using early direct injection to achieve diesel HCCI. Nissan Motor Company developed a process called modulated Kinetics that falls in the regime of late direct-injection diesel HCCI. The principles of this process were described by Mase et al. (1998) and Kimura et al. (1999). For this process, a long ignition delay period and rapid mixing was required, which assures premixed combustion and hence low smoke. Large amounts of EGR reduced the combustion temperature, resulting in low NO_x. The ignition delay was also extended by increased EGR and retarded injection (near the top dead center, TDC). Rapid mixing was achieved by combining high swirl with improved combustion-bowl geometry. The modulated Kinetics process achieved low emissions with appropriate combustion control.

Gasoline has a lower boiling point and higher octane number. For this reason, using gasoline fuel in HCCI engines is the reason for early combustion, which limits the operating range of HCCI engines (Zhao, 2003). Ultimately, high combustion pressure and knock are created (Zhao, 2003). To solve these two major problems, delayed combustion is necessary. Several approaches have been used by many researchers (He et al., 2013; He et al., 2014b; Yeom et al., 2007). Yeom et al. (2007) used LPG with gasoline. LPG has a higher octane number than gasoline and it has a high latent heat of vaporization, which can bring down the compression pressure and temperature (Iida et al., 2000). In addition, LPG contains fewer carbon atoms than gasoline or diesel, and thus CO₂ can be diminished by using LPG as part of the fuel mix in the engines (Campbell et al., 2004). Some scientists (Cedrone et al., 2011; He et al., 2013; He et al., 2014a, 2014b) blended n-butanol with gasoline to solve these problems. They observed that the onset of the auto-ignition occurs earlier and combustion duration becomes shorter when an increasing amount of n-butanol is used in place of gasoline.

Other fuels besides gasoline and diesel are also used for HCCI engines. Since natural gas is the second most abundant fuel, many researchers have studied the feasibility of using natural gas (Christensen et al., 1997; Flowers et al., 2001a; Hiltner et al., 2000; Olsson et al., 2002b; Stanglmaier et al., 2001) as a fuel in HCCI engines. Due to the high octane rating of natural gas (of the order of methane, which has an octane rating of 107), high compression ratio (Christensen et al., 1999a), high intake

temperatures or additives promoting auto-ignition like NO_x (Ricklin et al., 2002) and dimethyl ether (Chen et al., 2000) are required in natural-gas-fuelled HCCI engines. Performance aspects of propane-fuelled HCCI engines are discussed in (Au et al., 2001; Flowers et al., 2001b). Alcohols (Iida, 1994; Oakley et al., 2001) exhibit good auto-ignition properties and hence are excellent HCCI fuels, with a significantly larger operating range than most other fuels. Hydrogen is also studied as an alternative HCCI fuel (Shudo et al., 2002). In addition to the above-mentioned neat fuels, many fuel blends and additives like dimethyl ether, diethyl ether, dimethoxy methane or di-tertiary butyl peroxide (Eng et al., 2003) can be used in HCCI combustion.

2.5.2 Effects of Additives

Some chemical segments can advance the heat release process of auto-ignition. Along these lines, HCCI auto-ignition can be controlled by altering the fuel with the goal of making it more chemically responsive or inhibitive by including an ignition promoter or inhibitor. Christensen et al. (1999a) and Iida et al. (2001) injected water into the fuel and observed a lower initial gas temperature. It was presumed that water injection can control the ignition timing and combustion duration. Verhelst et al. (2009) studied HCCI combustion using a hydrogen-enriched natural gas mixture. It was observed that hydrogen expansion in a natural gas mixture has the capacity to build in-cylinder peak pressure, reduce ignition delay time and ignition temperature, and expand indicated power (Raitanapaibule et al., 2005). It additionally permits the augmentation of the lean limit of the natural gas mixture, without entering the lean misfire region, while accomplishing amazingly low emissions (Verhelst et al., 2009). Hydrogen expansion in ultra-low sulfur diesel advances incompletely premixed compression ignition and results in better performance and decreased emissions (Tsolakis et al., 2005). Szwaja and Grab-Logarinski (2009) considered hydrogen expansion (in HCCI mode) with diesel in a CI engine and found that the expansion of hydrogen in small amounts (e.g. about 5% in energy ratio) was able to diminish the ignition delay and enhance engine performance. They likewise reasoned that the expansion of hydrogen to diesel ought not to be more than 15% in energy ratio, to avoid extreme knock. (Shahbakhti et al., 2008) utilized a heptane/iso-octane mixture in an HCCI engine and found that this mixture is not suitable to control the ignition timing, but at low temperature the thermal efficiency was quite similar to that of a CI engine. Furthermore,

formaldehyde-doped lean butane/air mixtures (Christensen et al., 1998b) exhibited ignition timing retardation and a decrease in combustion efficiency.

2.6 Numerical Study of HCCI Engines

In order to apply the actuators and sensors to a closed-loop HCCI combustion timing control system, it is useful to have a model for control analysis and synthesis. Modeling has been a focus of HCCI engine research for some time. Most of the models are based on chemical kinetics and not suitable for control analysis or synthesis. Zhao (2003) provided an extensive summary of these models and categorize them into zero-dimensional single-zone thermo-kinetic models, quasi-dimensional models that include some geometric effects and computational fluid dynamic based multi-zone models. These types of models are complex and usually focus on producing a single cycle of data. For control analysis and synthesis, a model capable of quickly simulating seconds or even minutes worth of data is desirable.

2.6.1 Chemical Kinetics

In a CI engine, the fuel is direct-injected in the chamber with a high injection pressure when the piston is nearly at TDC. Then, the fuel ignites rapidly in the hot air environment. In SI engines, the spark plug is triggered when the piston is approximately at TDC to initiate the combustion. HCCI engines, on the other hand, have no mechanism to control the ignition timing and rely solely on chemical kinetics for combustion. The combustion in an HCCI engine is triggered when the heat in the chamber has reached the fuel activation energy. To numerically investigate the combustion behavior, chemical kinetic mechanisms which represent the actual fuels have been developed (Curran et al., 1998; Lee et al., 2010; Mehl et al., 2011b).

It is common to use n-heptane as a surrogate fuel for diesel (Guo et al., 2010; Hernandez et al., 2008; Pitz et al., 2011; Westbrook et al., 2006) because the chemical properties between those two are very similar, particularly in terms of cetane number. The intake temperature when n-heptane is used as a fuel in an HCCI engine is not as high as methane or natural gas. A study by Guo et al. (2010) showed that n-heptane can easily be ignited when the inlet temperature is 313K on a low CR engine (CR=10).

Methane, on the other hand, is reported to have no ignition when the inlet temperature is less than 400K on a high CR engine (CR=15) (Fiveland et al., 2000). Thus, it is important to have the right fuel and its chemical kinetic mechanism in order to study the combustion behavior of an HCCI engine. Curran et al. (1998) developed a detailed mechanism for n-heptane and validated the result over a wide range of operating conditions. They found that the ignition delay is in very good agreement with experiments using flow reactors, shock tubes and rapid compression machines. Seiser et al. (2000) and Ogink et al. (2002) developed a reduced mechanism for n-heptane because a detailed mechanism uses more computational resources. Patel et al. (2004) reduced the mechanism by more to obtain 26 species and 52 reactions. The author reported that the CPU time is reduced by 50-70% and the validation was completed under both constant-volume reactor and HCCI engine conditions. The ignition delay result is similar to those of detailed mechanisms. The use of n-heptane as the only main component in the mechanism is not sufficient to predict the soot emission from CI and HCCI engines. Thus, Wang et al. (2013) improved the mechanism by blending the n-heptane and toluene mechanisms. They reported that the mechanism gives reliable soot predictions and combustion phasing under various engine conditions.

An iso-octane mechanism was used as a surrogate fuel for gasoline and it can also be blended with n-heptane to represent a real fuel (Curran et al., 2002; Tanaka et al., 2003). A real gasoline fuel consists of thousands of HC compounds (Ogink et al., 2001; Zheng et al., 2002) and the fuel should be modeled using a combination of a few components. Mehl et al. (2011b) developed a mechanism that represents a commercial grade gasoline, which consists of n-heptane, iso-octane, toluene and olefins. They reported that the result is in good agreement over a wide range of pressures and temperatures relevant to IC engine applications. A reduced mechanism was also developed by Mehl et al. (2011a) and further reduced by (Kwon et al., 2011). A reduced mechanism shows an advantage when used in a complex CFD model, which requires more computational resources (Lee et al., 2010).

2.6.2 Single Zone Model

A single-zone model is where the combustion chamber area is treated as one homogeneous block. The single-zone model has some limitations due to the assumption

that the whole combustion chamber is treated as homogeneous (Fiveland et al., 2001). Peak cylinder pressure and rate of pressure rise can be over-predicted. It also predicts a short burn duration and cannot accurately predict CO and HC emissions, which primarily depend on crevices (Su, 2010). Crevices and the boundary layer are the cold areas for HC and CO to react during combustion. The earliest example of this type of model was developed by Najt et al. (1983) to help analyze experimental work on a premixed-charge, compression-ignited CFR engine. Their model employed the Shell ignition model and an empirical Arrhenius single step combustion model. By fitting the model constants to a wide range of engine combustion rate data, the authors were able to suggest that the combustion process was dominated by kinetics, a view that is widely accepted today. Recent examples of zero-dimensional models use more sophisticated and detailed chemical kinetics (Aceves et al., 2001b; and Dec, 2002). In general, these models have been successful in exploring the effects of fuel composition, compression ratio, air-fuel ratio, EGR rates and other operating parameters, as well as the lean limits of HCCI operation. Ogink et al. (2001) have combined the single zone approach with existing zero-dimensional engine models to provide accurate estimates of the effects of the gas exchange process and have used the resulting simulations to evaluate unconventional engine concepts or variable valve timing strategies. Fiveland et al. (2000) proposed a full cycle, thermo-kinetic single zone model. The fresh charge was assumed to be perfectly homogeneous, with fluid mechanics assumed to have no impact on combustion phasing and rate besides their effect through cylinder wall heat transfer. Detailed chemical kinetics mechanisms for natural gas were applied to predict the ignition timing and HRR. Their model contributed to understanding how mixture preparation and in-cylinder thermodynamics conditions affect ignition timing, as well as engine performance. While the zero-dimensional, single zone, thermo-kinetic models have presented the ability to yield satisfactory accuracy against measurements of engine performance, they suffer significant shortcomings in predicting the rate of heat release, combustion completeness, and emissions, largely due to the simplifying assumption of strict homogeneity throughout the combustion chamber. Inaccurate estimates of residual temperature and species composition critically affect predictions of subsequent cycles, temperature and species composition critically affect predictions of subsequent cycles, thus limiting the ability of the simulation to track transients. Thus, this type of model cannot be directly used as a control and design tool, despite its computational

efficiency. The potential problem of this type of model is to expand the engine operating range into unrealistic region.

2.6.3 Multi Zone Models

A multi-zone model separates the combustion chamber into several zones and the zone distribution depends on the type of the engine, either based upon flame propagation or homogeneous mixtures, thereby representing the inhomogeneity in the cylinder prior to combustion (Yao et al., 2009). Multi-zone modeling of HCCI engines is organized in such a way because the heat generated in an HCCI engine comes from the core of the combustion chamber. This is different to SI engines where the zone is started from the spark plug (the location of the heat source), and propagated according to the flame front motion. The multi-zone model predicts the pressure trace and the peak cylinder pressure very well, but it also cannot consider boundary layer effect and crevices and thus cannot predict CO and HC emissions (Aceves et al., 2000). Szybist et al. (2013) explored the effect of temperature stratification by modeling multiple zones with different temperatures imposed parametrically in an otherwise zero dimensional model. Ogink et al. (2002) used a similar approach, but introduced an empirical temperature distribution among the zones to better match the experimental energy release data. A comprehensive quasi-dimensional model was proposed by Fiveland et al. (2002) with the intent to bridge the gap between zero-dimensional and sequential fluid mechanic–thermo kinetic models. This model is based on a full-cycle simulation code and includes an adiabatic core, a predictive boundary layer model and a crevice flow model. The thermal boundary layer is driven by compressible energy considerations, and hence is of varying thickness, and is solved at multiple geometric locations along the piston-liner interface. A full dynamic ring pack model is used to compute the crevice flows. The model provided good agreement with experimental performance data for a natural gas fueled engine, and gave reasonably good agreement for unburned HCs. CO predictions were less satisfactory due to lack of detailed thermal resolution in the near wall regime. The key limitation of multi-zone, quasi-dimensional models is their inability to predicatively describe stratification or in-homogeneities in residual fraction that are likely to exist in practical applications, especially in direct injection systems. With suitable calibration, the quasi-dimensional models have shown that they can include key geometric effects without excessive computational times. As

such, they show promise as a rapid computational tool which can be used as the basis of practical in-vehicle system simulations.

2.7 Summary

This chapter has developed pertinent background information relevant to the experiments, numerical modeling, and discussion that follows in following chapters. A literature search on HCCI engine research was presented in order to show the progression of the field and how this study fits into the overall picture. This is by no means a comprehensive list of all research activity but a good starting point when discussing the subjects addressed in later sections. Many studies show that HCCI engine has low NO_x emissions, soot and particulates. The HCCI engine can achieve a higher or similar BTE compared to CI engines by using a high CR engine configuration. One of the advantages of the HCCI engine is that it does not suffer from throttling losses, which also improves the BTE. A higher BTE helps in reducing the fuel consumption of the engine and it might be able to match the fuel consumption of a hybrid engine. Engine parameters like intake temperature and pressure, compression ratio etc. as well as fuels and blends of fuels have great significance to achieve successful HCCI operation. However, HCCI engines still have unsolved issues, which are ignition control, knocking and high levels of unburned HC and CO emissions. Further studies have to be performed in order to solve these remaining issues. To achieve this, the numerical method shows a great advantage over experiments to simulate the combustion behavior in terms of cost and time. To this end, a simulation model has to be developed to investigate the behavior and, once completed; it has to be validated against experiments. In this thesis, zero-dimensional single model was chosen for modeling a HCCI engine. A zero-dimensional model requires less computational time compared to multi-dimensional model. Thus, a zero-dimensional simulation would be an interim solution until the cost and time of running a multi-dimensional model is comparable with the current cost of the zero-dimensional model. The use of chemical kinetics mechanisms also helps in investigating the combustion behavior of an HCCI engine. The details of the modeling will be discussed in Chapter 3.

CHAPTER 3

NUMERICAL MODELING

3.1 Introduction

Modeling combustion engines using computer codes is an important investigative technique. There are a number of different factors to be considered when developing a numerical model - chemistry, heat transfer, mechanical behavior, and fluid dynamics to name a few. In this study, a zero-dimensional single zone model for HCCI engine was established using MATLAB. The model is called zero-dimensional model because time is the only independent variable used in this model. The proposed method takes into account the detailed thermodynamic aspects of engine. The model integrates the ordinary differential equation system corresponding to the chemical and thermal evolution of a closed homogeneous system under an imposed volume history reproducing the engine cycle. This single-zone in time model treats the cylindrical combustion chamber as a uniform reactor with uniform temperature, pressure, and composition throughout. The reactor volume changes based on slider-crank relations that determine the motion of the piston in the engine cylinder. This kind of model aims to simulate the auto-ignition process in the core of the air-fuel mixture and enables the use of detailed chemical kinetic models with which we can investigate the chemical reactions contributing to cylinder inside pressure and temperature. The accumulated gas is assumed to be ideal gas. The models used two different types of chemical reaction mechanisms to model the fuels because two types of engine configurations were used. This is to ensure that the model works in both engine conditions. This Chapter will describe chemical kinetics mechanisms for diesel, gasoline and other test fuels first as well as emissions formation. Then the equations used in zero-dimensional single zone modeling will be presented in detail. To understand how the numerical code works an algorithm flow chart will be presented. Combustion and performance parameters will be

described in brief. At the end of the Chapter chemical properties of the test fuels will be presented.

3.2 Chemical Kinetics Mechanisms

A combustion event involves an extraordinary amount of elementary chemical reactions. Each reaction has a designated pre-exponential term (A , $\text{l/cm}^3\text{mol}^{-1}\text{sec}^{-1}$), temperature dependent exponent (b , no units), and activation energy (E_A , in kJ/mol) which are used to describe the reaction rate coefficient (k) according to Eq. (3.1).

$$k = AT^b \exp\left(\frac{-E_A}{RT}\right) \quad (3.1)$$

The development of chemical mechanisms for numerical modeling is an ongoing research. The researchers are testing, refining, and updating the values. Validation through comparisons with experimental results from shock tube and rapid compression machine experiments is one of the appropriate approaches. These mechanisms which can include on the order of 1000's of species (in the case of diesel fuel, for example) can quickly become cumbersome when running complex models. Therefore, another approach in the development of chemical mechanisms focuses on coming up with smaller mechanisms which still provide a desired degree of accuracy. This is done by constraining the conditions considered in the validation steps so that certain intermediate species and reactions can be ignored. These smaller mechanisms are often called skeletal or reduced mechanisms, with reduced mechanisms being the most drastically constrained and application-specific.

3.2.1 Diesel Mechanism

A chemical reaction mechanism is used to solve the chemical reactions during combustion. For diesel fuelled HCCI engines, a reduced diesel fuel surrogate mechanism (Pei et al., 2015) was used to simulate the diesel combustion. Pei and his co-workers assembled a kinetic mechanism describing the oxidation of n-dodecane/m-xylene mixture based on recently published kinetic mechanisms developed by the Lawrence Livermore National Laboratory. The detailed multi-component mechanism

for n-dodecane and m-xylene was developed by combining the previously developed n-dodecane mechanism (Sarathy et al., 2011) with a recently developed mechanism detailing the combustion of the xylene isomers (Pei et al., 2015). The two parent mechanisms were individually validated against an extensive set of experimental data for both fuels, including ignition delay time, speciation and laminar flame speed data. The detailed mechanisms, containing 2885 species and 11754 reactions, has been reduced using a combination of directed relation graph with expert knowledge (Lu et al., 2011a) and directed relation graph aided sensitivity analysis algorithms coupled with isomer lumping. The resulting mechanism, including 163 species and 887 reactions, has been successfully applied to the simulation of 3D diesel-like spray combustion using a commercially available CFD code. This reduced mechanism for diesel surrogate was used in this study.

3.2.2 Gasoline Mechanism

In this study a 4-component surrogate was used to model gasoline fuel. This surrogate was developed by Mehl et al. (2011a) at Lawrence Livermore National Laboratory. The surrogate is comprised of isooctane, *n*-heptane, toluene and 2-pentene, and the relative proportion of each component by mass fraction is given in Table 3.1.

Table 3.1 Gasoline surrogate composition

Component	Mass fraction
iso-octane	0.5413
<i>n</i> -heptane	0.1488
Toluene	0.2738
2-pentene	0.0361

In order to determine the composition of the surrogate, Mehl and coworkers used both composition of real gasoline (in terms of aromatics, olefins, alkanes and average molecular weight) as well as reactivity of gasoline (autoignition properties) to formulate a surrogate having a similar overall representation of various kinds of HCs and having similar $(RON + MON)/2$ as gasoline where RON stands for Research Octane Number and MON stands for Motor Octane Number. The choice of isooctane, *n*-heptane and toluene has been attributed to historical reasons, since they fit well within

the molecular weight range of interest, and have been traditionally well understood within the combustion community. The addition of 2-pentene to represent olefins has been attributed to this molecule matching the typical molecular weight of olefins found in gasoline, and also because it has the highest octane number and sensitivity.

A detailed chemical kinetic mechanism for this surrogate was developed by Mehl et al. (2011b), which consists of roughly 1400 species and 5000 reactions. This mechanism was validated against gasoline shock tube data over a range of temperatures and pressures. However, it is computationally infeasible to incorporate such a large mechanism within a 3-D CFD simulation; hence the same group (Mehl et al., 2011a) also developed a reduced 312-species, 1488-reaction chemical kinetic mechanism based on the detailed mechanism, intended for 3-D CFD simulation of HCCI engines. This model was validated against HCCI engine experiments by Mehl et al. (2012) over a range of intake pressure and load conditions, and was found to capture features such as intermediate temperature heat release (Dec et al., 2010) which are thought to be unique to gasoline fuel chemistry at higher pressures near TDC. This 312-species mechanism along with the 4-component gasoline surrogate was used in this study.

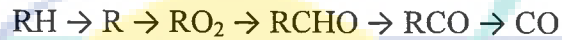
3.2.3 Mechanisms for Different Fuels and Blends of Fuels

A reduced *n*-heptane mechanism (Seiser et al., 2000) was used to simulate *n*-heptane fuel in the HCCI combustion. The mechanism consists of 159 species and 770 elementary reactions. For *n*-heptane/ethanol blend fuel a reduced ethanol mechanism was combined with the *n*-heptane mechanism (Dagaut et al., 2010). The final mechanism consists of 167 species and 1591 elementary reactions. In addition, for *n*-heptane/butanol blend fuel a reduced *n*-butanol mechanism was combined with the *n*-heptane mechanism (Dagaut et al., 2009). The final mechanism consists of 181 species and 1703 elementary reactions.

3.2.4 Mechanism of Emissions Formation

Exhaust emissions consist mainly of direct combustion products, such as water and CO₂, and pollutants such as CO, unburned HC and NO_x (which refers to the combination of NO and NO₂). The CO and unburned HC pollutants are a consequence

of incomplete combustion. With rich air-fuel mixtures there is not enough oxygen to ensure oxidation of the carbon in the fuel to CO₂, also the CO oxidation also freeze with the drop in temperature during the expansion stroke. To improve drivability during cold starts, the fuel flow is increased to compensate for slow fuel vaporization. However, this strategy leads to an increase in CO emissions as well as UHC. The CO formation can be summarized in the following reaction,



where R is the HC radical. The CO formed is then oxidized to CO₂ at a slower rate via the principal oxidation reaction,

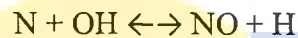
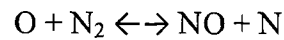


There are several ways leading into the formation of unburned HCs. Due to the increasing cylinder pressure forces during the compression stroke part of the air-fuel mixture is trapped into the crevices, this mixture will not be exposed to the high temperatures and it will remain unburned. These unburned gases will then leave the crevices during exhaust stroke. Other sources of formation of unburned HC are the cold cylinder walls that lead to flame termination before the completion of the oxidation reactions. Engine oil left in thin films on the cylinder wall and piston can absorb and desorb HCs before and after combustion, contributing as well to the formation of unburned HC.

The formation of NO_x is a complex process that involves the reactive combination of nitrogen found within the combustion air and organically bound nitrogen within the fuel itself. NO_x is a thermally produced gas and therefore its formation is largely dependent on the control of the combustion temperature. There are many other mechanisms from which NO_x can be produced, but thermal and prompt NO are the more relevant in the IC engines application (Amnéus et al., 2005; Golub et al., 1999; Miller et al., 1989; Miller et al., 2005).

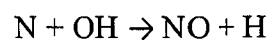
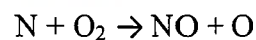
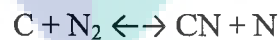
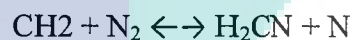
In the combustion of clean fuels (fuels not containing nitrogen compounds), oxidation of atmospheric nitrogen by the thermal mechanism is a major source of NO_x

emissions. The three principal reactions that comprise the thermal NO formation mechanism are,



The first two reactions compose a chain sequence in which a small amount of atomic oxygen can produce large amounts of NO. This mechanism, often called the Zeldovich mechanism, is very sensitive to temperature not only because the high activation energy of the first reaction, but also because the concentration of oxygen atoms in flames increases rapidly with increasing temperature (Amnéus et al., 2005; Golub et al., 1999; Miller et al., 1989; Miller et al., 2005).

Nitric oxide formation rates in combustion of HC fuels can exceed those attributable to the thermal mechanism discussed above, especially for fuel-rich conditions. This rapidly formed NO was termed prompt NO, since it's rapid and is confined to regions near the flame zone.



It has been shown that, prompt NO in HC flames is formed primarily by a reaction sequence of HC radicals with molecular nitrogen, leading to formation of amines or cyano compounds that subsequently react to form NO. Numerous studies showed that CH and CH₂ are the HC radicals that most contribute to the formation of prompt NO (Amnéus et al., 2005; Golub et al., 1999; Miller et al., 1989; Miller et al., 2005).

Table 3.2 NO_x kinetic mechanism reaction rates parameters for *A*, *b*, and *E_A*

S/L	Reaction (cm ³ – mol – sec – cal – k)	<i>A</i>	<i>b</i>	<i>E_A</i>
1	NO+O(+M)=NO ₂ (+M)	3x10 ¹³	0.00	0.0x10 ⁰
2	NO+H(+M)=HNO(+M)	1.52x10 ¹⁵	-0.41	0.0x10 ⁰
3	NO+OH(+M)=HONO(+M)	1.1x10 ¹⁴	-0.30	0.0x10 ⁰
4	NO ₂ +H ₂ =HONO+H	0.733 x10 ¹²	0.0x10 ⁰	2.881x10 ⁴
5	NO ₂ +O=O ₂ +NO	1.05x10 ¹⁴	-0.52	0.0x10 ⁰
6	NO ₂ +O(+M)=NO ₃ (+M)	1.33x10 ¹³	0.00	0.0x10 ⁰
7	NO ₂ +H=NO+OH	1.32x10 ¹⁴	0.00	3.62x10 ²
8	HO ₂ +NO=NO ₂ +OH	2.11x10 ¹²	0.00	-4.790x10 ²
9	NO ₂ +NO ₂ =NO ₃ +NO	9.64x10 ⁰⁹	0.73	2.092x10 ⁴
10	NO ₂ +NO ₂ = ₂ NO+O ₂	1.63x10 ¹²	0.00	2.612x10 ⁴
11	HNO+H=NO+H ₂	4.4x10 ¹¹	0.72	650.0
12	HNO+O=OH+NO	1.81x10 ¹³	0.00	0.0x10 ⁰
13	HNO+OH=H ₂ O+NO	1.3x10 ⁷	1.88	-956.0
14	HNO+NO=N ₂ O+OH	2x10 ¹²	0.00	26000.0
15	HNO+NO ₂ =HONO+NO	6.02x10 ¹¹	0.00	1.987x10 ³
16	HNO+HNO=H ₂ O+N ₂ O	8.51x10 ⁸	0.00	3.080x10 ³
17	HONO+O=OH+NO ₂	1.20x10 ¹³	0.00	5.961x10 ³
18	HONO+OH=H ₂ O+NO ₂	1.7x10 ¹²	0.00	-5.200x10 ²
19	N ₂ O(+M)=N ₂ +O(+M)	7.91x10 ¹⁰	0.00	56,024
20	N ₂ O+O=O ₂ +N ₂	1x10 ¹⁴	0.00	2.80x10 ⁴
21	N ₂ O+O=NO+NO	1x10 ¹⁴	0.00	2.80x10 ⁴
22	N ₂ O+H=N ₂ +OH (DUP)	2.53x10 ¹⁰	0.00	4.550x10 ³
23	N ₂ O+H=N ₂ +OH (DUP)	2.23x10 ¹⁴	0.00	1.675x10 ⁴
24	N ₂ O+OH=HO ₂ +N ₂	2.0x10 ¹²	0.00	40000.0
25	NO+N ₂ O=NO ₂ +N ₂	1.0x10 ¹⁴	0.00	50000.0
26	CH ₃ O ₂ +NO=CH ₃ O+NO ₂	2.53x10 ¹²	0.00	-358.00
27	CH ₃ +O ₂ (+M)=CH ₃ O ₂ (+M)	1.006x10 ⁸	1.630	0.00

In HCCI, combustion occurs through chemical oxidation, thus, the reached maximum temperature is determined by the energy content of the fuel/air/residuals mixture, giving lower maximum temperatures than comparable with SI or CI. While the Zeldovich mechanism (thermal NO) is adequate for calculating NO_x emissions in SI or CI engines, it is safe to say that it doesn't accurately predict these emissions on HCCI combustion. Studies on lean combustors showed that NO_x is largely formed through

N₂O paths. It appears believable that N₂O reaction pathways would play an important role for NO_x formation also for HCCI engines (Amnéus et al., 2005; Golub et al., 1999; Miller et al., 1989; Miller et al., 2005).

To predict the NO_x formation accurately, an NO_x mechanism prepared by Miller et al. (1989) was integrated with all the mechanisms. For this reason, 7 extra species were added. The species are NO, NO₂, NO₃, N₂O, HONO, HNO, and CH₃O₂. Ultimately, 27 reactions were added with all the mechanisms. The reaction rates for all the reactions were taken from Miller et al. (1989) and Mueller et al. (2000). For completeness, the added NO_x mechanism reaction rates are summarized in Table 3.2.

3.3 Engine Parameters

The engine movements are defined from the engine parameters, which have to be defined before employing the energy equation of the first law of thermodynamics in the zero-dimensional model. Figure 3.1 presents the geometry of the piston and crank mechanisms.

The crank radius (a) is defined as half the stroke length (L) which is expressed in Eq. (3.2).

$$a = \frac{L}{2} \quad (3.2)$$

The ratio of connecting rod length (l) to crank radius is given by Eq. (3.3).

$$R = \frac{l}{a} \quad (3.3)$$

The rotational speed of the engine is expressed by Eq. (3.4).

$$\omega = \frac{2\pi N}{60} \quad (3.4)$$

where N is the engine speed in rotations per minute (rpm).

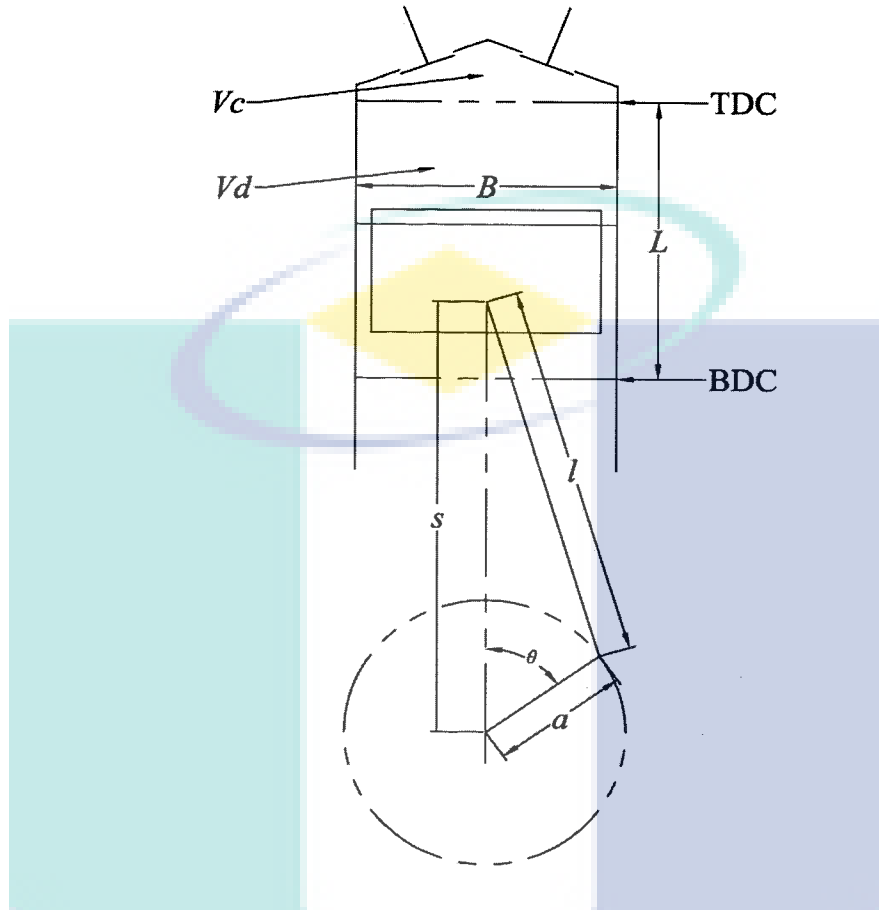


Figure 3.1 Engine geometry of the piston and crank mechanisms

Source: Heywood (1988)

For a flat piston crown, the area is given by Eq. (3.5).

$$A_p = \frac{\pi B^2}{4} \quad (3.5)$$

where B represents the bore diameter of the engine.

When the piston is at TDC, the clearance volume is defined as Eq. (3.6).

$$V_c = \frac{V_d}{(R_c - 1)} \quad (3.6)$$

where V_d is the displacement volume and R_c is the compression ratio, which are given as

$$V_d = A_p L \quad (3.7)$$

$$R_c = \frac{\text{maximum cylinder volume}}{\text{minimum cylinder volume}} = \frac{V_d + V_c}{V_c} \quad (3.8)$$

From these parameters, the instantaneous piston speed can be obtained from Eq. (3.9).

$$S_p = \frac{\pi}{2} \overline{S_p} \sin \theta \left(1 + \frac{\cos \theta}{\sqrt{R^2 - \sin^2 \theta}} \right) \quad (3.9)$$

where $\overline{S_p}$ is the mean piston speed.

The mean piston speed can be defined as Eq. (3.10).

$$\overline{S_p} = \frac{2LN}{60} \quad (3.10)$$

The instantaneous piston speed is zero at the beginning of the stroke and approaches its maximum at the middle of the stroke. It goes to zero again at the end of the stroke, as shown in Figure 3.2. The instantaneous cylinder volume at any crank angle location can be determined by Eq. (3.11).

$$V = V_c + A_p(l + a - s) \quad (3.11)$$

where s is the distance between crank axis and piston pin axis, which is given by Eq. (3.12).

$$s = a \cos \theta + \sqrt{(l^2 - a^2 \sin^2 \theta)} \quad (3.12)$$

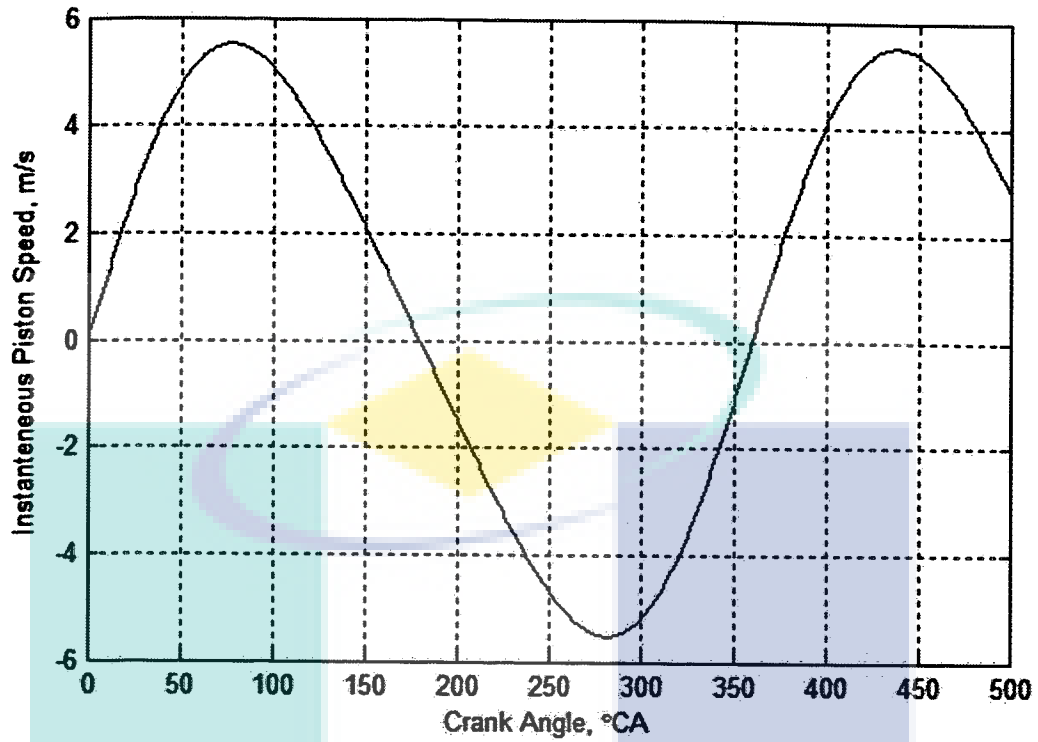


Figure 3.2 Instantaneous piston speed: zero at TDC and BDC, maximum at the middle of the stroke

After manipulation of Eqs. (3.11) and (3.12), the instantaneous cylinder volume is expressed as Eq. (3.13).

$$V = V_c \left[1 + \frac{R_c - 1}{2} \left(R + 1 - \cos \theta - \sqrt{R^2 - \sin^2 \theta} \right) \right] \quad (3.13)$$

The rate of change of volume can be expressed by Eq. (3.14).

$$\frac{dV}{d\theta} = V_c \left[\frac{R_c - 1}{2} (\sin \theta) \left(\frac{1 + \cos \theta}{\sqrt{R^2 - \sin^2 \theta}} \right) \right] \quad (3.14)$$

Cylinder volume is an important parameter because it determines the piston work in the energy equation.

3.4 Valve Geometry

Valve geometry is an important parameter to be considered because the mixing begins in the inlet manifold and it determines the mass flow rate to the combustion chamber. In engine configurations, the valve head is circular with a slightly different diameter between inlet and exhaust valves. Typical valve geometry for most engines is shown in Figure 3.3.

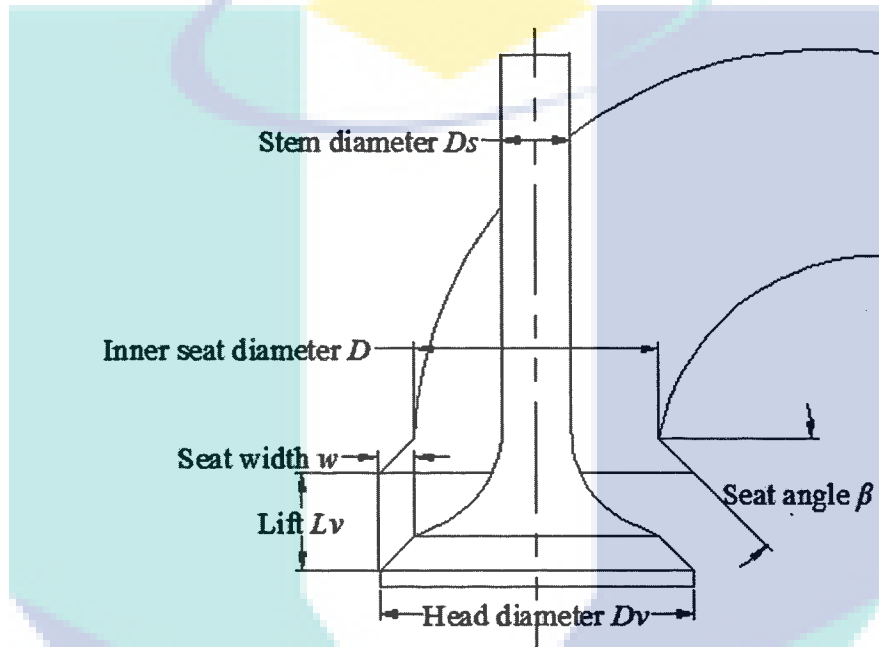


Figure 3.3 Valve geometry for most engines with parameters defining the valve

Source: Heywood (1988)

Based on Heywood's definition (Heywood, 1988) on valve configurations for most engines, the valve head diameter is taken as

$$D_v = 1.1D \quad (3.15)$$

where D is the inner seat diameter, as shown in Figure 3.3. Then, the valve seat width is

$$S_w = D_v - D \quad (3.16)$$

with the valve stem diameter defined as

$$D_s = 0.2D \quad (3.17)$$

In order to determine the mass flow rate of the mixture to the combustion chamber, the valve lift profile has to be defined. The valve lift profile is determined by using the desired maximum valve lift (L_v) and half-event angle (c). The half-event angle is defined as half of the total valve opening duration. The profile as a function of crank angle (Assanis et al., 1990) is then given by Eq. (3.18).

$$y = L_v + C_2 \theta^2 + C_w \theta^w + C_q \theta^q + C_r \theta^r + C_s \theta^s \quad (3.18)$$

where w , q , r and s are constants to match the desired valve lift curve, which are selected as $w = 6$, $q = 8$, $r = 10$ and $s = 12$.

$$C_2 = \frac{-wqrs L_v}{[(w-2)(q-2)(r-2)(s-2)c^2]} \quad (3.19)$$

$$C_w = \frac{-wqrs L_v}{[(w-2)(q-2)(r-2)(s-2)c^2]} \quad (3.20)$$

$$C_q = \frac{-2wrs L_v}{[(q-2)(q-w)(r-q)(s-q)c^q]} \quad (3.21)$$

$$C_r = \frac{-2wrs L_v}{[(r-2)(r-w)(r-q)(s-r)c^r]} \quad (3.22)$$

$$C_s = \frac{-2wqrs L_v}{[(s-2)(s-w)(s-q)(s-r)c^s]} \quad (3.23)$$

Using Eq. (3.18), a typical valve lift profile with tappet mechanism (mechanical lifters) is illustrated in Figure 3.4 (Heywood, 1988). Once the valve lift is known, the effective

valve open area can be obtained. In this case, the effective valve open area is taken as its curtain area, which is given by

$$A_c = \pi D_v L_v \quad (3.24)$$

Figure 3.4 presents a typical profile of valve lift for poppet valves with mechanical lifters. Generally, larger valve sizes (or more valves per cylinder) give higher maximum air flow in and out of the chamber.

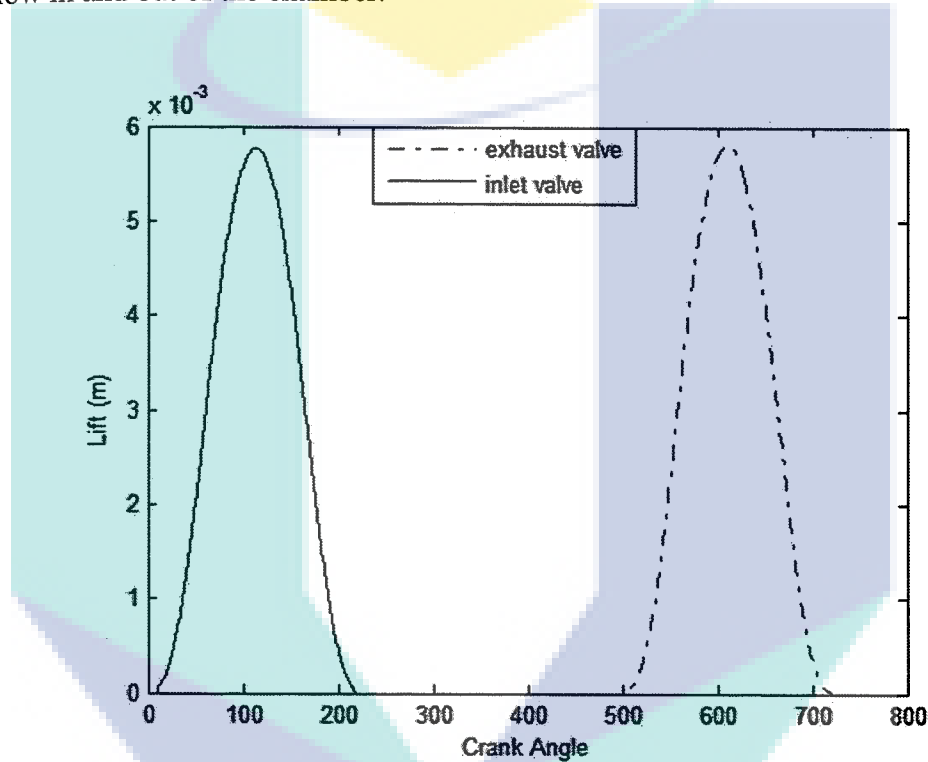


Figure 3.4 Valve lift profile for typical poppet valves with mechanical lifters

The mass flow rate to the combustion chamber can be obtained by using the equation of compressible flow through a flow restriction (Heywood, 1988). The equation includes the real gas flow effects with discharge coefficient C_d obtained from the experiments. In principle, the mass flows in or out of the combustion chamber when there is a pressure difference between the chamber and ports. The equation is separated into two cases: choked and subsonic flows. For choked flow, the following conditions are obeyed:

$$\frac{p_T}{p_0} \leq \left[\frac{2}{\gamma+1} \right]^{\frac{\gamma}{\gamma+1}}$$

$$\dot{m}_{in} = \frac{C_d A_c p_0}{\sqrt{R T_0}} \sqrt{\gamma} \left[\frac{2}{\gamma+1} \right]^{\frac{\gamma+1}{2(\gamma+1)}} \quad (3.25)$$

While for subsonic flow,

$$\frac{p_T}{p_0} > \left[\frac{2}{\gamma+1} \right]^{\frac{\gamma}{\gamma+1}}$$

$$\dot{m}_{in} = \frac{C_d A_c p_0}{\sqrt{R T_0}} \left(\frac{p_T}{p_0} \right)^{\frac{1}{\gamma}} \left[\frac{2\gamma}{\gamma-1} \left\{ 1 - \left(\frac{p_T}{p_0} \right)^{\frac{\gamma-1}{\gamma}} \right\} \right]^{\frac{1}{2}} \quad (3.26)$$

where p_T , p_0 , T_0 and γ are the downstream static pressure, upstream stagnation pressure, upstream stagnation temperature and ratio of specific heats, respectively. These Eqs., (3.25) and (3.26), are a function of gas properties, valve geometry and thermodynamics states upstream and downstream of the valves. For flow into the combustion chamber, p_0 is the intake port pressure and p_T is the cylinder pressure. On the other hand, p_0 is the cylinder pressure and p_T is the exhaust port pressure for the flow out of the combustion chamber. The value C_d is obtained experimentally from Stiesch (2013) and interpolated for the whole valve lift event as shown in Figure 3.5.

Once the mass flow rate was determined, it was used in the energy equation and also to obtain the total mass in the combustion chamber. The next section discusses the conservation equations which were used in the zero-dimensional model that is a simplified version of the multi-dimensional model.

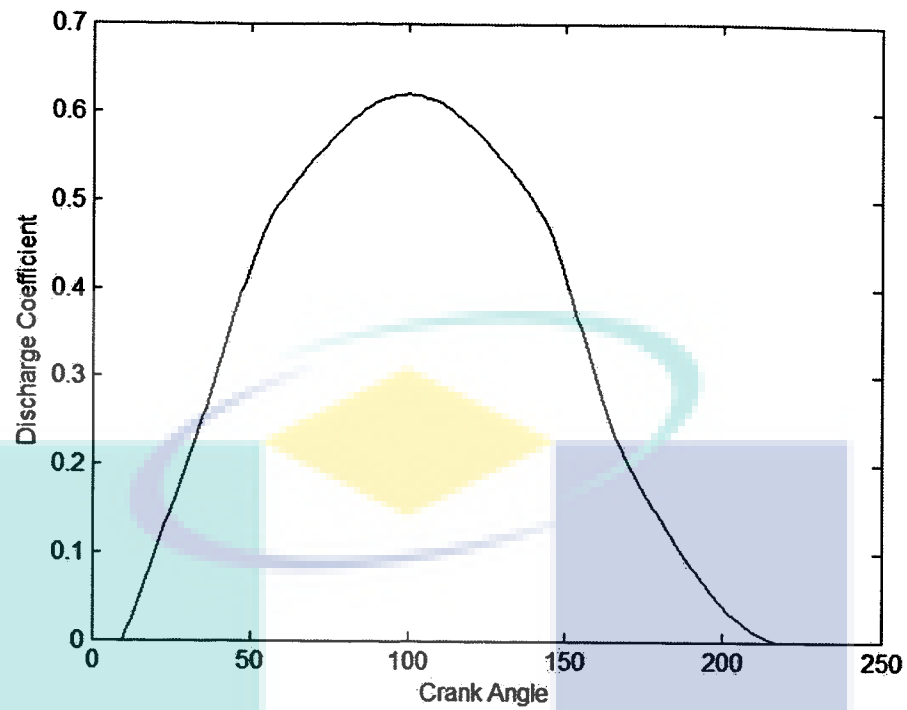


Figure 3.5 Discharge coefficient for one valve event

3.5 Combustion Process Model

3.5.1 Conservation of Mass

The combustion chamber is assumed to be the control volume of the system, where it has mass transfer in and out of the system through the intake and exhaust valves. Thus, the mass in the system is defined as Eq. (3.27) (Kuo, 1986)

$$\frac{dm}{dt} = \sum_j \dot{m}_j \quad (3.27)$$

where j is the number of flows in (\dot{m}_j positive) or out of the system and m is the total mass in the system.

3.5.2 Conservation of Species

Conservation of species is used to determine the evolution of species inside the combustion chamber due to the chemical reactions. The rate of change of the mass fraction of species i is given by Eq. (3.28) (Kuo, 1986)

$$\frac{dY_i}{dt} + \frac{(Y_i - Y_{in})}{\rho V} \dot{\rho} = \omega_i \quad (3.28)$$

where Y_{in} is the inlet mass fraction and ω_i is the mass reaction rate of the species i .

3.5.3 Conservation of Energy

The first law of thermodynamics equation in differential form is used to model the combustion in the single-zone model. The control volume of the combustion chamber is assumed to be an open thermodynamics system, by ignoring the changes in potential energy. The derivation of the first law of thermodynamics for engine simulations is described extensively by Assanis et al. (1986). In differential form, the first law of thermodynamics is expressed as Eq. (3.29).

$$\frac{dU}{dt} = \frac{dQ_h}{dt} - \frac{dW}{dt} + \sum_j \frac{dH_j}{dt} \quad (3.29)$$

where U is the internal energy, Q_h is the heat transfer, W is the work and H_j is the enthalpy of flows entering or leaving the system. By using the definition of each term, Eq. (3.29) then becomes Eq. (3.30).

$$\frac{d(mu)}{dt} = \frac{dQ_h}{dt} - \frac{pdV}{dt} + \sum_j \frac{h_j dm_j}{dt} \quad (3.30)$$

After manipulating Eq. (3.30), the final equation for the temperature change in the single-zone model is given by Eq. (3.31).

$$\frac{dT}{dt} = \frac{1}{C_A} \left[\sum_i \left[\left(\frac{pv R_i}{R} - h_i \right) \frac{dY_i}{dt} \right] - \frac{C_B}{m} \frac{dm}{dt} + \frac{1}{m} \left(\frac{dQ_h}{dt} - \frac{pdV}{dt} + \sum_j \dot{m}_j h_j \right) \right] \quad (3.31)$$

where Q_h is the heat transfer, W is the work and h_j is the enthalpy of flows entering and leaving the system as well as C_A and C_B are defined as

$$C_A = \overline{c_p} - \frac{\rho v}{T} \quad (3.32)$$

$$C_B = h - \rho v \quad (3.33)$$

The derivation of Eq. (3.31) is given in Appendix A.

Once the temperature is obtained, the in-cylinder pressure is determined by using the ideal gas law

$$p = \frac{\rho R_u T}{\overline{W}_{mv}} \quad (3.34)$$

where R_u is the universal gas constant and \overline{W}_{mv} is the mean molecular weight of the mixture.

3.6 Heat Release Model

Heat transfer from the combustion chamber to the cylinder wall occurs by convection and radiation. In HCCI engines, radiation heat transfer is negligible because its effect is very small, due to low soot and low temperature combustion (Bengtsson et al., 2004) therefore it is ignored (Soyhan et al., 2009). The convective heat transfer was modeled to match the experimental results so that the in-cylinder gas motion can be predicted (Stone, 2012). The convective heat transfer rate can be described by Newton's law of cooling (Stiesch, 2013) as Eq. (3.35).

$$\frac{dQ_h}{dt} = h_c A_w (T - T_w) \quad (3.35)$$

where h_c is the heat transfer coefficient, A_w is the wall area and T_w is the wall temperature. The wall area is the sum of the piston, cylinder head and cylinder wall area, which is expressed by Eq. (3.36).

$$A_w = \frac{\pi B^2}{4} + \left(\frac{\pi B^2}{4} + \frac{4V_c}{B} \right) + \left[\left(\frac{\pi BL}{2} \right) (R+1 - \cos \theta - \sqrt{R^2 - \sin^2 \theta}) \right] \quad (3.36)$$

In single zone modeling, an empirical sub-model is used for the heat transfer coefficient, where the model does not contain any physical or chemical principles. Instead, the model attempts to reproduce the characteristics of heat loss obtained from experiments (Stiesch, 2013). In this study, the heat transfer coefficient is modeled using the Woschni correlation, which has been calibrated in an HCCI engine mode. The details of the correlation are discussed as below

The Woschni heat transfer coefficient uses bore, B , as the characteristic length and mean piston speed, \bar{S}_p as the characteristic velocity:

$$h_c = 129.8 B^{-0.2} p^{0.8} T^{-0.55} (2.228 \bar{S}_p)^{0.8} \quad (3.37)$$

In above Equation, SI units are used for all variables (B in m, T in K, V in m³ and \bar{S}_p in m/s) except for p , the instantaneous in-cylinder pressure, which is in bars.

Determining the heat release of a combustion process through analysis of the in-cylinder pressure trace is a common technique. HRR was calculated using cylinder pressure and cylinder volume.

$$\frac{dQ}{d\theta} = \frac{\gamma}{\gamma-1} p \frac{dV}{d\theta} + \frac{1}{\gamma-1} V \frac{dp}{d\theta} + \frac{dQ_h}{dt} \quad (3.38)$$

dQ is the heat release dependent on the variation of crank angle $d\theta$ and γ is the ratio of specific heat values. The integral of Eq. (3.38) is the cumulative heat release.

3.7 Numerical Solutions

A zero-dimensional model solves the first law of thermodynamics equations, as presented in Eq. (3.31). The numerical solution for the temperature change is straightforward because the equation is in the form of a first-order ordinary differential equation. The equation was rearranged so that the change in temperature is on the left hand side. Then, a stiff solver was used to solve Eqs. (3.28) and (3.31) simultaneously. A flow chart of the model is presented in Figure 3.6. The model was coded so that the simulation runs based on the value of crank angle, instead of the pre-defined process with pre-defined combustion, as done by Shaver et al. (2003), Canova et al. (2005) and Killingsworth et al. (2006). A pre-defined or segregated process is where the simulation code is divided according to the engine cycle: intake, compression, power and exhaust. Each cycle uses a different set of equations to obtain temperature or pressure change across the CA, which is based on the ideal gas law equation. Then, the ignition occurs based on the pre-defined ignition location with estimated combustion duration, where the ignition delay has been measured according to the experiment. There is no detailed chemical reaction involved. For the simulation based on the value of CA, it uses the energy equation for the entire engine cycle to solve the temperature change in the chamber with detailed chemical reactions involved. This method gives an advantage in predicting the chemical reaction behavior along the CA step, because the chemical reactions fully control the HCCI engines. At the beginning of the simulation, the engine parameters and initial operating condition were defined, which were based on the experimental data (Gotoh et al., 2013; Guo et al., 2010). Then, the mixture composition in the combustion chamber and inlet manifold was initialized. It was assumed that the initial composition in the combustion chamber before IVO consists of only air and a mixture of air and fuel is introduced after the IVO. A typical valve profile was determined based on Eq. (3.18), which was used to represent the valve motion and also to get the inlet mass flow rate (\dot{m}_{in}). The simulation began from 0°CA, where the piston was at TDC, and finished at EVO. The entire simulation consists of three parts: before IVO, before IVC and before EVO, as shown in Figure 3.6.

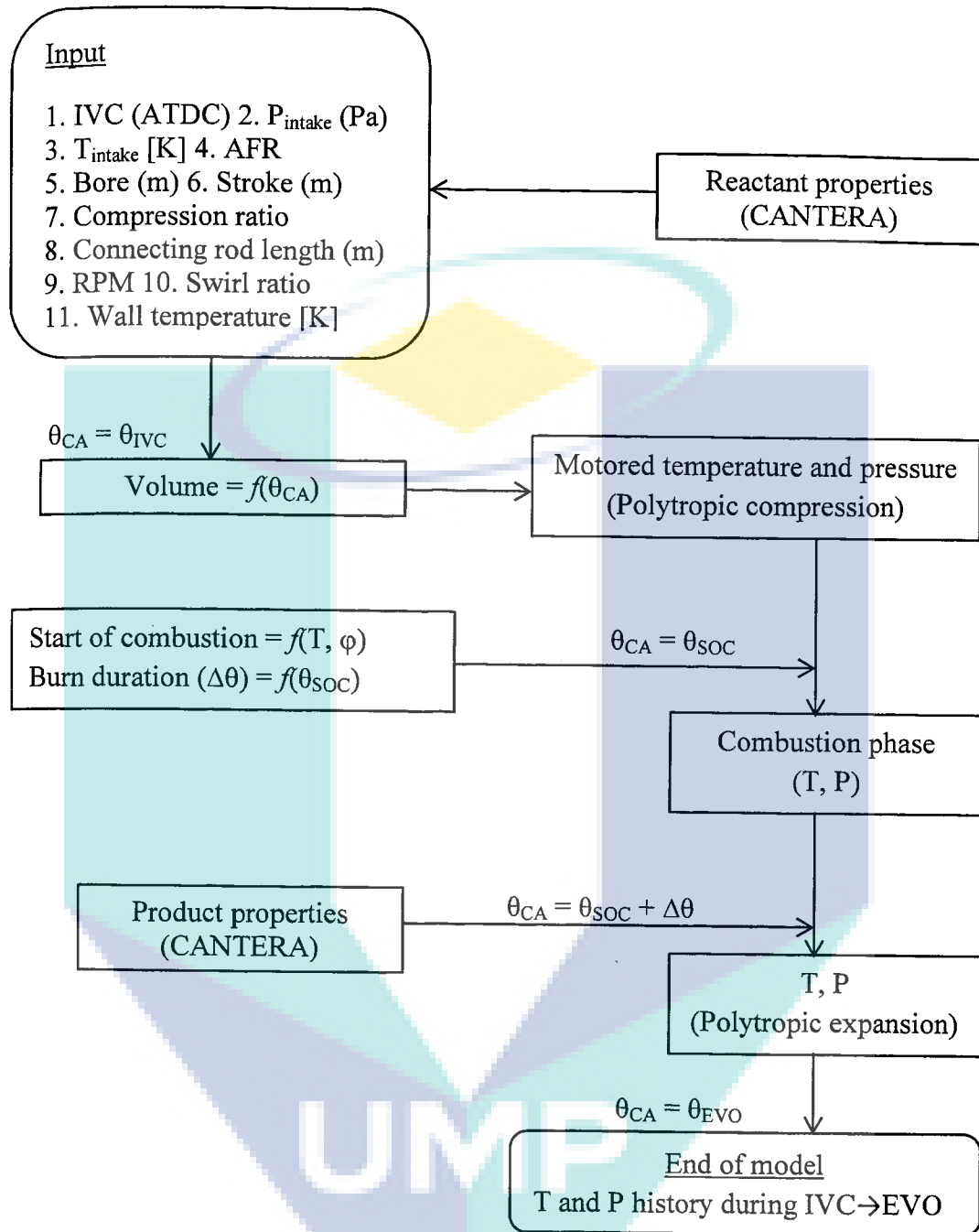


Figure 3.6 An algorithm flow chart for zero-dimensional single-zone model simulation

For the first part, the piston was in downward motion and the air was expanded before being mixed with the intake mixture. Once the intake valve was opened (second part), the air in the combustion chamber was mixed with the intake mixture. In this process, the mass was added to the combustion chamber based on Eq. (3.27). The cylinder volume was expanding and it is expected that the mixture temperature was

decreasing at this stage. The final part is where the main combustion occurred, which was after IVC and before EVO. At this stage, the piston was in upward motion after IVC, compressing the gas mixture. The chemical kinetics plays an important role as it determines the SOC. Once the piston passes the TDC mark, it is in downward motion again, expanding the mixture and the simulation stops at EVO. The simulation solves the energy and species equations for the entire process. Therefore, this technique has eliminated the segregated process as usually done in zero-dimensional modeling. Segregated process is where the simulation is divided into four parts in one engine cycle: intake, compression, expansion and exhaust. Thus, the simulation uses four different sets of equations to cater for each process. In this study, the simulation uses only one set of equations for all the processes. This ensures the in-cylinder properties are consistent from one process to another.

Cantera is an open source software package for chemical kinetics mechanism and is widely used (Andrae, 2011). New researchers could easily adopt Cantera for their research needs given the software's capability to integrate with MATLAB, FORTRAN and Python languages. The chemical kinetics mechanism files can be obtained in Chemkin format, where the file is then be converted to a Cantera-readable file. The use of a chemical reaction mechanism enables the study of the chemical species interaction, where the interaction is influenced by the temperature, pressure and species mass fraction. Furthermore, the chemical reaction mechanism would be able to give a better understanding in the combustion study. The base code used in this study for zero-dimensional single zone engine model written in MATLAB and using Cantera for the chemical kinetics calculations is included in Appendix C.

3.8 Combustion Parameters

The heat release profiles obtained from the in-cylinder pressure traces can be used to develop a characterization of the SOC. The HCCI combustion is considered to start as the crank angle at 10% of the cumulative heat release occurs. A graphical representation of this metric is shown in Figure 3.7 (Mack, 2007b).

The combustion duration is often defined as the time between 10% and 90% cumulative heat releases. This is often referred to as CA10-90. The heat release duration

is a good measure of the combustion event's time interval. A typical HCCI engine experiences an extremely rapid pressure event and thus short combustion duration. Therefore, an elongated heat release profile is desirable as it shows a less violent (smaller pressure rise rate) event. A graphical representation of this metric is shown in Figure 3.7.

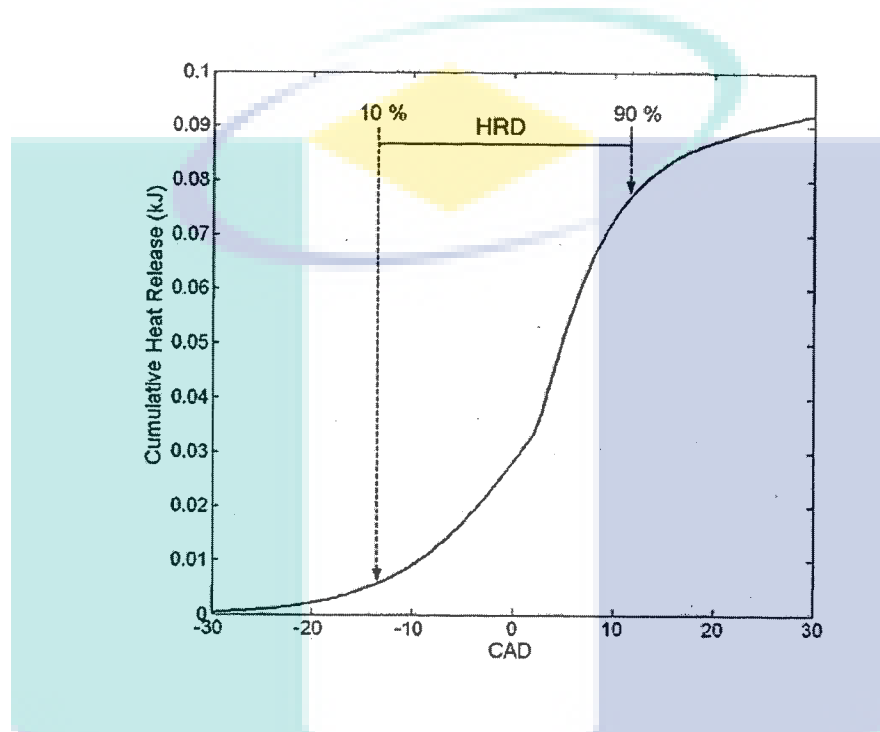


Figure 3.7 Process of determining SOC and combustion duration (CA10-90)

Source: Mack (2007b)

The combustion duration (CA50) is often defined as the crank angle at which 50% of the cumulative heat release occurs. This is often referred to as CA50. Figure 3.8 graphically depicts this process.

3.9 Performance Parameters

In this section, some basic parameters which are commonly used to characterize engine operation are illustrated. These include the mechanical output parameters of work, torque, and power as well as the input requirement of air, fuel and combustion efficiencies (Heywood, 1988; Pulkrabek, 1997).

Torque is a good indicator of an engine's ability to do work. It is defined as force acting at a moment distance and has units of N-m or lbf-ft. The equation used for indicated torque is expressed as (Pulkrabek, 1997):

$$\tau = \frac{W_{net}}{4\pi} \quad (3.39)$$

Where τ is the indicated torque and W_{net} is the net work done which can be calculated by

$$W_{net} = \int p dV \quad (3.40)$$

where p is the cylinder pressure and dV is the variation of cylinder volume.

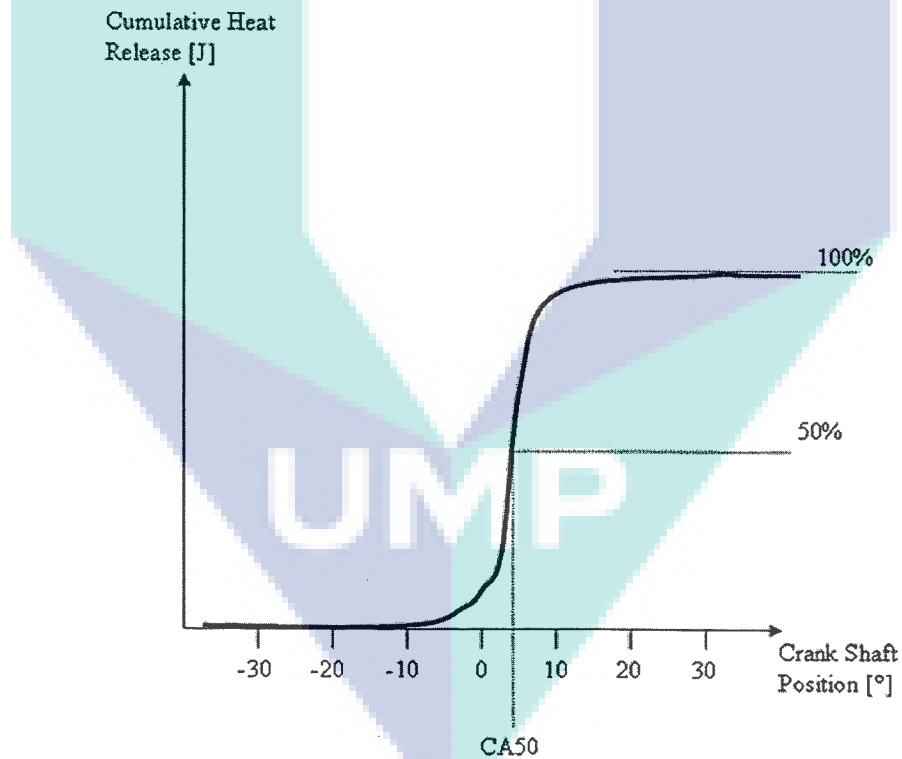


Figure 3.8 Process of determining CA50

Source: Hakansson (2007)

Power is defined as the rate of work of the engine. If N = engine speed, then indicated power is expressed as (Pulkrabek, 1997):

$$ip = \frac{2\pi N\tau}{60} \quad (3.41)$$

IMEP is a good parameter for comparing engines with regard to design or output because it is independent of both engine size and speed. It can be calculated by:

$$imep = \frac{W_{net}}{V_d} \quad (3.42)$$

where V_d is the cylinder swept volume and W_{net} is the net work done.

ITE η_{ith} is the ratio of energy in the indicated power (ip) to the input fuel energy in appropriate units (Ganesan, 2012) and it is expressed as Eq. (3.43):

$$\eta_{ith} = \frac{ip}{\text{mass of fuel consumption} \times \text{calorific value of fuel}} \quad (3.43)$$

Indicated power (ip) gives the indicated specific fuel consumption:

$$isfc = \frac{\text{mass of fuel consumption}}{ip} \quad (3.44)$$

3.10 Chemical Properties Of Fuels

In this study, different fuels are used in HCCI engines, including diesel, gasoline, n -heptane, ethanol, butanol and blends of n -heptane and ethanol as well as blends of n -heptane and butanol using 15% and 30% of both ethanol and butanol in blends. The properties of all test fuels are shown in Table 3.3, Table 3.4 and Table 3.5 respectively.

Table 3.3 The properties of diesel fuel

Properties	Value
Chemical formula	$C_{12}H_{26}$
Density (kg/m^3)	779.5
Octane number	-----
Lower heating value (MJ/kg)	44.56
Boiling point($^{\circ}C$)	254
Molar mass (g/mol)	170.26

Source: Guo et al. (2011)

Table 3.4 The properties of gasoline fuel

Properties	Value
Chemical formula	C_4-C_{12}
Density (kg/m^3)	747
Octane number	94
Lower heating value (MJ/kg)	44
Boiling point($^{\circ}C$)	210

Source: Gotoh et al. (2013)

Table 3.5 The chemical properties of the test fuels

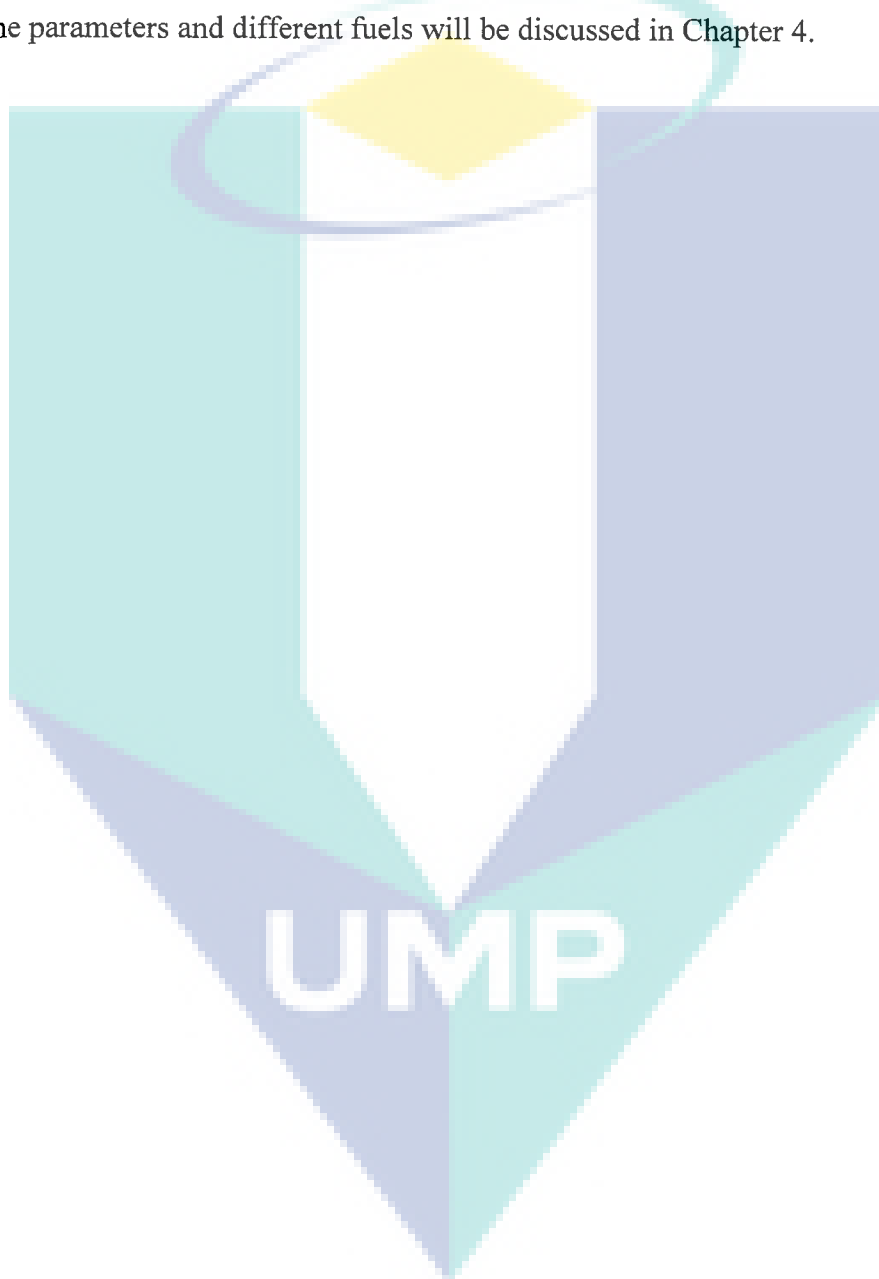
Properties	n-heptane	E15	E30	Bu15	Bu30
Chemical formula	C_7H_{16}	-	-	-	-
Density (kg/m^3)	679.5	697	713	700	808
Lower heating value (MJ/kg)	44.56	41	39	43	41
Boiling point($^{\circ}C$)	98	95	92	101	117.7
Molar mass (g/mol)	100.16	92	84	96	74.12

Source: Holtzapfel et al. (1999) and Saisirirat et al. (2011)

3.11 Summary

This chapter has discussed the methodology used in developing the simulation model. The use of numerical models in engine research is a useful tool which provides both greater insight and rapid feedback. Experiments are oftentimes costly (in both terms of money and time) so the information gained through computer modeling is invaluable. Chemical kinetic mechanisms and geometric representations of the combustion chamber are coupled to predict engine behavior. Chemical kinetic

mechanisms are used to simulate combustion chemistry in numerical models. Development of chemical kinetic mechanisms specific to the experiments (i.e. the mechanism used in this study) is an ongoing research in the combustion community. Single zone models, using the slider crank relationship for combustion chamber geometry, provide idealized but useful information. The validation of the model against previously published experimental results and details analysis of the effect of different engine parameters and different fuels will be discussed in Chapter 4.



CHAPTER 4

RESULTS AND DISCUSSION

4.1 Introduction

The validation of the zero-dimensional single zone model against the experimental results from the literature will be presented in this chapter. Two experimental data sets were used for validation purpose: one is the HCCI engine fuelled with diesel (Guo et al., 2010) and the other with gasoline (Gotoh et al., 2013). This Chapter also presents the results of numerical modeling. The engine conditions including intake temperature, intake pressure, engine speed and the compression ratio will be varied to analyze the ability of the model to predict the combustion, performance and emissions characteristics of HCCI engines. The numerical results will be compared with experimental results from CI and SI engines to understand the advantages of HCCI engines over CI and SI engines. The use of fuel blends is an important concept for HCCI engine. It helps to study the ability of HCCI engines to use variety of fuels. This Chapter will describe the performance and emissions characteristics of HCCI engines and compare the results with CI and SI engines first. Then the effect of engine parameters on combustion and performance characteristics of both diesel and gasoline HCCI engines will be presented. After that the effects of fuel blends in HCCI engines will be described. The summary will conclude the Chapter.

4.2 Model Validation

4.2.1 Diesel HCCI

In this section, the simulation models were validated by the experimental results that were conducted by Guo et al. (2010) on a four stroke single cylinder diesel engine

which was modified for HCCI operation at a fixed engine speed of 900 rpm under the full engine load condition for diesel fuel. The detail specifications of the engines are presented in Table 4.1. The schematic diagram of the engine setup is presented in Figure 4.1.

Table 4.1 Engine model specifications

Engine parameters	Value
Type	4 stroke, single cylinder
Bore (mm)	82.55
Stroke (mm)	114.3
Displacement (L)	0.6117
No. of cylinders	1
Compression ratio	4.6-16
Connecting rod length (mm)	254
Combustion chamber	Pancake shape
Intake Valve Close (°CA)	-144
Exhaust Valve Open (°CA)	140
Fuel system	Air-assist port fuel injection

Source: Guo et al. (2010)

The engine was modified from the standard ASTM guideline by the addition of an air-assist port fuel injection system and other hardware and software needed for the control of critical engine parameters such as intake air temperature, air/fuel ratio, exhaust gas recirculation and intake and exhaust back pressure. A port fuel injector for flexible fuel vehicles was modified to provide air-assist atomization of liquid fuels. Surge tanks were installed in the intake and exhaust systems to minimize pressure pulsations of the intake and exhaust gasses, thereby improving engine operational stability and airflow measurement. The low-speed data acquisition system is based on National Instruments' PXI hardware platform. The hardware is controlled by data acquisition and control software (Sakor Technologies, Inc., DynoLAB™ PT), which provided stable control of the engine speed and load conditions, as well as critical parameters such as engine coolant and lubricating oil temperatures, intake air pressure and temperature, exhaust back pressure, fuel injection timing, and the quantity of fuel injected. The engine was coupled to an eddy current dynamometer that absorbed engine load. A variable-speed ac motor, coupled to the dynamometer with an overdrive clutch,

was used to start and motor the engine before stable HCCI combustion was initiated, as well as to maintain engine speed when HCCI combustion was unstable.

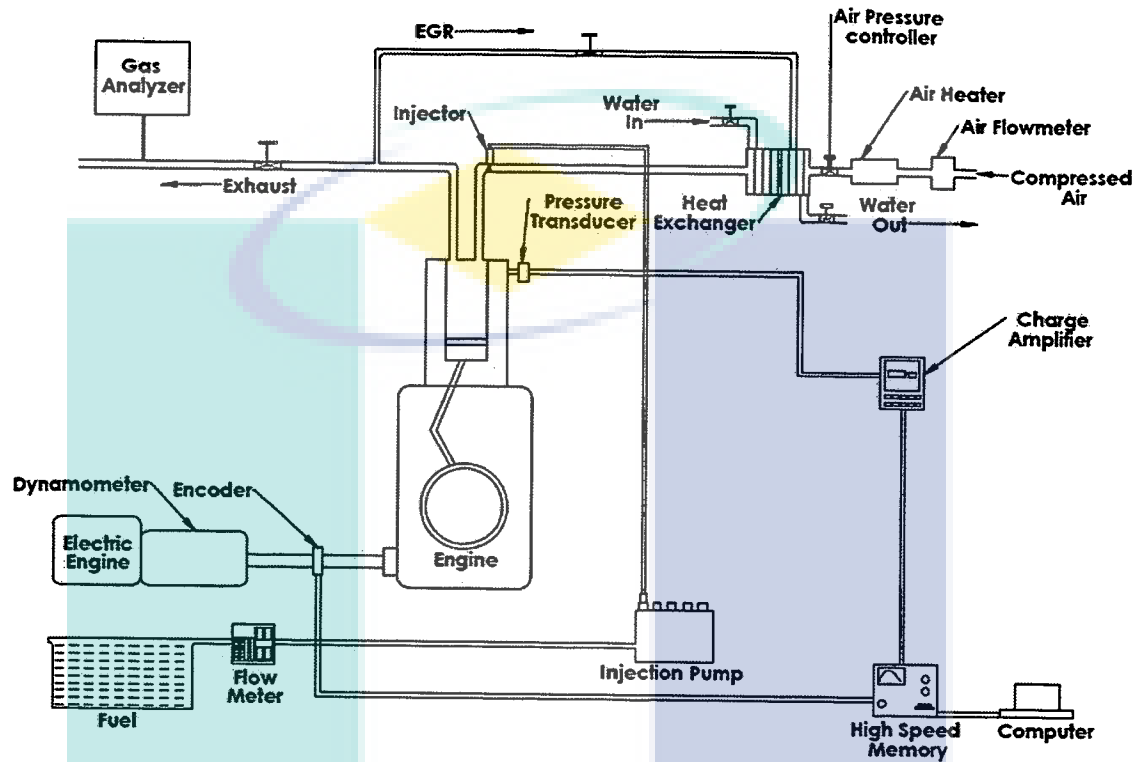


Figure 4.1 Schematic diagram of the HCCI engine set up, reproduced from Guo et al. (2010)

In this study, the initial conditions for the intake pressure and temperature were set as $P_{\text{intake}}=100$ kPa and $T_{\text{intake}}=333$ K. The intake air temperature was set 20K higher than the actual temperature to account for the mixing effects (Guo et al., 2010). A different study also stated that the intake temperature for a single-zone model has to be increased up to 30K, while up to about 10K for a multi-zone model (Bunting et al., 2008). The assumption of uniform wall temperature for the entire engine cycle, uniform in-cylinder temperature and pressure, and a potential limitation of the chemical chemistry as well may contribute to the adjustment of the intake temperature (Guo et al., 2010). The wall temperature (T_{wall}) was set to be 530K for a CI engine (Zheng et al., 2005). However, the wall temperature used in the numerical studies varies from one engine to another (Soyhan et al., 2009; Wang et al., 2006; Zheng et al., 2005), where the wall temperature ranges from 293K (Barroso et al., 2005) to approximately 800K

(Soyhan et al., 2009). The exhaust temperature and pressure were approximated at 1000K and 101.3kPa, respectively (Heywood, 1988), where the approximated value is close to measurement of a diesel engine (Zhou et al., 2006). At the beginning of the simulation, where CA is less than IVO, the mixture composition in the chamber was assumed to be only air with no fuel. The fuel is being introduced into the chamber during the IVO period, where the fuel quantity is based on the air-fuel ratio used in the experiment.

To further validate the applicability of the developed reaction mechanism for engine simulations, numerical simulations were performed and compared against the HCCI engine experiments. The obtained results show good agreement with the experimental published results and capture important combustion phase trends as engine parameters are varied with maximum percentage of error which is less than 6%. As presented in Figure 4.2, the numerical simulation was able to capture elements of HCCI combustion of diesel, particularly the low-temperature reaction (LTR). Figure 4.2(a) plots the in-cylinder pressure and Figure 4.2(b) plots the HRR obtained from experiments done by (Guo et al., 2010) and present study, at a fixed engine speed of 900 rpm under constant intake temperature of 333 K and air-fuel ratio of 50 conditions.

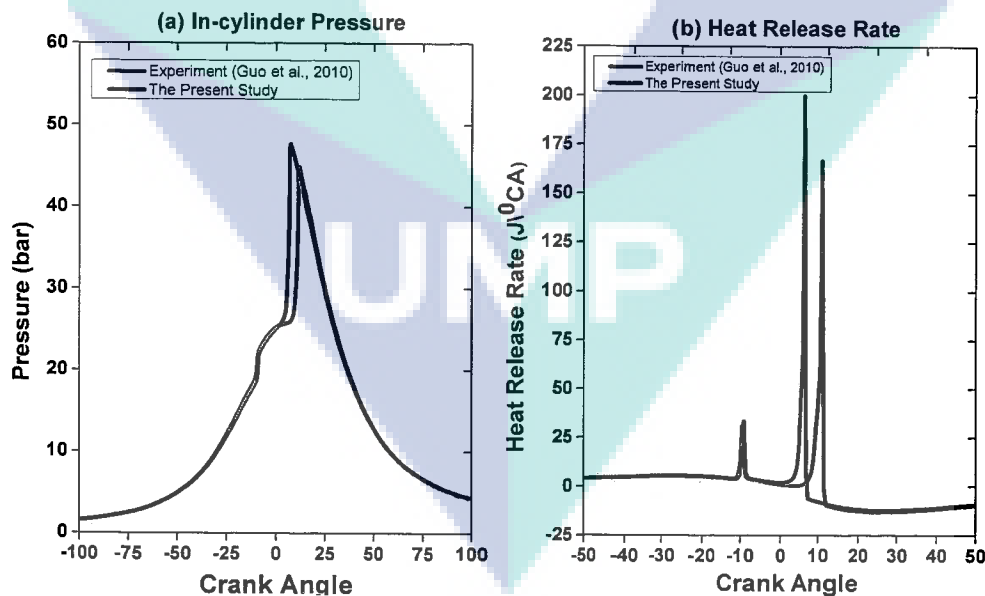


Figure 4.2 Comparison between zero-dimensional single zone model with experimental data from Guo et al. (2010). CR=10, N=900 rpm, T_{in} =333 K, P_{in} =100 kPa, AFR=50

As can be seen, the peak cylinder pressure is adequately reproduced, indicating that the important reaction pathways are very well represented. In comparison, the main combustion stage (MCS) predicted by the numerical simulation is advanced compared to the experimental results as presented in Figure 3.10(b). A spike in the predicted HRR was observed during the MCS. This spike was caused by the rapid oxidation of all CO accumulated to this point in the simulation to CO₂ (An et al., 2012). The conversion of CO to CO₂ is predicted to happen rapidly once the required temperature is reached because only a few reactions are involved. Rapid oxidation of CO to CO₂ has not been observed experimentally or reported in this study. The assumption of uniform mixture temperature and mixture composition contributes to this overly-rapid HRR.

4.2.2 Gasoline HCCI

In this section, the simulation models were validated by the experimental results that were conducted on a four stroke inline-4 cylinders gasoline engine which was modified for HCCI operation at a fixed engine speed of 1500 rpm under the full engine load condition for gasoline fuel surrogate. The detail specifications of the engines are presented in Table 4.2 (Gotoh et al., 2013). The schematic diagram of the engine setup is presented in Figure 4.3. The engine was modified from the standard setup by the addition of hardware and software needed for the control of critical engine parameters such as intake air temperature, air-fuel ratio, exhaust gas recirculation and intake and exhaust back pressure. The intake mean pressure was adjusted by varying the motor drive speed. The intake gas temperature was adjusted by a water-cooled intercooler. The partition ratio of a three-way valve was controlled to realize given intake temperature. The mean pressure in the exhaust pipe was controlled using an exhaust throttle valve. The cylinder pressure of the cylinder was measured by a piezoelectric pressure transducer (Kistler 6052c, 6117b). The crank angle of the 50% burn (CA50) was used to monitor the combustion phasing, and grossIMEP was used to recognize the output power of individual cylinder. To balance the cylinder-to-cylinder variation of CA50 and grossIMEP, the amount of supplied fuel for the each cylinder were adjusted. All of the pressure analysis data including apparent HRR, mean effective pressures and pressure rise rate were computed from the ensemble-averaged pressure trace taken over 100 cycles. Piezo-resistive pressure transducers (Kistler 4005B) were mounted on the intake

and the exhaust manifolds for the measurements of intake and exhaust pressure pulsations.

Table 4.2 Engine model specifications

Engine parameters	Value
Type	4 stroke, Inline-4 cylinder
Bore (mm)	86
Stroke (mm)	86
Displacement (L)	0.5
No. of cylinders	4
Compression ratio	12
Connecting rod length (mm)	200
Fuel	Gasoline (RON 91)
Intake Valve Close (°CA)	-180
Exhaust Valve Open (°CA)	156
Fuel system	Air-assist port fuel injection

Source: Gotoh et al. (2013)

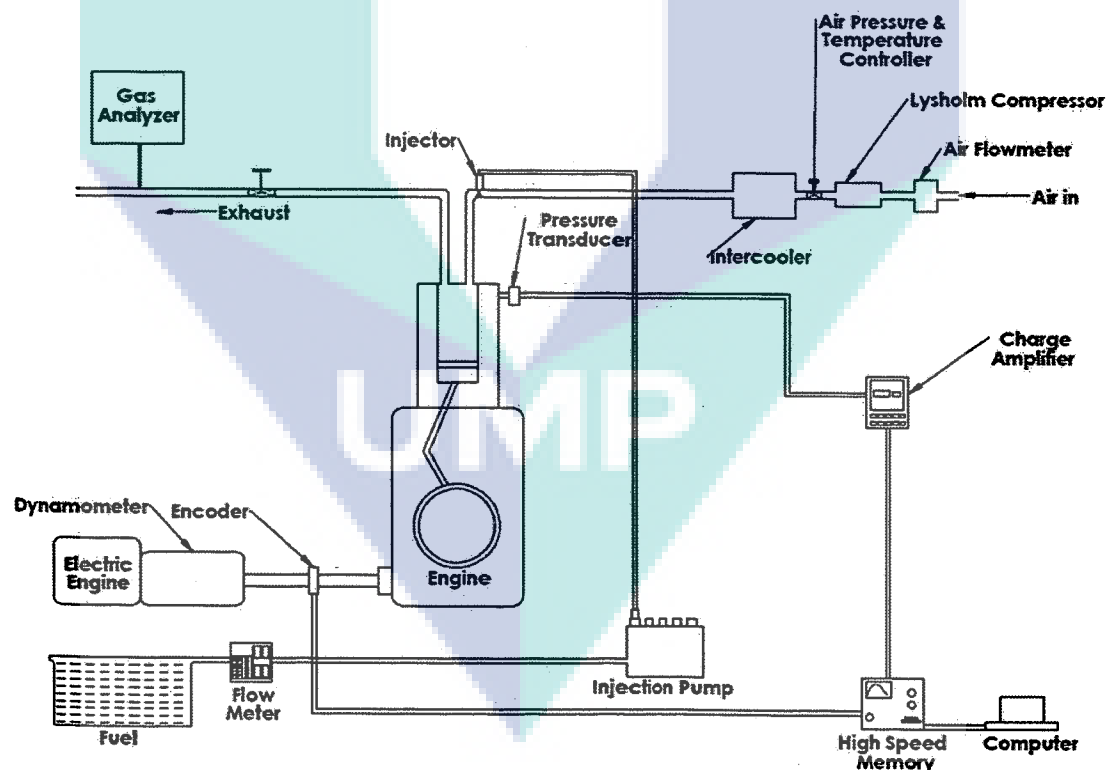


Figure 4.3 Schematic diagram of the HCCI engine set up, reproduced from Gotoh et al. (2013)

In this study, the initial conditions for the intake pressure and temperature were set as $P_{\text{intake}}=100$ kPa and $T_{\text{intake}}=393$ K. The intake temperature for the zero-dimensional model was set 15°C higher than the actual to account for the mixing effects. This is consistent with Bunting et al. (2008) and Guo et al. (2010), where the intake temperature for the zero-dimensional model was set 10 – 30 K higher than the actual. The wall temperature (T_{wall}) was set to be 353K which is consistent with Barroso et al. (2005) and Su et al. (2007). However, the wall temperature used in the numerical studies varies from one engine to another (Soyhan et al., 2009; Wang et al., 2006; Zheng et al., 2005), where the wall temperature ranges from 293K (Barroso et al., 2005) to approximately 800K (Soyhan et al., 2009). The exhaust temperature and pressure were approximated at 700K and 101.3kPa, respectively (Heywood, 1988), where the approximated value is close to measurement of a gasoline engine (Zhou et al., 2006). At the beginning of the simulation, which is before the IVO, the mixture in the chamber was assumed to be only air and the fuel-air mixture was added according to the pre-set air-fuel ratio value after the IVO.

To further validate the applicability of the developed reaction mechanism for engine simulations, numerical simulations were performed and compared against the HCCI engine experiments. The obtained results show good agreement with the experimental published results and capture important combustion phase trends as engine parameters are varied with maximum percentage of error which is less than 4%. As presented in Figure 4.4, the numerical simulation was able to capture elements of HCCI combustion of gasoline surrogate fuel, particularly the LTR. Figure 4.4(a) plots the in-cylinder pressure and Figure 4.4(b) plots the HRR obtained from experiments done by Gotoh et al. (2013) and present study, at a fixed engine speed of 1500 rpm under constant intake temperature of 393 K and air-fuel ratio of 40 conditions. As can be seen, the peak cylinder pressure is predicted higher than the experiment. The predicted maximum in-cylinder pressure is evidently slightly higher than that of the experiment due to the limitation of the zero-dimensional model, where the entire combustion chamber is assumed to be homogenous. In comparison, MCS predicted by the numerical simulation is advanced compared to the experimental data as presented in Figure 4.4(b). A spike in the predicted HRR was observed during the MCS. This spike was caused by the rapid oxidation of all CO accumulated to this point in the simulation to CO₂. The conversion of CO to CO₂ is predicted to happen rapidly once the required

temperature is reached because only a few reactions are involved. The assumption of uniform mixture temperature and mixture composition contributes to this overly-rapid HRR. Overall, the combustion phasing is in good agreement with the experimental data, demonstrating that the zero-dimensional single-zone model can be used in HCCI engine simulations.

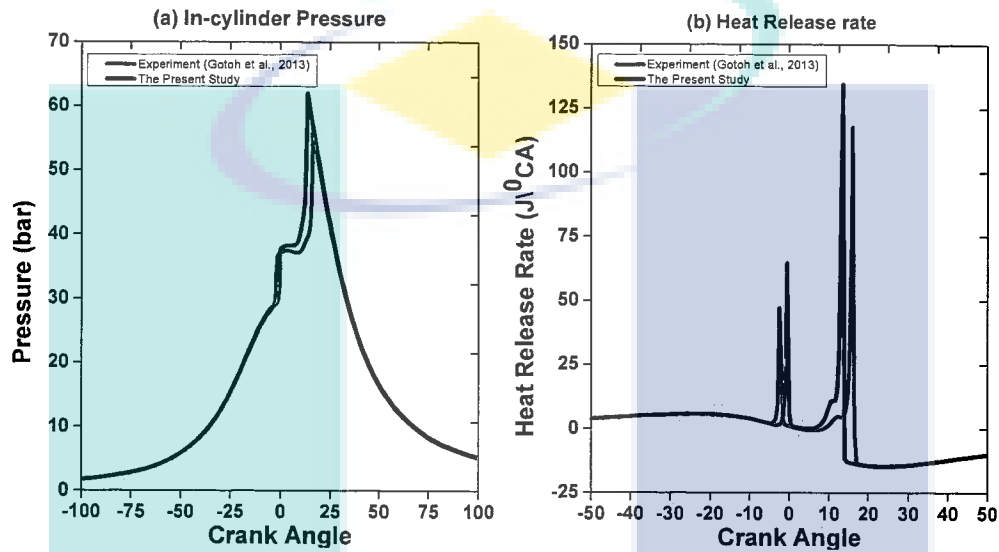


Figure 4.4 Comparison between zero-dimensional single zone model with experimental data from Gotoh et al. (2013). CR=12, N=1500 rpm, $T_{in}=393$ K, $P_{in}=100$ kPa, AFR=40

4.2.3 Comparison of Different Models

In this section, the simulation results from the zero-dimensional single-zone model are compared with the experimental results as well as also compared with another zero-dimensional single-zone model from Maurya et al. (2016) and one-dimensional model from Mo (2008) as presented in Figures 4.5 and 4.6. From Figure 4.5, it is seen that both zero-dimensional models predict higher in-cylinder pressure compared to the experiment. While comparing between two zero-dimensional models, prediction of in-cylinder pressure from zero-dimensional model of the present study is slightly better than the prediction from zero-dimensional of Maurya et al. (2016). The predicted maximum in-cylinder pressure is evidently slightly higher than that of the experiment due to the limitation of the zero-dimensional model, where the entire combustion chamber is assumed to be homogenous.

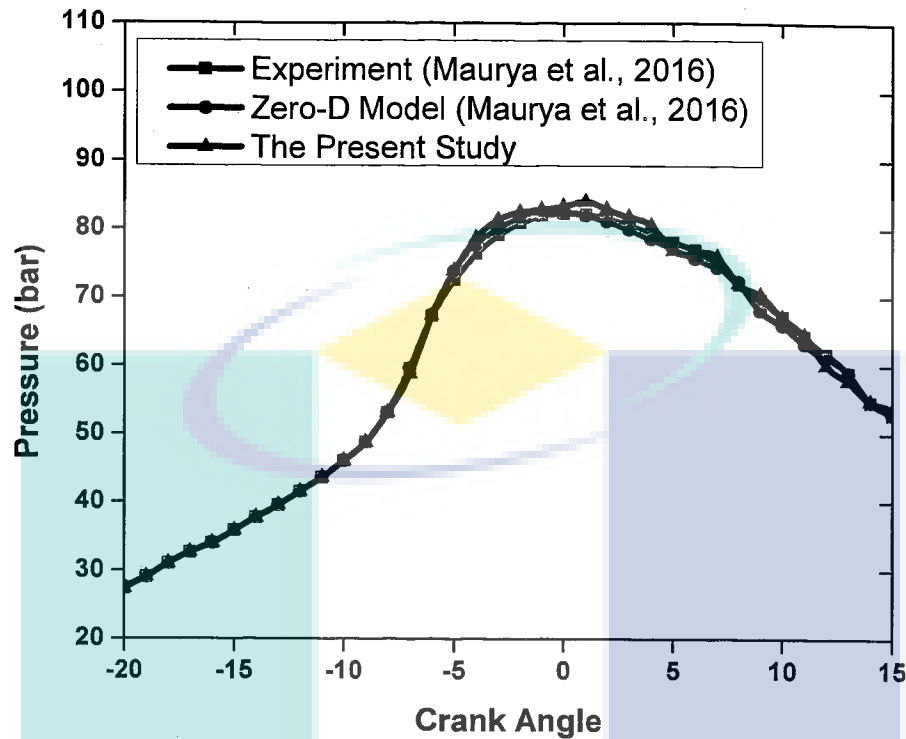


Figure 4.5 Comparison between zero-dimensional single zone model with experimental data and another zero-dimensional model from Maurya et al. (2016). CR=21, N=1000 rpm, $T_{in}=365$ K, $P_{in}=100$ kPa, $\lambda = 3$

From Figure 4.6, it is seen that zero-dimensional model predicts the in-cylinder pressure properly. Very good agreement is seen between experiment and simulation in terms of combustion phasing and MCS prediction. While comparing between zero-dimensional model and one-dimensional model, prediction of in-cylinder pressure from one-dimensional model of Mo (2008) is slightly better than the prediction from zero-dimensional of the present study because of the prediction of knocking in one-dimensional model. The reason behind this phenomenon is that the limitation of zero-dimensional modeling of assuming the whole combustion chamber is homogeneous. However, the combustion phasing is in good agreement with the simulation results of other types of numerical models, demonstrating that the zero-dimensional single-zone model of the present study can be used in HCCI engine simulations.

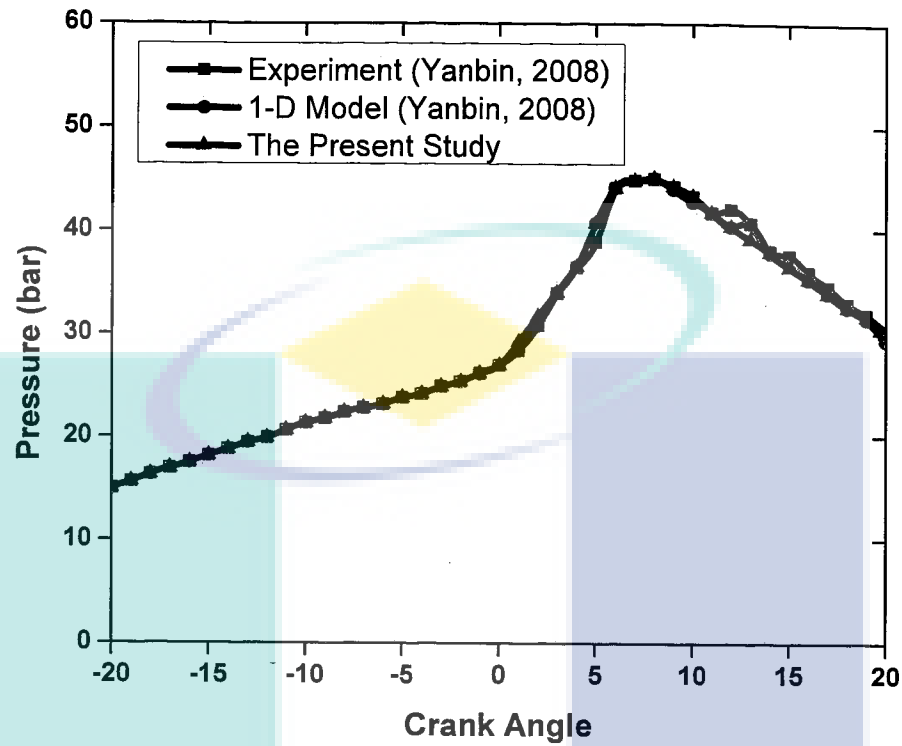


Figure 4.6 Comparison between zero-dimensional single zone model with experimental data and one-dimensional model from Mo (2008). CR=12, N=1995.7 rpm, $T_{in}=388.96$ K, $P_{in}=93.99$ kPa, $\lambda = 1.5$

4.3 Comparison of HCCI with CI

In this section, the comparison of performance and emissions characteristics between diesel and HCCI is discussed. The experimental performance and emissions characteristics for diesel engine using diesel fuel was done by An et al. (2012). The detail specifications of the engines are presented in Table 4.3. The simulations were run for HCCI engine on same operating condition and using same fuel.

4.3.1 Engine Performance

Figure 4.7 presents the variation of in-cylinder pressure between diesel engine and HCCI engine at a constant speed of 2400 rpm and full load condition using diesel as a fuel. The in-cylinder pressure condition of the HCCI engine was selected at a best case condition of 333 K intake temperature, when less knocking occurred. The in-cylinder

pressure for the HCCI engine is higher than for the CI engine. The maximum pressure for the HCCI engine is 117 bar and 109.73 bar for the CI engine.

Table 4.3 Engine model specifications

Engine parameters	Value
Type	4 stroke, DI, water cooled
Bore (mm)	92
Stroke (mm)	93.8
Displacement (L)	0.6117
No. of cylinders	4
Compression ratio	18.5
Connecting rod length (mm)	158.5
Combustion chamber	Pancake shape
Intake Valve Close (°CA)	-144
Exhaust Valve Open (°CA)	140

Source: An et al. (2012)

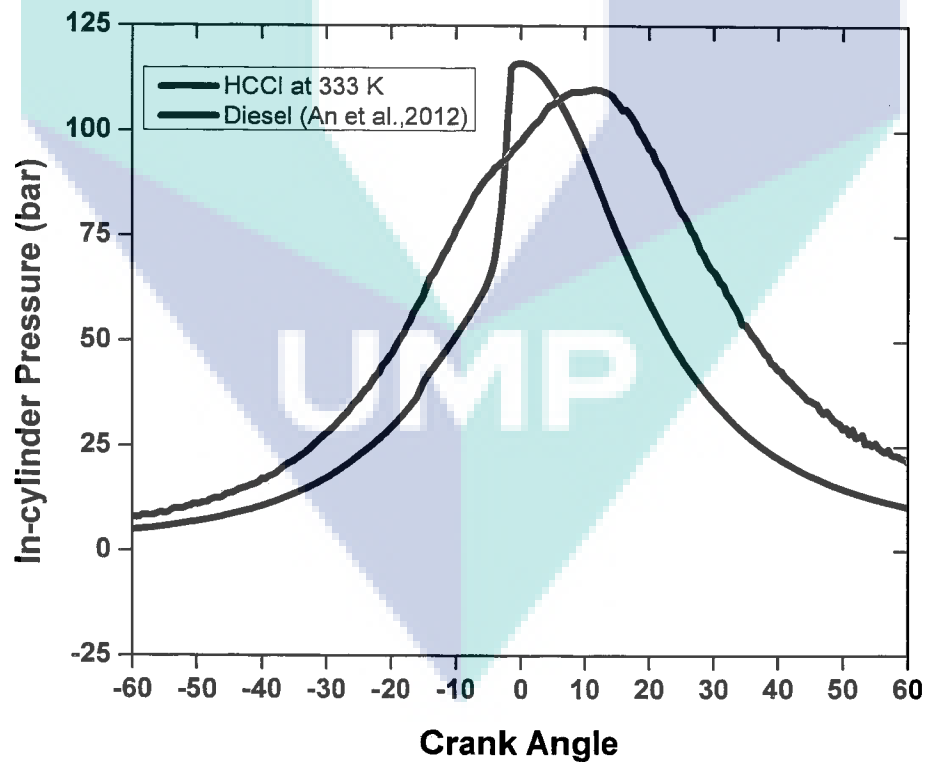


Figure 4.7 The variation of in-cylinder pressure between diesel engine and HCCI engine at a constant speed of 2400 rpm and full load condition

Note that from the Figure 4.7 the combustion event for the HCCI engine occurs in a short time. The in-cylinder pressure increases faster and reaches the peak in approximately 8°CA with the combustion starting at 5°CA BTDC. With the CI engine, the pressure increases steadily and the combustion is slower compared to the HCCI engine. The combustion event for the CI engine starts at approximately 30°CA BTDC before the pressure reaches the peak at 10°CA ATDC. Thus, the combustion event for the CI engine occurred in approximately 40°CA , which is five times slower than for the HCCI. Hence, the combustion in the HCCI engine occurs instantaneously with a very fast combustion, as has been discussed by Raitanapaibule et al. (2005) and Tomita (2004). Therefore, the HCCI combustion requires very well controlled operating conditions to achieve the desired in-cylinder pressure behavior, otherwise knocking will take place.

Figure 4.8 presents the variation of engine power between diesel engine and HCCI engine at variable speed ranging from 1200 rpm to 3200 rpm and full load condition. It is seen that the HCCI engine power is higher than diesel engine in every speed condition except in 3200 rpm. The maximum power for the CI engine is 6.63 kW at 3200 rpm and 6.08 kW for the HCCI engine at 2800 rpm. An improvement in HCCI engine power was described in Figure 4.1, where the in-cylinder peak pressure is higher than CI engine. This improves the combustion efficiency which helps to increase power. In addition, the charge for HCCI engine is considered as homogeneous which is favorable for complete combustion. Thus combustion efficiency is improved and ultimately higher power is produced (Kook et al., 2007).

Figure 4.9 presents the variation of BSFC between diesel engine and HCCI engine at variable speed ranging from 1200 rpm to 3200 rpm and full load condition. When compared with the HCCI engine, the BSFC for HCCI is better than the CI in every speed condition, as presented in Figure 4.3. The HCCI engine has the best BSFC at 215.64 g/kW-hr, where the CI has a minimum BSFC of 219.57 g/kW-hr. When the diesel engine operates in highest speed condition, the BSFC marginally increases to 238.57 g/kW-hr. Thus, the HCCI engine has up to 1.65% lower BSFC than the diesel engine at highest speed. This is because the power generated by the HCCI engine is higher due to the high compression ratio of the engine (Fiveland et al., 2000).

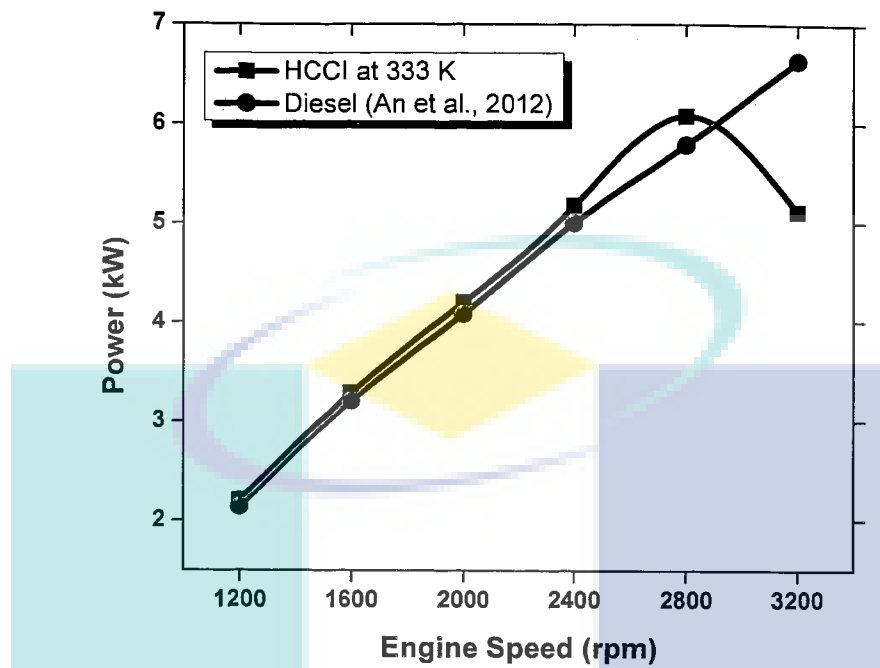


Figure 4.8 The variation of engine power between diesel engine and HCCI engine at variable speed and full load condition

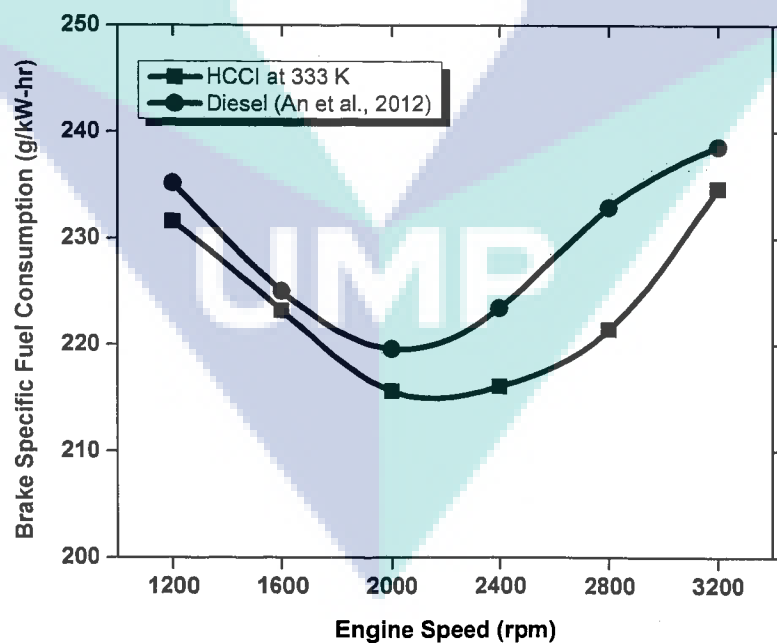


Figure 4.9 The variation of BSFC between diesel engine and HCCI engine at variable speed and full load condition

Figure 4.10 presents the variation of BTE between diesel engine and HCCI engine at variable speed ranging from 1200 rpm to 3200 rpm and full load condition. It is seen that HCCI provides highest BTE at 2800 rpm whereas diesel engine provides at 2000 rpm. BTE of the HCCI engine increases with the increase of engine speed up to 2800 rpm and then decreases. When the BTE between the two modes of combustion is compared, the HCCI engine yields a higher efficiency than the diesel engine. The HCCI engine has a maximum efficiency of 44.98%, where the diesel engine has efficiency up to 36.75%. This is because the power generated by the HCCI engine is higher due to the high compression ratio of the engine (Fiveland et al., 2000).

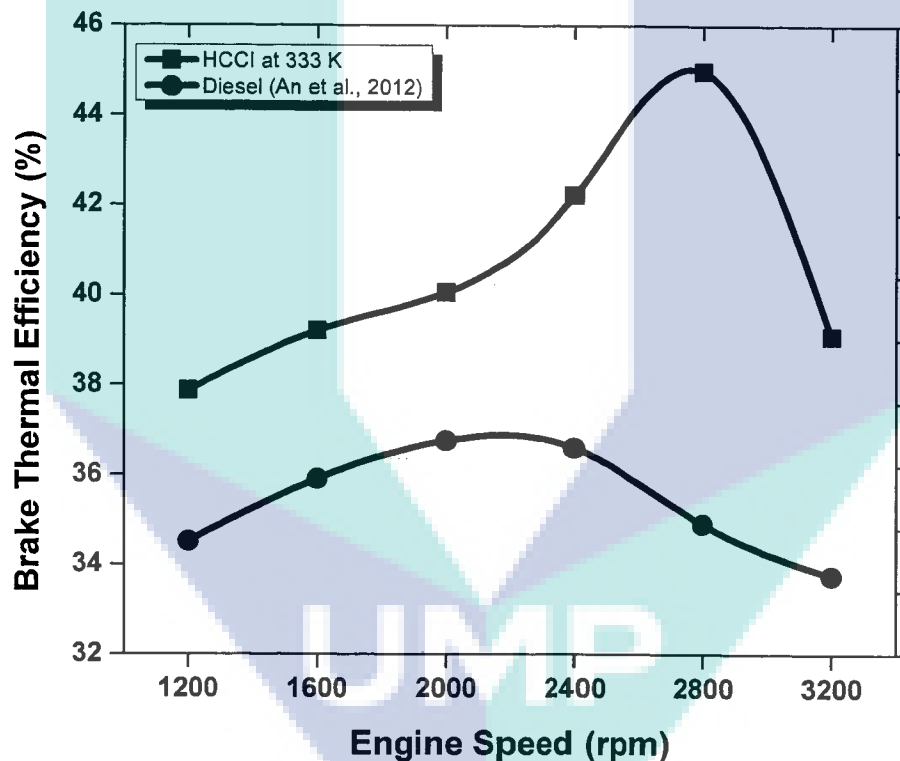


Figure 4.10 The variation of BTE between diesel engine and HCCI engine at variable speed and full load condition

4.3.2 Engine Emissions

Figure 4.11 presents the variation of HC emission between diesel engine and HCCI engine at variable speed ranging from 1200 rpm to 3200 rpm and full load

condition. A big difference in HC emission is seen between diesel engine and HCCI engine. This is one of the disadvantages of HCCI engine which is already mentioned in literature review. The HC emission from HCCI engine increases with the increase of engine speed up to 2400 rpm and then gradually decreases. When the HC emission between the two modes of combustion is compared, the HCCI engine yields a very higher amount of HC than the diesel engine. The HCCI engine has a maximum HC emission of 143 ppm, where the diesel engine has HC emission up to 9.94 ppm. This is due to the nature of this type of combustion. For low combustion temperature, incomplete combustion is occurred and ultimately HC emissions is produced (Bression et al., 2008; Ganesh et al., 2008). HC is mainly formed in the crevices of the cylinder which are so cold for complete consumption (Aceves et al., 2001a). Higher concentrations of hydrogen and natural gas in diesel engines have the ability to reduce UHC and CO emission levels, because the gaseous state of hydrogen and natural gas will reduce the wall wetting effect on the cylinder liner (Cho et al., 2007).

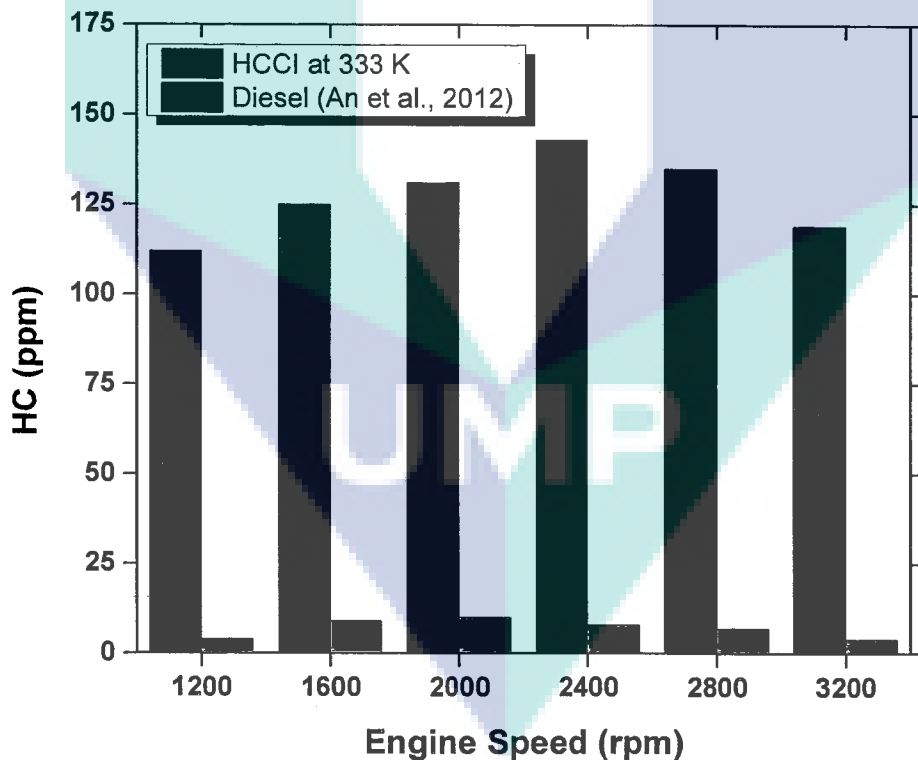


Figure 4.11 The variation of HC emission between diesel engine and HCCI engine at variable speed and full load condition

Figure 4.12 presents the variation of CO emission between diesel engine and HCCI engine at variable speed ranging from 1200 rpm to 3200 rpm and full load condition. A significant difference in CO emission is seen between diesel engine and HCCI engine. This is one of the disadvantages of HCCI engine which is already mentioned in literature review. When the HC emission between the two modes of combustion is compared, the HCCI engine yields a very higher amount of CO than the diesel engine. The HCCI engine has a maximum CO emission of 78 ppm, where the diesel engine has HC emission up to 4.22 ppm. This is due to the nature of this type of combustion. The amount of CO₂ and CO are dependent on the combustion efficiency, where the combustion efficiency can be defined as the ratio of CO₂ to the total of fuel carbon present in the exhaust including CO, CO₂ and UHC (Li et al., 2007). CO is formed by following RH-R-RO₂-RCHO-RCO-CO equation, where R is the HC radical (Heywood, 1988). CO is mainly formed in the crevices of the cylinder which are so cold for complete consumption (Aceves et al., 2001a). In addition, for complete reaction of the conversion from CO to CO₂ needs temperature above 1500 K (Dec, 2002). However, CO formation is occurred in case of HCCI combustion at low load peak burned gas temperature remains below that required level.

Figure 4.13 presents the variation of NO_x emission between diesel engine and HCCI engine at variable speed ranging from 1200 rpm to 3200 rpm and full load condition. A significant difference in NO_x emission is seen between diesel engine and HCCI engine. This is one of the advantages of HCCI engine which is already mentioned in literature review. When the NO_x emission between the two modes of combustion is compared, the HCCI engine yields a very lower amount of NO_x than the diesel engine. The HCCI engine has a maximum NO_x emission of 10.8 ppm, where the diesel engine has NO_x emission up to 974.33 ppm. This is due to the nature of this type of combustion. The pollution formation process in CI engines is strongly dependent on fuel distribution system and the process of changing the distribution with time because of mixing. In case of diesel engines fuel distribution system is non-uniform and the NO_x formation is occurred in the high temperature burned gas region which is non-uniform as well as formation rates are highest in these region close to stoichiometric ratio (Heywood, 1988).

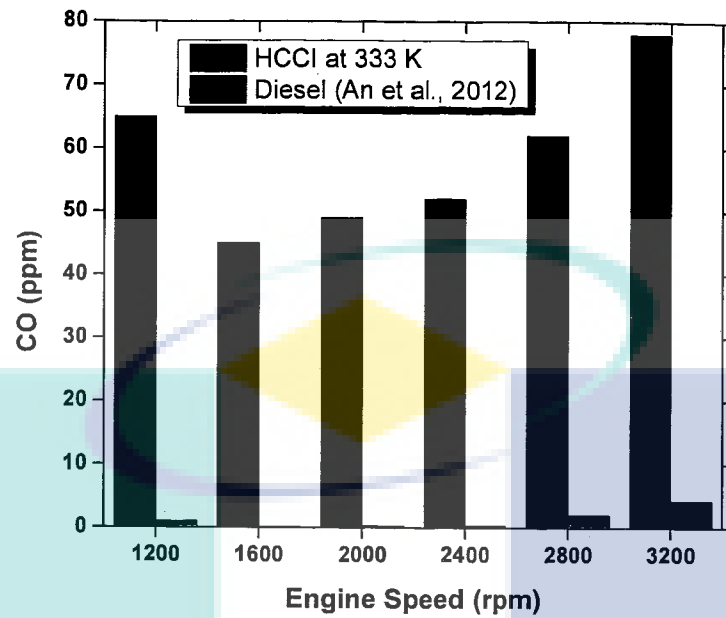


Figure 4.12 The variation of CO emission between diesel engine and HCCI engine at variable speed and full load condition

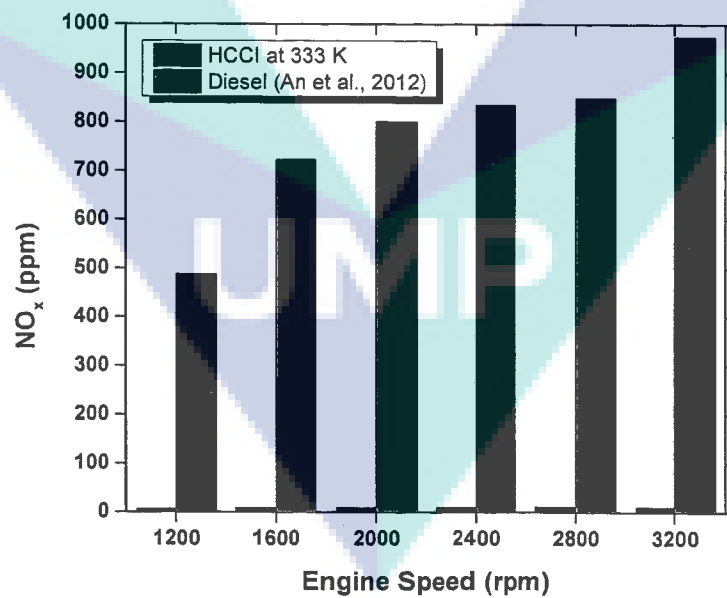


Figure 4.13 The variation of NO_x emission between diesel engine and HCCI engine at variable speed and full load condition

Since HCCI engines typically operate fuel lean, the final flame temperature is usually well below 2000 K. At this low post-combustion temperature chemical reactions that produce NO_x are essentially inactive (Mack, 2007a). NO_x is generally formed in a high temperature reaction, where the nitrogen in air dissociates into nitrogen radicals to form NO when reacting with oxygen. Some NO is converted to NO_2 when further reactions occur in the chamber.

4.4 Comparison of HCCI with SI

In this section, the comparison of performance and emissions characteristics between gasoline and HCCI is discussed. The experimental performance and emissions characteristics for gasoline engine using gasoline fuel surrogate was done by Topgül (2015). The detail specifications of the engines are presented in Table 4.4. The simulations were run for HCCI engine on same operating condition and using same fuel.

Table 4.4 Engine model specifications

Engine parameters	Value
Type	4 stroke, SI
Bore (mm)	80.26
Stroke (mm)	88.9
Displacement (L)	0.5117
No. of cylinders	1
Compression ratio	5.1-13.1
Connecting rod length (mm)	150
Intake Valve Close ($^{\circ}\text{CA}$)	-144
Exhaust Valve Open ($^{\circ}\text{CA}$)	140

Source: Topgül (2015)

4.4.1 Engine Performance

Figure 4.14 presents the variation of in-cylinder pressure between gasoline engine and HCCI engine at a constant speed of 3000 rpm and full load condition using gasoline as a fuel. The in-cylinder pressure condition of the HCCI engine was selected at a best case condition of 393 K intake temperature, when less knocking occurred. The

in-cylinder pressure for the HCCI engine is higher than for the SI engine. The maximum pressure for the HCCI engine is 48.41 bar and 43.56 bar for the SI engine.

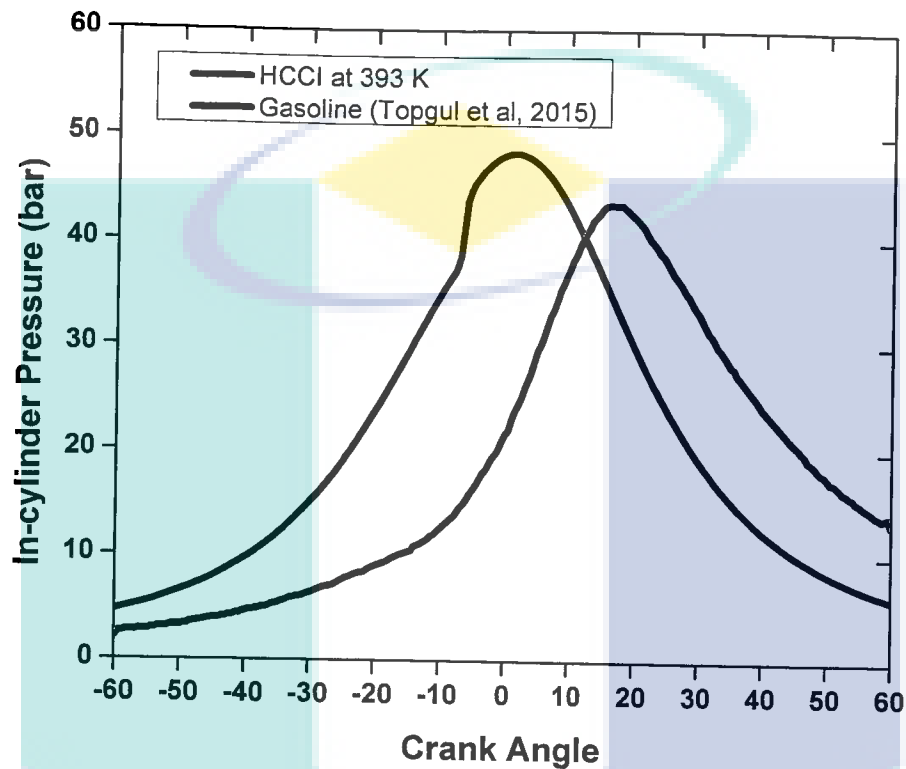


Figure 4.14 The variation of in-cylinder pressure between gasoline engine and HCCI engine at a constant speed of 3000 rpm and full load condition

It can be seen from Figure 4.14 that the combustion was happened in HCCI engine in a short time compared to SI engine. The combustion was started at 9°CA BTDC and the in-cylinder pressure was increased faster and reached the peak approximately within 10°CA. On the other hand, combustion of SI engine was started at 14°CA BTDC and the in-cylinder pressure was increased slowly and reached the peak approximately within 30°CA which is three times slower than for the HCCI. Hence, the combustion in the HCCI engine occurs instantaneously with a very fast combustion, as has been discussed by Raitanapaibule et al. (2005) and Tomita (2004). Therefore, the HCCI combustion requires very well controlled operating conditions to achieve the desired in-cylinder pressure behavior, otherwise knocking will take place.

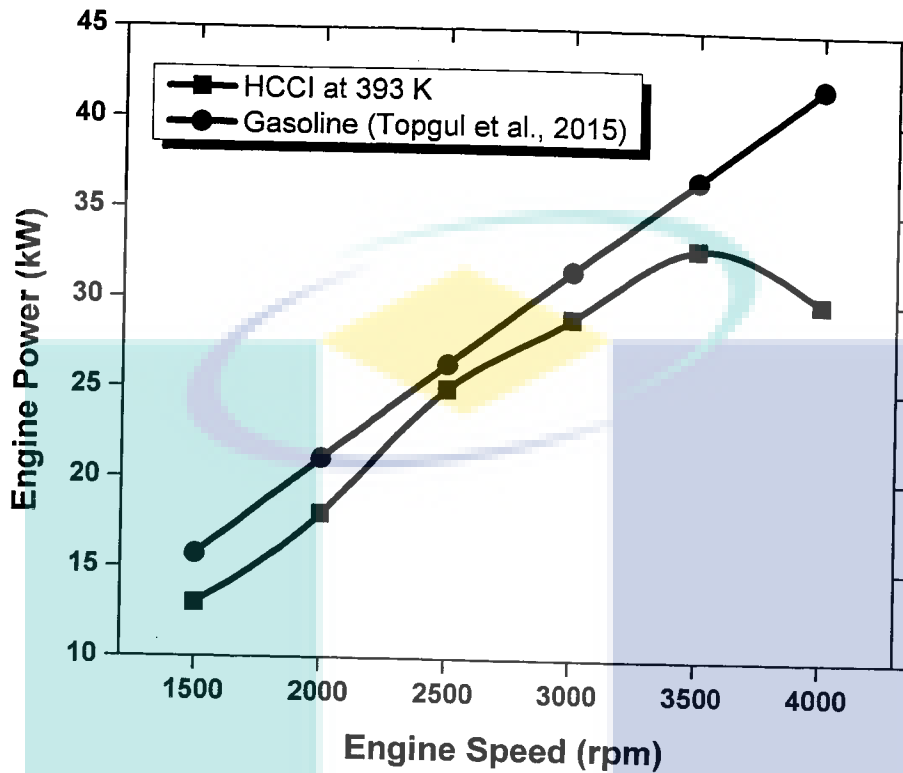


Figure 4.15 The variation of engine power between gasoline engine and HCCI engine at variable speed and full load condition

Figure 4.15 presents the variation of engine power between gasoline engine and HCCI engine at variable speed ranging from 1500 rpm to 4000 rpm and full load condition. From Figure 4.9 it is seen that the HCCI engine power is lower than gasoline engine in every speed condition. The maximum power for the HCCI engine is 33 kW at 3500 rpm and 42.01 kW for the SI engine at 4000 rpm. A reduction in HCCI engine power was described in Figure 4.8, where the in-cylinder pressure trace experienced a rapid increase in pressure when combustion occurred. This, in turn, will reduce the area under the curve: meaning the work produced by the HCCI engine decreases. Integrating the in-cylinder pressure over the volume produces work. Hence, the work produced by the HCCI and SI engines by using the in-cylinder pressure in Figure 4.8 is 275.94 J and 299.80 J respectively. Thus, the HCCI engine produces less work than its SI counterpart, which translates into low power.

Figure 4.16 presents the variation of BSFC between gasoline engine and HCCI engine at variable speed ranging from 1500 rpm to 4000 rpm and full load condition. When compared with the HCCI engine, the BSFC for HCCI is higher than the SI in every speed condition, as presented in Figure 4.10. The HCCI engine has the best BSFC at 264.99 g/kW-hr, where the SI has a minimum BSFC of 260.22 g/kW-hr. When the gasoline engine operates in highest speed condition, the BSFC marginally increases to 275.68 g/kW-hr. Thus, the HCCI engine has up to 3.60% higher BSFC than the gasoline engine at highest speed. This is because the power generated by the HCCI engine is lower due to the low compression ratio of the engine. However, if the BSFC can be maintained lower than SI, the HCCI engine would be a good option in the near future. The BSFC for the HCCI engine can be improved by using other parameters to control the combustion such as intake temperature, leaner mixture, exhaust gas recirculation etc.

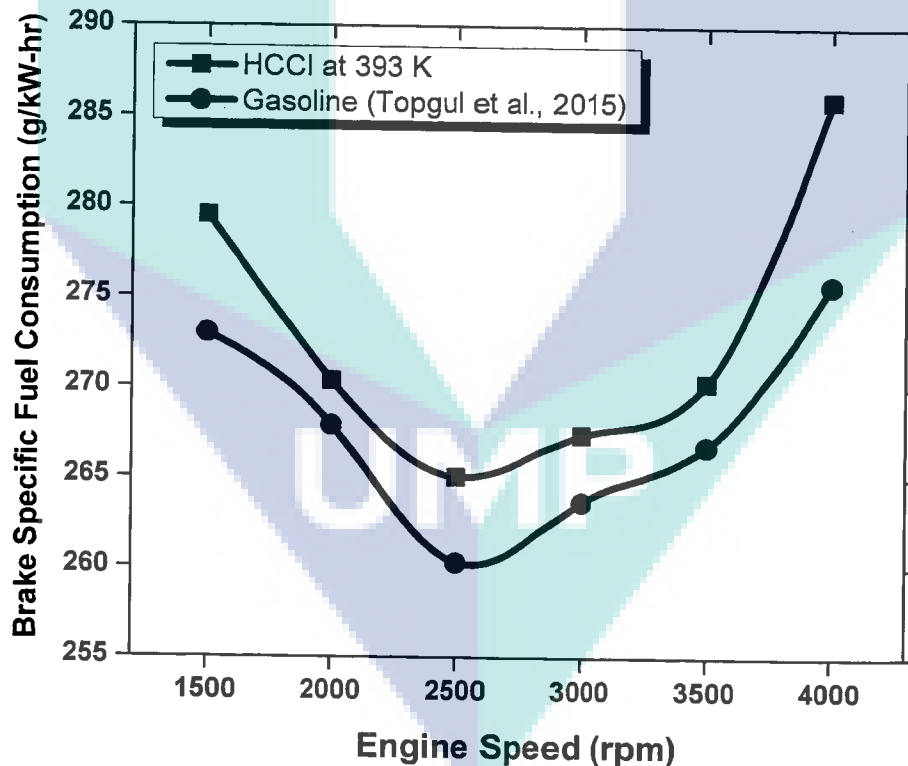


Figure 4.16 The variation of BSFC between gasoline engine and HCCI engine at variable speed and full load condition

Figure 4.17 presents the variation of BTE between gasoline engine and HCCI engine at variable speed ranging from 1500 rpm to 4000 rpm and full load condition. From Figure 4.17, it is seen that HCCI provides highest BTE at 3500 rpm whereas gasoline engine provides at 2500 rpm. The HCCI engine BTE increases with the increase of engine speed up to 3500 rpm and then gradually decreases. When the BTE between the two modes of combustion is compared, the HCCI engine yields a lower efficiency than the gasoline engine. The HCCI engine has a maximum efficiency of 30.8%, where the gasoline engine has efficiency up to 31.44%. This is because the power generated by the HCCI engine is lower due to the low compression ratio of the engine. Therefore, given a small difference in engine efficiency between gasoline and HCCI engines at the same operating condition, the HCCI engine can produce a better result if more tuning is carried out.

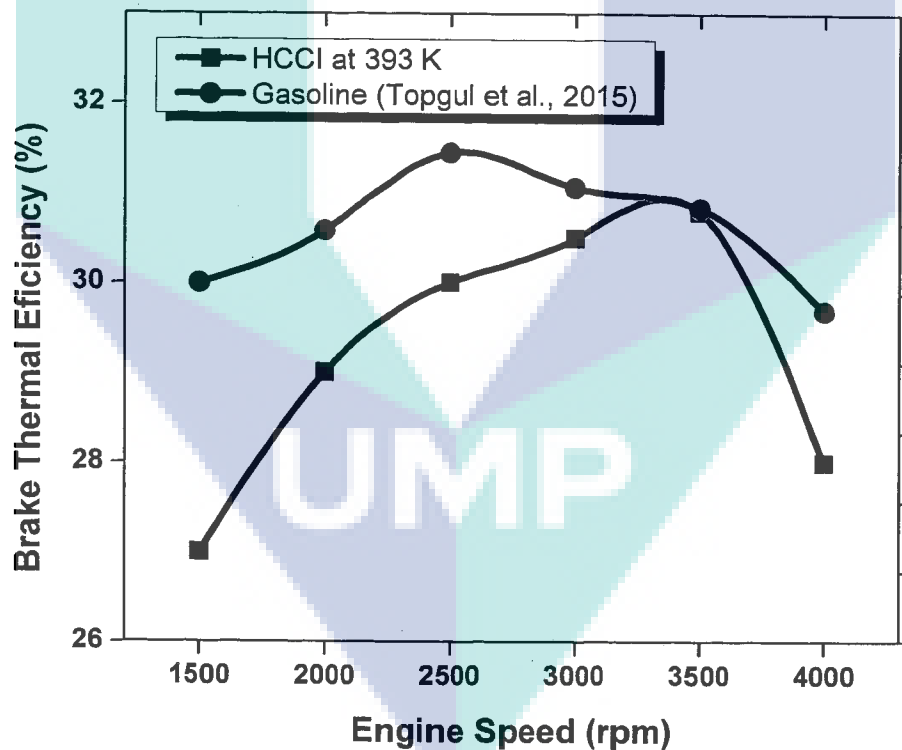


Figure 4.17 The variation of BTE between gasoline engine and HCCI engine at variable speed and full load condition

4.4.2 Engine Emissions

Figure 4.18 presents the variation of HC emission between gasoline engine and HCCI engine at variable speed ranging from 1500 rpm to 4000 rpm and full load condition. A significant difference in HC emission is seen between gasoline engine and HCCI engine. The HC emission from HCCI engine decreases with the increase of engine speed. When the HC emission between the two modes of combustion is compared, the HCCI engine yields a very higher amount of HC than the gasoline engine. The HCCI engine has a maximum HC emission of 976 ppm, where the gasoline engine has HC emission up to 176.95 ppm. This is due to the nature of this type of combustion.

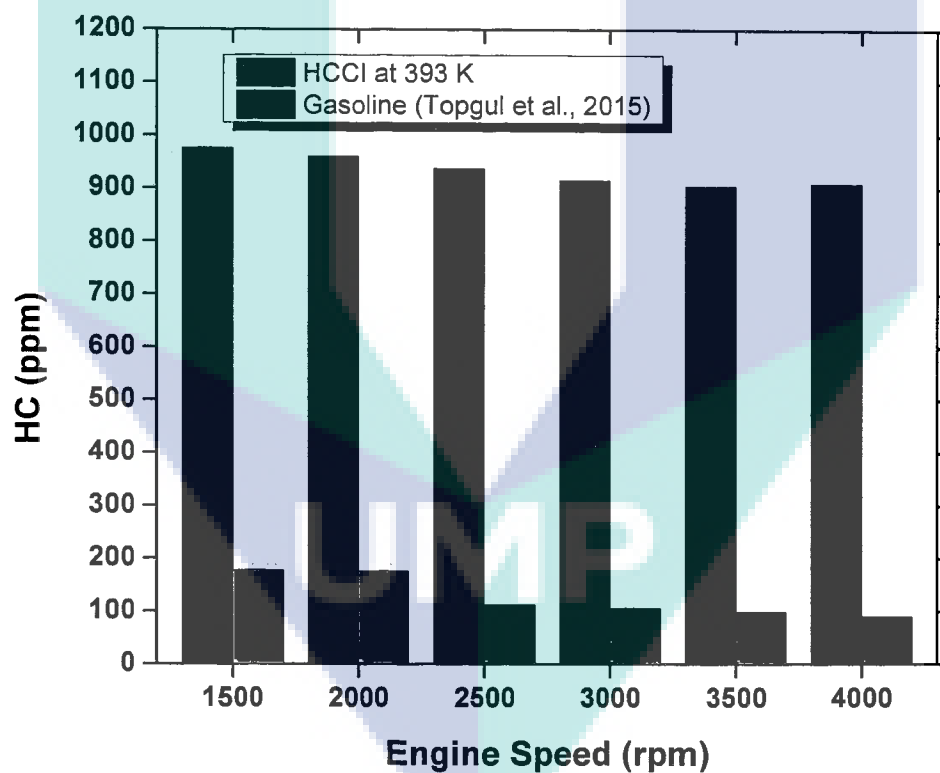


Figure 4.18 The variation of HC emission between gasoline engine and HCCI engine at variable speed and full load condition

For low combustion temperature, incomplete combustion is occurred and ultimately HC emissions is produced (Bression et al., 2008; Ganesh et al., 2008). HC is

mainly formed in the crevices of the cylinder which are so cold for complete consumption (Aceves et al., 2001a). Higher concentrations of hydrogen and natural gas in gasoline engines have the ability to reduce UHC emission level, because the gaseous state of hydrogen and natural gas will reduce the wall wetting effect on the cylinder liner (Cho et al., 2007).

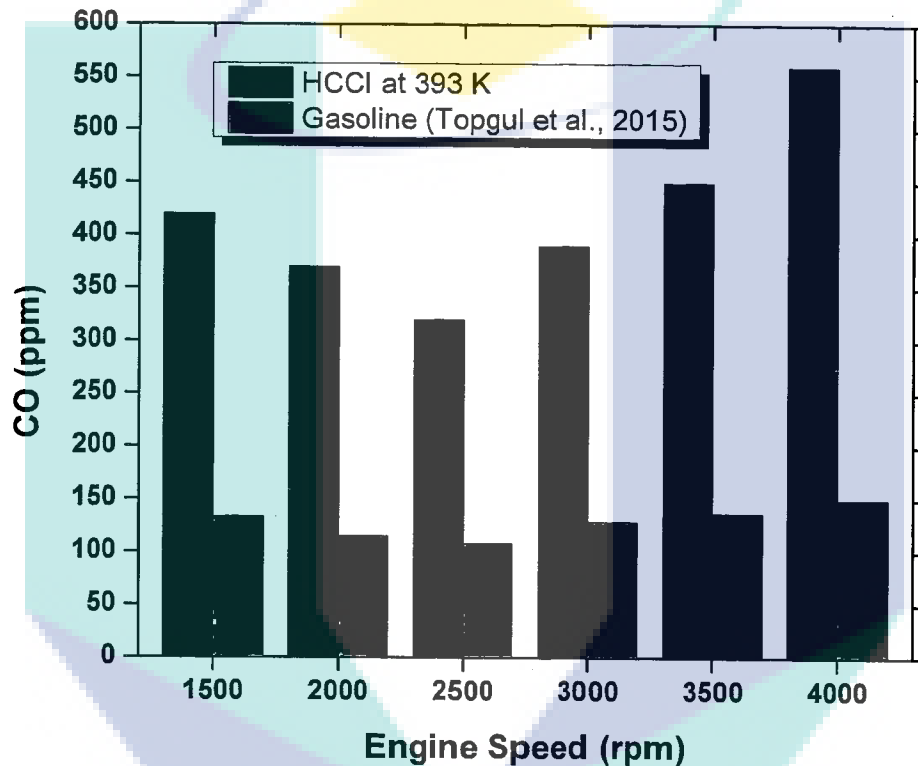


Figure 4.19 The variation of CO emission between gasoline engine and HCCI engine at variable speed and full load condition

Figure 4.19 presents the variation of CO emission between gasoline engine and HCCI engine at variable speed ranging from 1500 rpm to 4000 rpm and full load condition. A significant difference in CO emission is seen between gasoline engine and HCCI engine. This is one of the disadvantages of HCCI engine which is already mentioned in literature review. When the CO emission between the two modes of combustion is compared, the HCCI engine yields a very higher amount of CO than the gasoline engine. The HCCI engine has a maximum CO emission of 560 ppm, where the gasoline engine has HC emission up to 150 ppm. This is due to the nature of this type of combustion. The amount of CO₂ and CO are dependent on the combustion efficiency,

where the combustion efficiency can be defined as the ratio of CO_2 to the total of fuel carbon present in the exhaust including CO , CO_2 and UHC (Li et al., 2007). CO is formed by following $\text{RH-R-RO}_2\text{-RCHO-RCO-CO}$ equation, where R is the HC radical (Heywood, 1988). CO is mainly formed in the crevices of the cylinder which are so cold for complete consumption (Aceves et al., 2001a). In addition, for complete reaction of the conversion from CO to CO_2 needs temperature above 1500 K (Dec, 2002). However, CO formation is occurred in case of HCCI combustion at low load peak burned gas temperature remains below that required level.

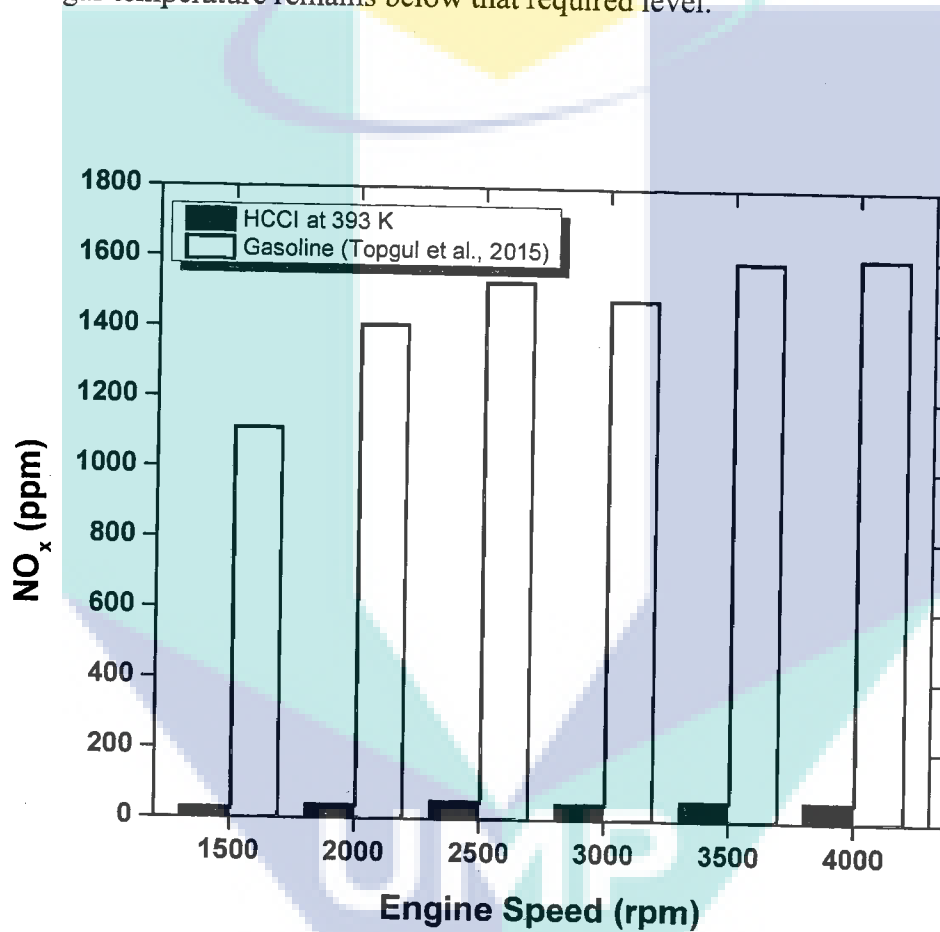


Figure 4.20 The variation of NO_x emission between gasoline engine and HCCI engine at variable speed and full load condition

Figure 4.20 presents the variation of NO_x emission between gasoline engine and HCCI engine at variable speed ranging from 1500 rpm to 4000 rpm and full load condition. A significant difference in NO_x emission is seen between gasoline engine and HCCI engine. This is one of the advantages of HCCI engine which is already mentioned in literature review. When the NO_x emission between the two modes of combustion is

compared, the HCCI engine yields a very lower amount of NO_x than the gasoline engine. The HCCI engine has a maximum NO_x emission of 60 ppm, where the diesel engine has NO_x emission up to 1609.24 ppm. This is due to the nature of this type of combustion.

4.5 Influence of Engine Parameters

In this section, the effect of engine speed, intake air temperature, intake air pressure and compression ratio on combustion and performance characteristics of HCCI engine is investigated using numerical simulations for both diesel HCCI and gasoline HCCI. The engine specifications and fuels used for validation purposes were also used here to investigate the effects of engine parameters.

4.5.1 Diesel HCCI

Engine speed is an important parameter which has a significant effect on combustion and performance of HCCI engines. Figure 4.21 illustrates the effect of engine speed on diesel HCCI combustion and performance for a constant intake temperature of 333 K. Engine speed was varied from 600 rpm to 1200 rpm. From the Figure 4.21(a) it is clearly seen that in-cylinder pressure increases with increasing engine speed up to 900 rpm and then decreases with further increasing engine speed. The most important reason is heat loss through cylinder wall during the compression stroke. With the engine speed increasing, the accumulated heat loss during the compression stroke reduced significantly because of the shorter cyclic period, which increases the in-cylinder temperature at the end of compression stroke. Therefore, the chamber could achieve a higher maximum pressure at higher engine speed due to less heat loss through the cylinder wall (Zhang et al., 2015). In addition, peak pressure location is retarded with the increase of engine speed. This is due to a significantly retarded MCS, as presented in Figure 4.21(b). The HRR during the MCS is also reduced with retarded combustion due to the increasing combustion chamber volume after top dead center. This leads to lower combustion chamber temperatures and a corresponding decrease in the oxidation reaction rates (García et al., 2009a). However, the effect of engine speed on the LTR phase tends to be relatively weak, reflecting its strong dependence on temperature history (Zhang et al., 2014a).

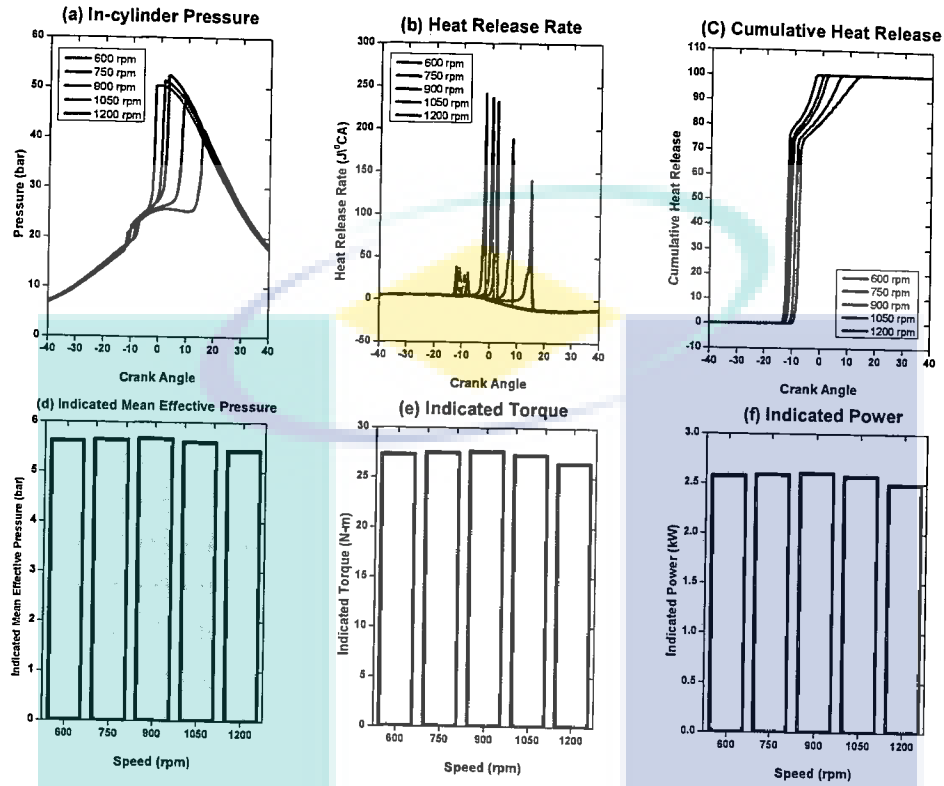


Figure 4.21 Influence of speed on combustion and performance characteristics in HCCI engine. CR=10.0, $T_{in}=333$ K, $P_{in}=100$ kPa, AFR=50

To observe the influence of engine speed on the performance of HCCI engines, five typical speeds were selected for the simulation. As are presented in Figures 4.21(d)-(f), IMEP, IT and IP increases with increasing engine speed up to 900 rpm and then decreases with further increasing engine speed. Maximum IMEP, IT and IP were obtained as 5.69 bar, 27.72 Nm and 2.61 kW. At higher engine speed the performance was less. This is because of that, with the increase of engine speed, the combustion duration is shortened with respect to time and affects the performance of HCCI engines (Canakci, 2008). Moreover, volumetric efficiency depends on engine speed. Because of the changing volumetric efficiency and increased friction forces at higher engine speed, the IMEP, IT and IP were less (Nishi et al., 2016).

Intake air temperature is the most critical and widely used engine operation parameter to control the phasing of HCCI combustion. Figure 4.22 illustrates the effect

of intake temperature on HCCI combustion and performance for a constant AFR of 50. Intake temperature of the air was varied from 333 K to 393 K. Stable HCCI combustion was obtained for a wide range of temperatures. As presented in Figure 4.22(a) the auto-ignition timing was advanced with the increase of intake air temperature. The phasing of both LTR and MCS were advanced. Furthermore, it can also be clearly seen from Figure 4.22(b) that rapid HRR occurs due to higher pressure rise rate. Thus, HCCI combustion deteriorated due to knocking and cylinder pressure decreased with the increase of inlet air temperature. The LTR heat release profiles were found to be quite similar, although they were advanced as temperature increased. However, increasing the intake temperature significantly enhances the HRR of the MCS. The increasingly advanced phasing of the MCS contributes to the increased HRR (Uyumaz, 2015). To investigate the influence of intake air temperature on the performance of HCCI engines, five typical temperatures were selected for the simulation. As are presented in Figures 4.22(d)-(f) IMEP, IT and IP decrease with increasing intake temperature. This is because there are key chemical reactions in the low-temperature phase. These reactions depend on the system temperature and AFR. $C_7H_{15}O_2=C_7H_{14}OOH$ is the most important reaction in low-temperature phase. $C_7H_{14}OOH$ retards the process of low-temperature oxidation, and it plays the most important role in the occurrence of the negative temperature coefficient (NTC) phase (Peng et al., 2005; Zhang et al., 2014a). Under the specific operating condition, the maximum IMEP, IT, and IP occur when intake temperature is 360 K. Obviously, the intake temperature is very critical, i.e., a small change of intake temperature leads to large variations in performance of HCCI.

Intake air pressure boosting has a significant effect on the combustion and performance of HCCI engines as well as is a common way to improve power output. In this study, the effect of boosting on HCCI combustion and performance was examined at a constant AFR and intake air temperature condition. As presented in Figure 4.23(a), boosting the intake pressure tends to significantly increase the peak cylinder pressure during the compression stroke. The reason is that the collision frequency among molecules increases with the increase of the boost pressure, which leads to the increase of the combustion reaction velocity (Liu et al., 2008). Since the quantity of fuel injected is increased as intake pressure increases to maintain a constant AFR, the LTR stage is advanced and intensified. This leads to a shorter NTC delay period and significantly advances phasing of the MCS, as presented in Figure 4.23(b). The reason for this is the

combustion reaction velocity which increases with the increasing boost pressure (Christensen et al., 2000; Olsson et al., 2004).

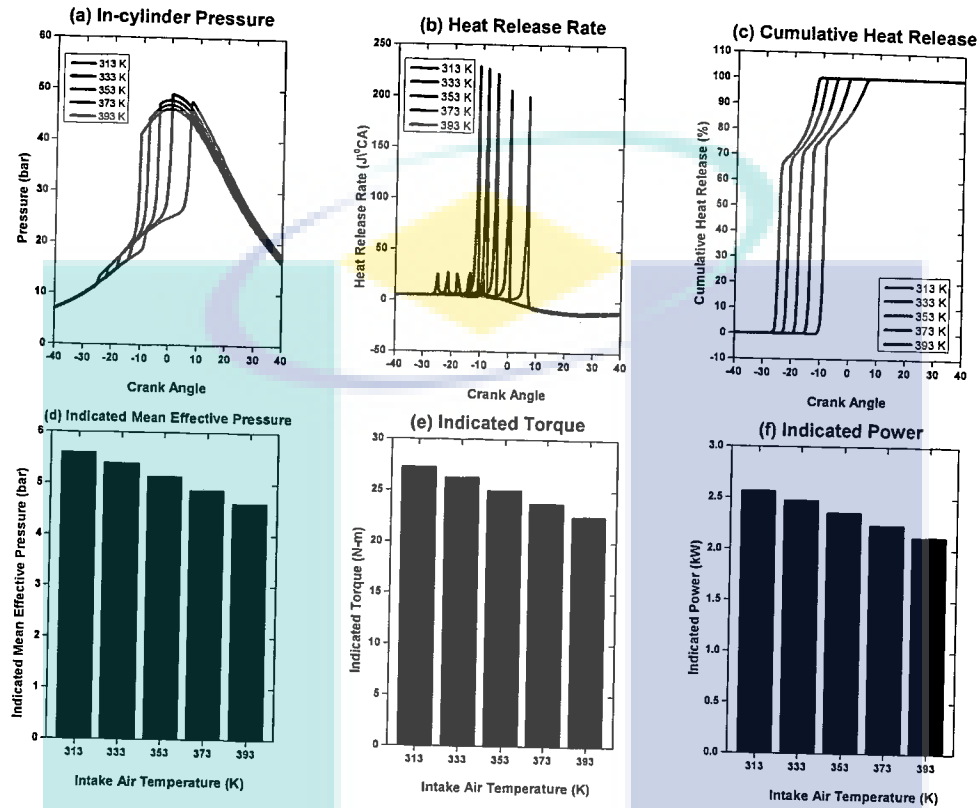


Figure 4.22 Influence of intake air temperature on combustion and performance characteristics in HCCI engine. CR=10.0, N=900 rpm, P_{in} =100 kPa, AFR=50

To investigate the influence of intake air pressure on the performance of HCCI engines, five typical pressures ranging from 100 kPa to 200 kPa were selected for the simulation. As are presented in Figures 4.23(d)-(f) IMEP, IT and IP increases with increasing intake air pressure. The maximum IMEP, IT, and IP were obtained at 200 kPa. The use of a higher inlet pressure can bring in more air, which leads to an increase of the amount of fuel that can be injected and an increase of the maximum IMEP, IT and IP those can be achieved. On the other hand, the engine can operate stably at a leaner air fuel ratio with an increasing inlet pressure, which leads to lower values of IMEP, IT and IP. However, the benefits of intake boost would have been much greater if the combustion phasing had been controlled independently using different intake temperature, EGR, or other methods. The results indicate that an increase in the boost

pressure causes the need of leaner mixture, and requires more advanced injection timing to achieve the maximum engine torque (Hosseini et al., 2007; Olsson et al., 2001).

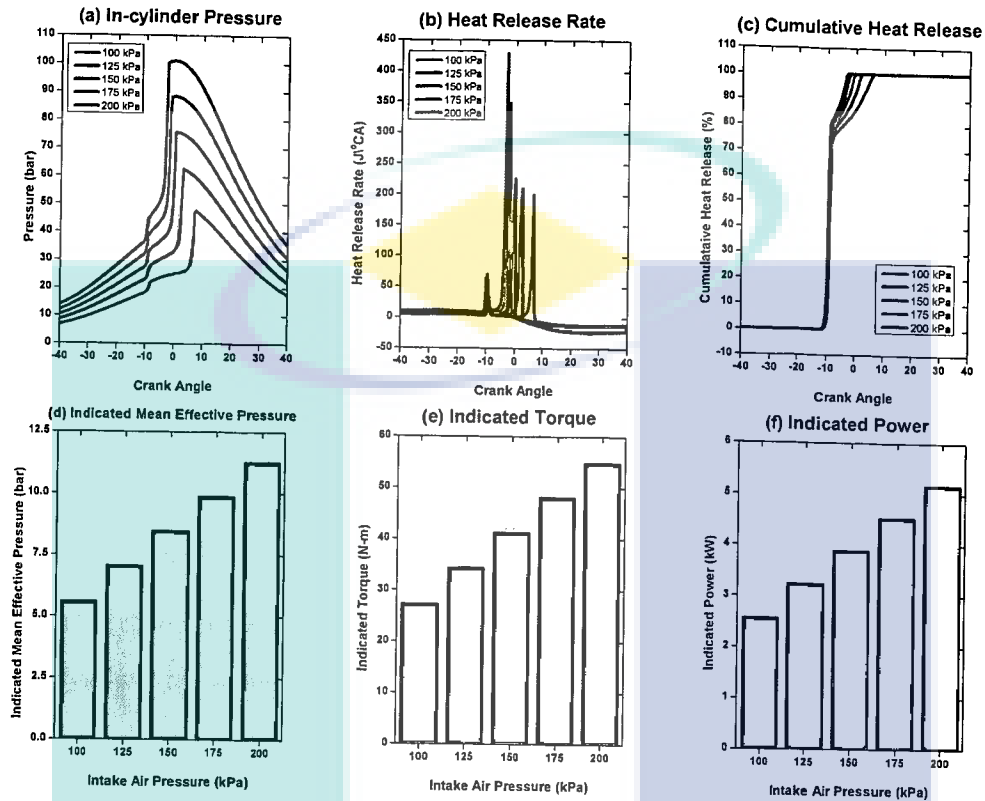


Figure 4.23 Influence of intake air pressure on combustion and performance characteristics in HCCI engine. CR=10.0, N=900 rpm, T_{in} =333 K, AFR=50

Compression ratio is another important engine parameter which also has a significant effect on combustion and performance characteristics of HCCI engines. Figure 4.24 presents that increasing the compression ratio advances the combustion process and increases the peak cylinder pressures. This is primarily due to the effect of increased compression temperatures and pressures as the compression ratio increases, which enhances diesel oxidation. As presented in Figure 4.24(b), the phasing of both LTR and MCS phases were advanced with increasing compression ratio (Li et al., 2006). To investigate the influence of compression ratio on the performance of HCCI engines, five typical compression ratios were selected for the simulation. As are presented in Figures 4.24(d)-(f) IMEP, IT and IP increases with increasing compression ratio. This is because there are key chemical reactions which occur during the compression stroke. These reactions depend on the in-cylinder pressure and

temperature. Due to increasing compression ratio oxidation of diesel is enhanced which ultimately help to increase IMEP, IT and IP (Peng et al., 2005). Under the specific operating condition, the maximum IMEP, IT, and IP occur when the compression ratio is 16. It is obvious that the compression ratio is very critical, i.e., a small change of compression ratio leads to large variations in performance of HCCI.

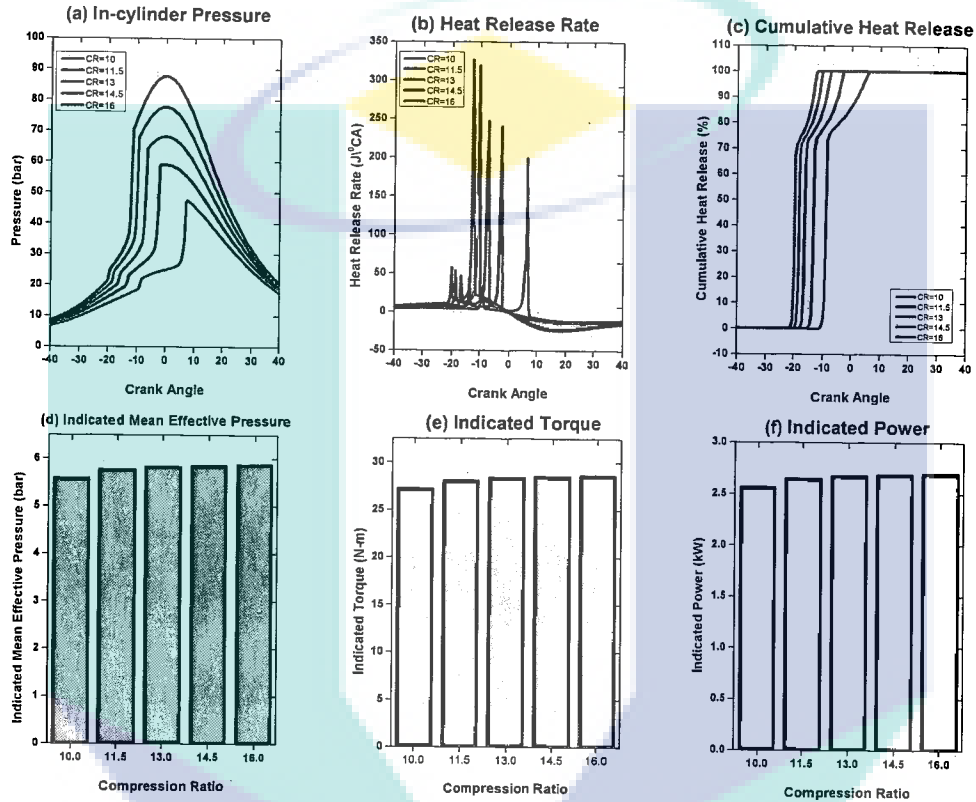


Figure 4.24 Influence of Compression Ratio on combustion and performance characteristics in HCCI engine. $N=900$ rpm, $T_{in}=333$ K, $P_{in}=100$ kPa, $AFR=50$.

4.5.2 Gasoline HCCI

Engine speed is an important parameter which has a significant effect on combustion and performance of HCCI engines. Figure 4.25 illustrates the effect of engine speed on HCCI combustion and performance for a constant intake temperature of 393 K. Engine speed was varied from 600 rpm to 1800 rpm. From the Figure 4.25(a) it is clearly seen that in-cylinder pressure increases with increasing engine speed up to 1500 rpm and then decreases with further increasing engine speed. Peak pressure location is retarded with the increase of engine speed. This is due to a significantly

retarded MCS, as presented in Figure 4.25(b). The HRR during the MCS is also reduced with retarded combustion due to the increasing combustion chamber volume after top dead center. This leads to lower combustion chamber temperatures and a corresponding decrease in the oxidation reaction rates. However, the effect of engine speed on the LTR phase tends to be relatively weak, reflecting its strong dependence on temperature history (Zhang et al., 2014a). To observe the influence of engine speed on the performance of HCCI engines, five typical speeds were selected for the simulation. As are presented in Figures 4.25(d)-(f), IMEP, IT and IP increases with increasing engine speed up to 1500 rpm and then decreases with further increasing engine speed. This is because of that, with the increase of engine speed, the combustion duration is shortened with respect to time and affects the performance of HCCI engines (Canakci, 2008).

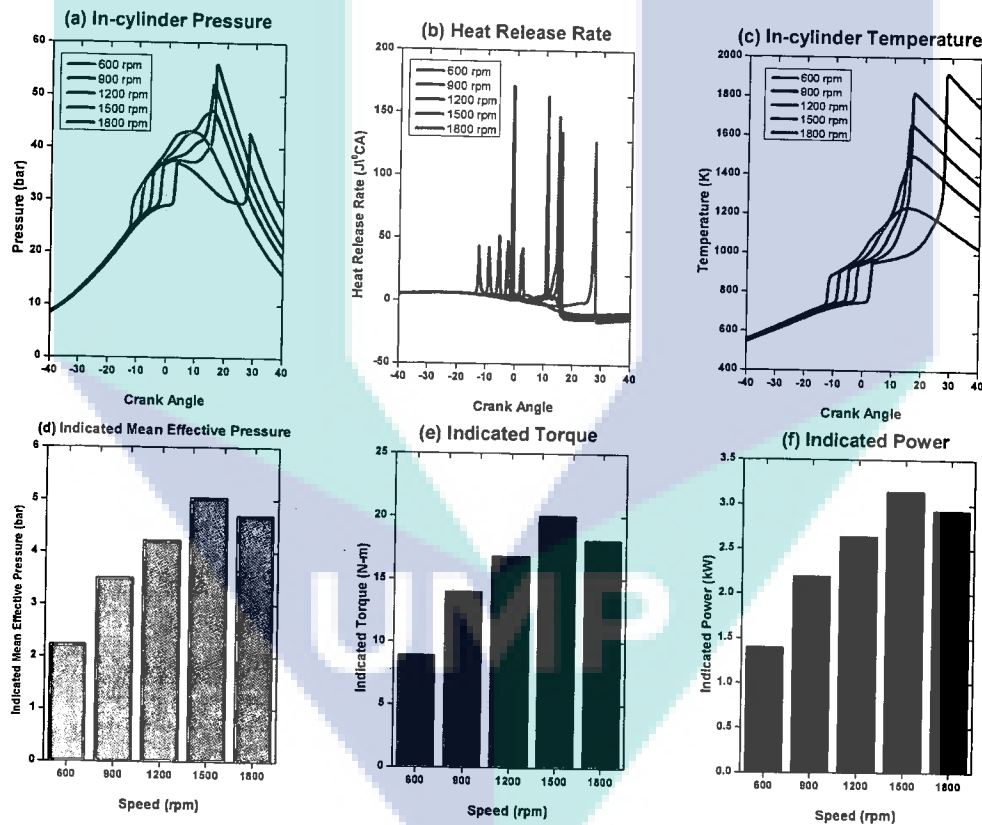


Figure 4.25 Influence of speed on combustion and performance characteristics in HCCI engine. CR=12.0, $T_{in}=393$ K, $P_{in}=100$ kPa, AFR=40

Intake air temperature is the most critical and widely used engine operation parameter to control the phasing of HCCI combustion. Figure 4.26 illustrates the effect of intake temperature on HCCI combustion and performance for a constant AFR of 40.

Intake temperature of the air was varied from 373 K to 453 K. Stable HCCI combustion was obtained for a wide range of temperatures. As presented in Figure 4.26(a) the auto-ignition timing was advanced with the increase of intake air temperature. The phasing of both LTR and MCS were advanced. Furthermore, it can also be clearly seen from Figure 4.26(b) that rapid HRR occurs due to higher pressure rise rate. Thus, HCCI combustion deteriorated due to knocking and cylinder pressure decreased with the increase of inlet air temperature. The LTR heat release profiles were found to be quite similar, although they were advanced as temperature increased. However, increasing the intake temperature significantly enhances the HRR of the MCS. The increasingly advanced phasing of the MCS contributes to the increased HRR (Uyumaz, 2015).

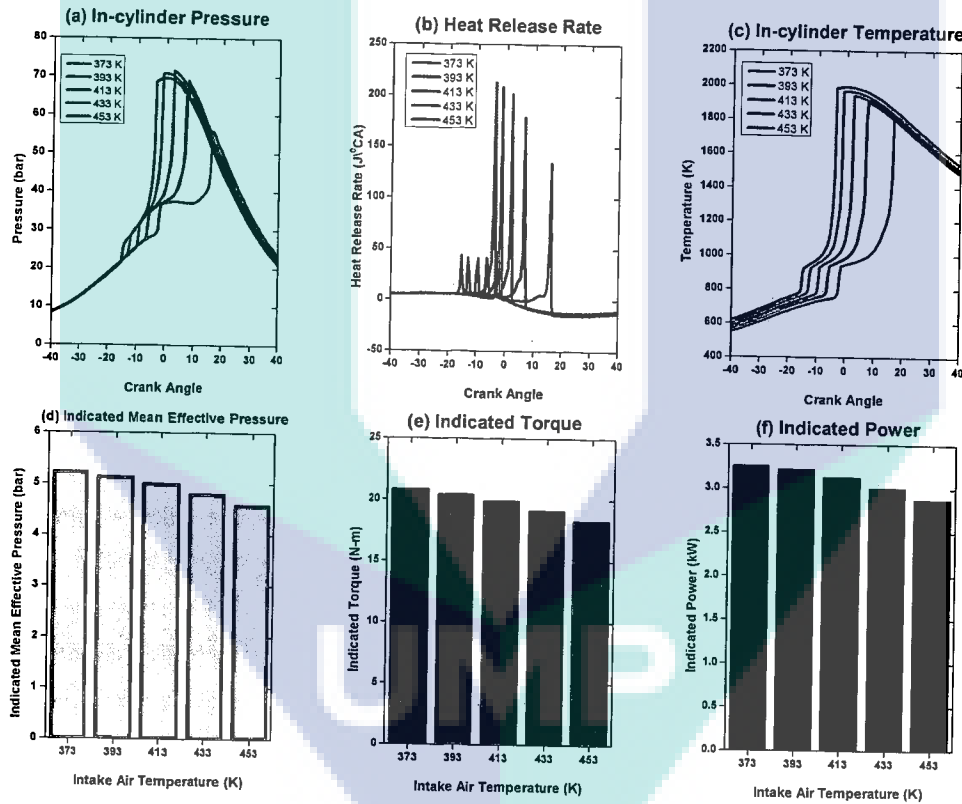


Figure 4.26 Influence of intake air temperature on combustion and performance characteristics in HCCI engine. CR=12.0, N=1500 rpm, P_{in} =100 kPa, AFR=40

To investigate the influence of intake air temperature on the performance of HCCI engines, five typical temperatures were selected for the simulation. As are presented in Figures 4.26(d), 4.26(e) and 4.26(f), IMEP, IT and IP decrease with increasing intake temperature. This is because there are key chemical reactions in the

low-temperature phase. These reactions depend on the system temperature and AFR. $C_7H_{15}O_2=C_7H_{14}OOH$ is the most important reaction in low-temperature phase. $C_7H_{14}OOH$ retards the process of low-temperature oxidation, and it plays the most important role in the occurrence of the negative temperature coefficient (NTC) phase (Peng et al., 2005; Zhang et al., 2014a). Under the specific operating condition, the maximum IMEP, IT, and IP occur when intake temperature is 373 K. Obviously, the intake temperature is very critical, i.e., a small change of intake temperature leads to large variations in performance of HCCI.

Intake air pressure boosting has a significant effect on the combustion and performance of HCCI engines as well as is a common way to improve power output. In this study, the effect of boosting on HCCI combustion and performance was examined at a constant AFR and intake air condition. As presented in Figure 4.27(a), boosting the intake pressure tends to significantly increase the cylinder pressure during the compression stroke. Since the quantity of fuel injected is increased as intake pressure increases to maintain a constant AFR, the LTR stage is advanced and intensified. This leads to a shorter NTC delay period and significantly advances phasing of the MCS, as presented in Figure 4.27(b). The reason for this is the combustion reaction velocity which increases with the increasing boost pressure (Christensen et al., 2000; Olsson et al., 2004). To investigate the influence of intake air pressure on the performance of HCCI engines, five typical pressures ranging from 100 kPa to 200kPa were selected for the simulation. As are presented in Figures 4.27(d), 4.27(e) and 4.27(f), IMEP, IT and IP increases with increasing intake air pressure. The maximum IMEP, IT, and IP were obtained at 200 kPa. The results indicate that an increase in the boost pressure causes the need of leaner mixture, and requires more advanced injection timing to achieve the maximum engine torque (Hosseini et al., 2007; Olsson et al., 2001).

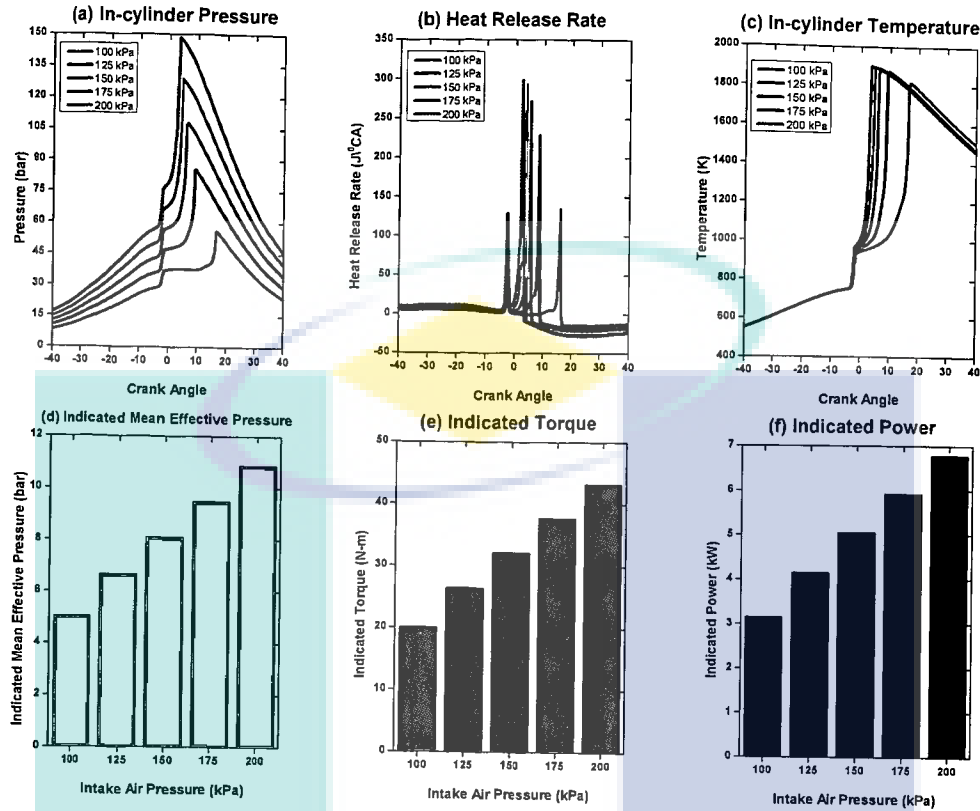


Figure 4.27 Influence of intake air pressure on combustion and performance characteristics in HCCI engine. CR=12.0, N=1500 rpm, $T_{in}=393$ K, AFR=40.

Compression ratio is another important engine parameter which also has a significant effect on combustion and performance characteristics of HCCI engines. Figure 4.28 presents that increasing the compression ratio advances the combustion process and increases the peak cylinder pressures. This is primarily due to the effect of increased compression temperatures and pressures as the compression ratio increases, which enhances gasoline surrogate fuel oxidation. As presented in Figure 4.28(b), the phasing of both LTR and MCS phases were advanced with increasing compression ratio (Li et al., 2006). To investigate the influence of compression ratio on the performance of HCCI engines, five typical compression ratios were selected for the simulation. As are presented in Figures 4.28(d), 4.28(e) and 4.28(f), IMEP, IT and IP increases with increasing compression ratio. This is because there are key chemical reactions which occur during the compression stroke. These reactions depend on the in-cylinder pressure and temperature. Due to increasing compression ratio oxidation of gasoline surrogate fuel is enhanced which ultimately help to increase IMEP, IT and IP (Peng et al., 2005).

Under the specific operating condition, the maximum IMEP, IT, and IP occur when the compression ratio is 16. It is obvious that the compression ratio is very critical, i.e., a small change of compression ratio leads to large variations in performance of HCCI.

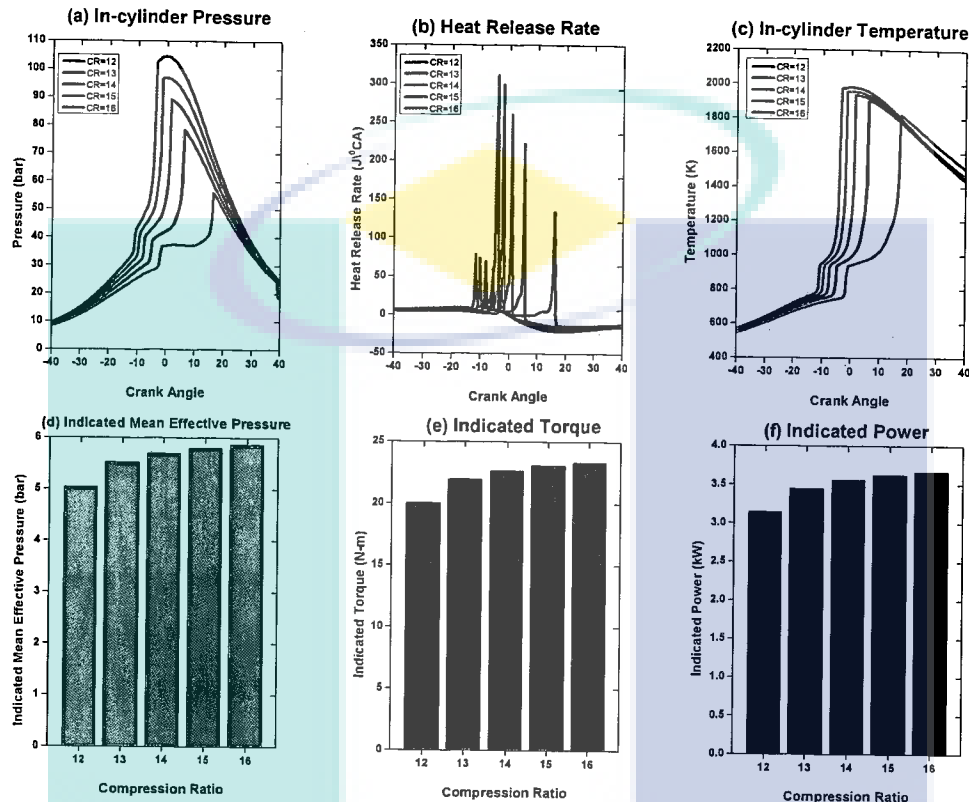


Figure 4.28 Influence of Compression Ratio on combustion and performance characteristics in HCCI engine. $N=1500$ rpm, $T_{in}=393$ K, $P_{in}=100$ kPa, $AFR=40$

4.6 Different Fueled HCCI

Intake temperature plays an important role in HCCI combustion because HCCI combustion depends on the chemical kinetics. Charge mixture is compressed until autoignition temperature reaches (Dec, 2009; Heywood, 1988). In addition, suitable fuel should be selected avoiding misfire and knocking. In this way, alcohols resist to not only knocking combustion but also reducing the harmful exhaust emissions in HCCI combustion (Padala et al., 2013). As an alternative fuel, alcohol seems to be the most promising choices among other fuels in order to control HCCI combustion. In this study, the effects of pure n-heptane, and ethanol/n-heptane mixtures and butanol/n-heptane mixtures were investigated on HCCI combustion, performance and emissions

using numerical simulations. N-heptane percentages used in the ethanol and butanol mixtures were chosen 70% and 85% by volume where E15 contains 85% n-heptane and 15% ethanol; E30 contains 70% n-heptane and 30% ethanol; Bu15 contains 85% n-heptane and 15% butanol as well as Bu30 contains 70% n-heptane and 30% butanol. A numerical study was performed at 900 rpm engine speed and constant lambda ($\lambda=2$) at different intake temperatures of 313 K, 333 K, 353 K, 373 K and 393 K in order to observe the controlling of HCCI combustion. The reason of selecting this range of intake temperatures is that lower intake air temperature cannot achieve the test fuels' auto-ignition temperature which ultimately is the reason for failing to achieve HCCI combustion. Similarly, higher intake air temperature creates higher in-cylinder pressure and temperature which ultimately causes knocking (Cinar et al., 2015; Uyumaz, 2015).

4.6.1 Combustion Characteristics

The effects of ethanol and butanol fuel blends with n-heptane and neat n-heptane on cylinder pressure and HRR dependent on the crank angle with different intake temperatures are presented in Figures 4.29 and 4.30. N-heptane was used as base fuel in the simulations and the test results were compared with n-heptane/ethanol and n-heptane/butanol blends. The pressure rise rate increased a little bit with E30 and Bu30 fuels. It can also be mentioned that SOC was delayed a little bit as the amount of ethanol and butanol increased in the test fuels. Autoignition was increased with the increase of intake temperature for all test fuels. More molecules participated in the chemical reactions. Besides, the chemical reactions were improved between fuel and oxygen molecules at higher intake temperatures (Ra et al., 2008). Thus autoignition occurred easily. Maximum cylinder pressure was obtained with E30 and Bu30. HRR increases with the increase of intake temperature up to 15% of ethanol and butanol but it decreases with increasing intake temperature when ethanol and butanol percentage increases up to 30%. It was observed that the most significant effect of intake temperature on HCCI combustion was autoignition timing. Although the SOC was affected by the intake temperature, there was a slight difference in cylinder pressure for all test fuels.

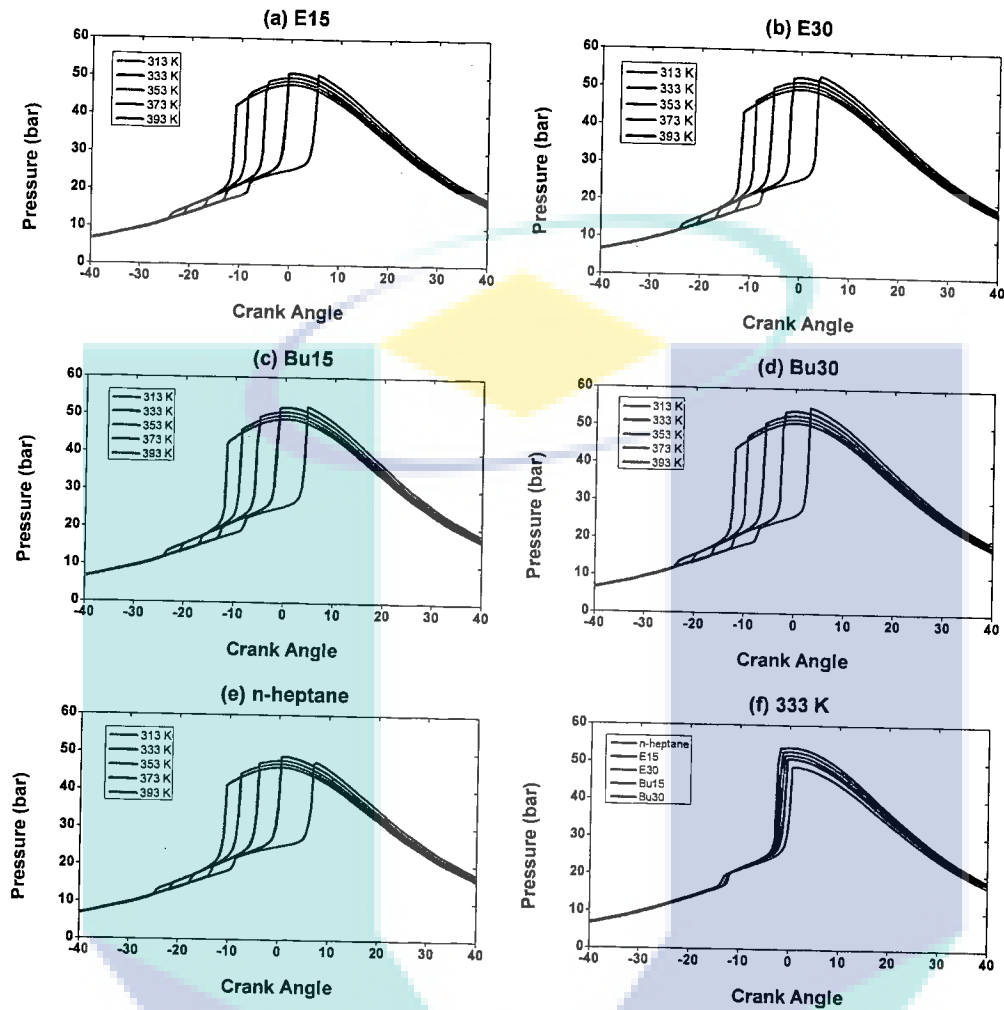


Figure 4.29 The variation of in-cylinder pressure of HCCI combustion at constant lambda $\lambda = 2$ and 900 rpm engine speed with different intake temperatures and test fuels

At high intake temperatures, autoignition can occur easily in HCCI combustion. As can be seen, in Figure 4.30 the SOC was delayed with the increase of the amount of the ethanol and butanol in the test fuels. N-heptane was auto-ignited earlier than all the other test fuels due to zero octane number and higher heating value. At 393 K maximum heat release was obtained with Bu15. Maximum cylinder pressure decreased with n-heptane due to earlier autoignition (Lü et al., 2006). In-cylinder temperature and pressure should be adequately high at the end of the compression stroke in order to start the chemical reactions in HCCI combustion. The in-cylinder temperature at the end of compression stroke increases with the increase of intake temperature. However, intake

temperature is limited because of the higher pressure rise rate on HCCI combustion (Dec, 2009). It also causes the cyclic variations which are the indication of durability and stability of the IC engines (Agarwal, 2007).

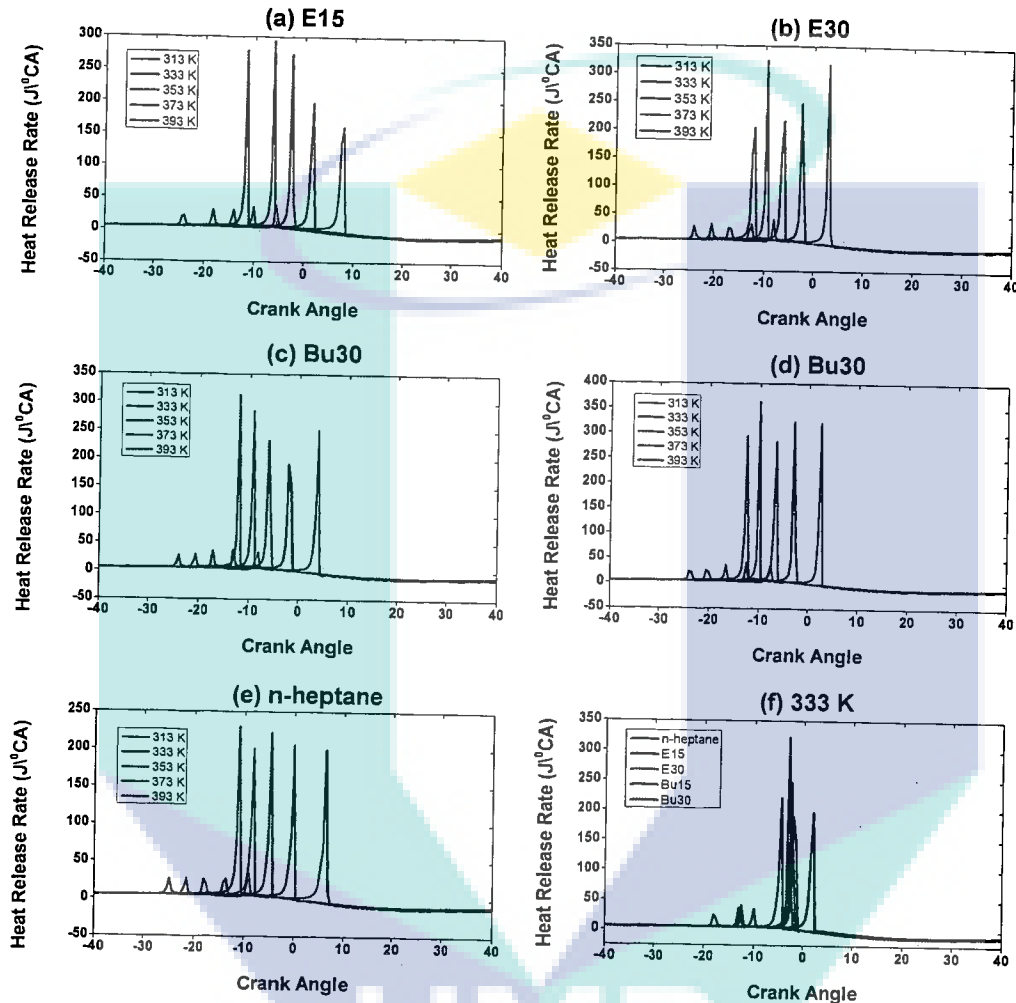


Figure 4.30 The variation of HRR of HCCI combustion at constant lambda, $\lambda = 2$ and 900 rpm engine speed with different intake temperatures and test fuels

The effects of intake temperature with different test fuels on SOC are presented in Figure 4.31. SOC is strongly controlled by chemical and physical properties of the fuel, temperature, and pressure at the end of the compression stroke in HCCI combustion (Olsson et al., 2002a). Among them, intake temperature is one of the most dominant factors affecting the start of autoignition. In this study, SOC was determined with the HRR which rises from zero to a positive value. It was found that increased

intake temperature caused combustion to advance for each test fuel. Simulation results showed that earliest autoignition was obtained with n-heptane. Minimum SOC was obtained with E30 test fuel. It could be implied that the SOC was delayed as the amount of ethanol and butanol increased in the test fuels because higher octane number alcohol tends to retard the autoignition. Earlier autoignition results in knocking combustion which damages the engine parts (Maurya et al., 2011). As a result, high octane number alcohol fuel seems to be the most promising alternative fuel in HCCI combustion in order to prevent knocking combustion and to extend operating range.

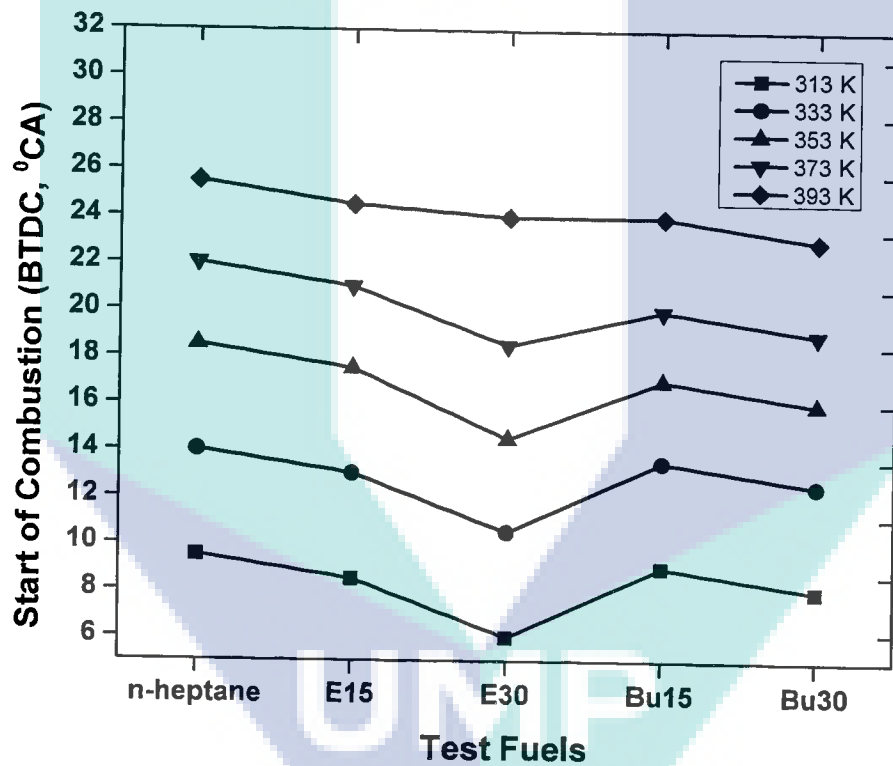


Figure 4.31 The variation of SOC of HCCI combustion at constant lambda, $\lambda = 2$ and 900 rpm engine speed with different intake temperatures and test fuels

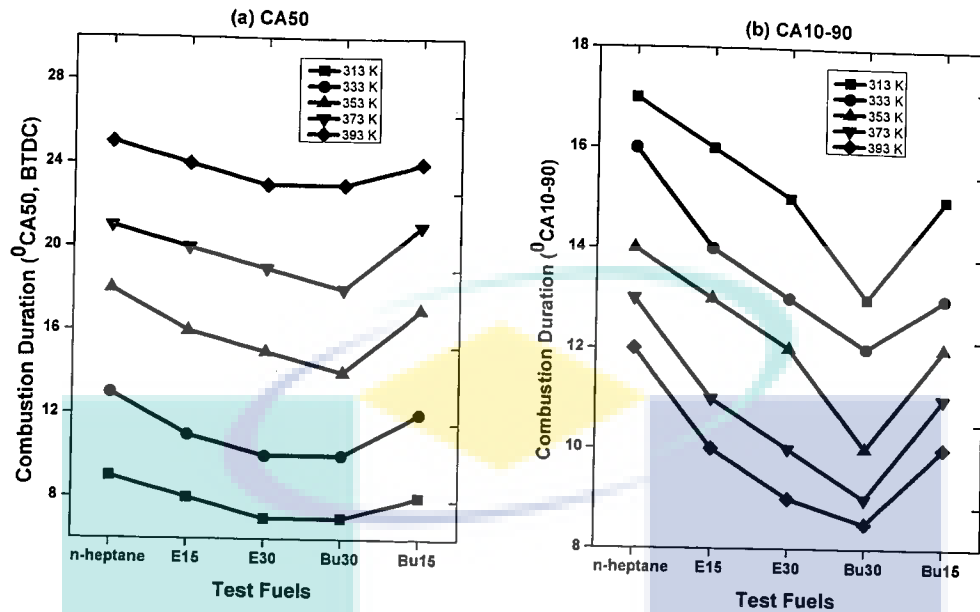


Figure 4.32 The variation of combustion duration (CA50 and CA10-90) of HCCI combustion at constant lambda, $\lambda = 2$ and 900 rpm engine speed with different intake temperatures and test fuels

Figure 4.32 presents the combustion duration (CA50 and CA10-90) of test fuels at different intake temperatures. Figure 4.32 (a) presents the variation of CA50 with test fuels at different intake temperatures. Crank angle degrees define the points versus crank angle where the CA50 was obtained before top dead center. It is seen that CA50 closes to TDC as the intake temperature decreases. CA50 was determined near TDC with Bu30 due to faster combustion. It can be inferred from Figure 4.32 (b) that CA10-90 decreases as intake temperature increases. Minimum combustion duration was obtained at 393 K for each test fuel. At high intake temperatures, CA10-90 decreases due to the improvement of chemical reactions and increasing of the activated molecules during the combustion reaction. It results in shorter combustion duration (Lu et al., 2011b). Furthermore, combustion duration (CA10-90) decreased when the mass fraction of ethanol and butanol increased in the test fuel. It was seen that the increase of octane number of test fuels caused the decrease on combustion duration. The longest combustion duration was obtained with n-heptane due to knocking (Lü et al., 2006).

4.6.2 Performance Characteristics

The variation of IMEP with test fuels at different intake temperatures on HCCI combustion is presented in Figure 4.33. It can be seen that IMEP decreases with the increase of intake temperature. It also causes the decrease of volumetric efficiency at high intake temperatures because hot air has lower density compared to cold air. The simulation has run with the leaner mixture at constant excessive air coefficient $\lambda = 2$ on HCCI combustion. So, the energy driven to the cylinder decreases. Thus, IMEP decreases especially at high intake temperatures as seen in Figure 4.33. It can be also concluded that IMEP decreases with n-heptane due to knocking although it has higher heating value compared to ethanol and butanol blends. There was no remarkable difference on imep when the E15 was used as a fuel in the simulations. However, IMEP of E30, Bu15 and Bu30 was higher than E15. Maximum imep was obtained with Bu30 as 6.51 bar at 313 K intake temperature. Imep increased by about 13.97% when compared to pure n-heptane at 313 K intake temperature. The reason of imep increase with Bu30 can be explained due to higher calorific value compared to ethanol. In addition, the density of ethanol and butanol is higher than n-heptane. It may be mentioned that it causes to drive more energy into the cylinder compared to n-heptane. Hence, the pressure at the end of combustion increases due to more fuel molecules participation into the chemical reactions (Uyumaz, 2015).

The effects of test fuels and intake temperatures on ITE of HCCI engine are presented in Figure 4.34. Thermal efficiency increased with the increase of intake temperature with n-heptane, E15, Bu15 and Bu30. It can be clearly noticed that autoignition can occur easily at high intake temperatures and autoignition conditions improve at each point of the combustion chamber. Thus, thermal efficiency increases. However, a small decrease was seen in thermal efficiency with n-heptane, E15, and E30 at 393 K intake temperature. It can be said that CA50 was determined a little bit far away from TDC with n-heptane, E15 and E30 compared to other test fuel at 393 K intake temperature as seen in Figure 4.28 because combustion occurred away from TDC. Maximum thermal efficiency was obtained as 54.36% with Bu30 test fuel at 393 K intake temperature. Similarly, CA50 was determined near TDC with Bu30 as seen in Figure 4.26(a).

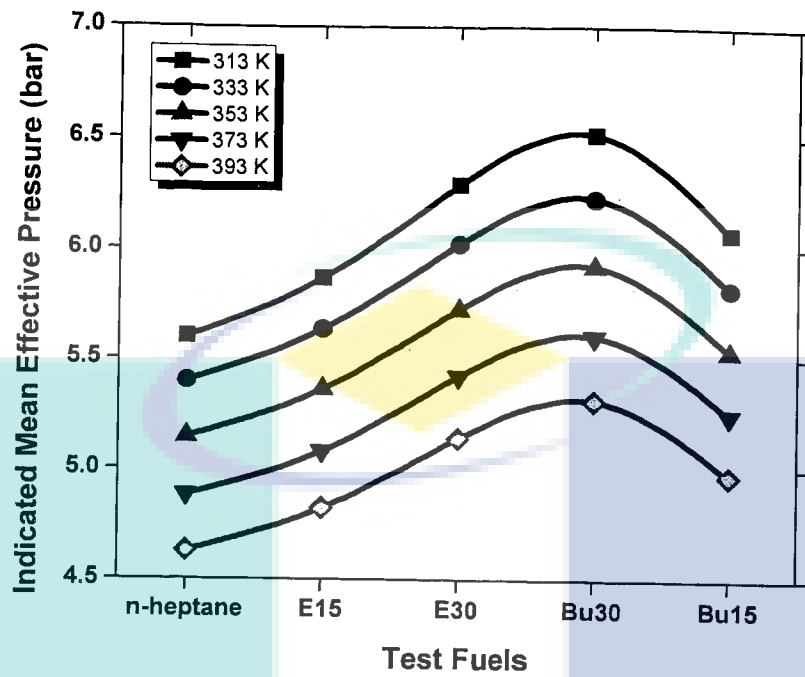


Figure 4.33 The variation of indicated mean effective pressure on HCCI combustion at constant lambda, $\lambda = 2$ and 900 rpm engine speed with different intake temperatures and test fuels

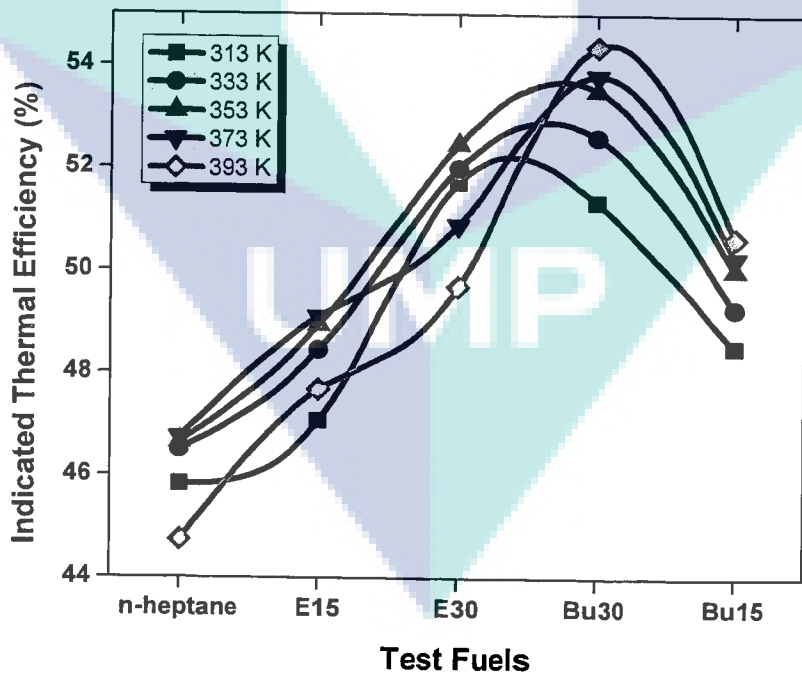


Figure 4.34 The variation of indicated thermal efficiency of HCCI combustion at constant lambda, $\lambda = 2$ and 900 rpm engine speed with different intake temperatures and test fuels

Chemical reactions improve when the combustion occurs near TDC due to higher cylinder pressure at smaller volume in the combustion chamber (Yu et al., 2002). In contrast, minimum thermal efficiency was obtained as 45.82% with n-heptane test fuel at 313 K intake temperature. Although combustion occurred close to the top dead center with n-heptane at 313 K intake temperature, knocking tendency was observed with n-heptane test fuel. Thus, thermal efficiency decreased. At 393 K inlet air temperature, thermal efficiency increased by about 17.71% with Bu30 compared to n-heptane. It is also clear that the addition of butanol improves the thermal efficiency compared to ethanol due to the higher heating value of butanol.

4.6.3 Emissions Characteristics

The variation of CO emissions is presented in Figure 4.29. As seen in Figure 4.35, minimum CO emissions were produced with n-heptane because of higher combustion temperature and faster combustion due to knocking. It can be also concluded that CO emissions decrease with the increase of intake temperature. In case of lower intake temperature, at the end of combustion, the temperature becomes too low for complete oxidation. Thus CO₂ formation is decreased and the amount of CO emissions increased (Lü et al., 2006). Maximum CO emissions were measured at 313 K intake temperature for all test fuels. It is also seen that CO emissions increase with the increase of the amount of ethanol and butanol in the test fuel. The reason behind this phenomenon is that close to the rich limit for HCCI and with early combustion phasing, very little CO is generated. However, close to the lean limit and with late combustion phasing, lot of CO can be formed (Maurya et al., 2011). The simulations were run with lean mixtures and using ethanol and butanol retarded the SOC. Maximum CO emissions were measured as 0.47% with E30 at 313 K intake temperature.

In Figure 4.36, the variation of HC emissions is presented at different intake temperatures using different fuels. HCCI features low temperature combustion, but this low combustion temperature results in higher emissions of HCs. The combustion temperature near the walls is even lower, due to heat losses.

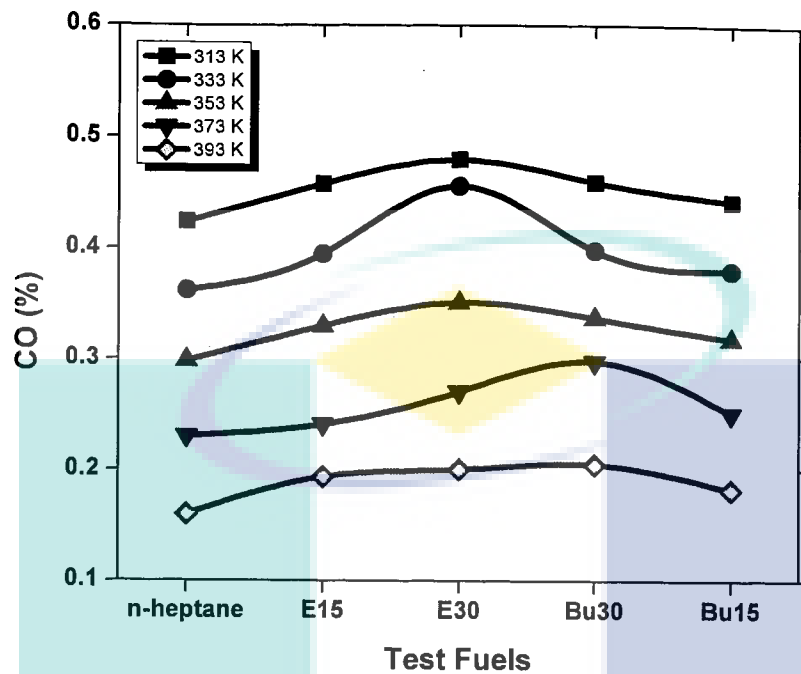


Figure 4.35 The variation of CO emissions on HCCI combustion at constant lambda, $\lambda = 2$ and 900 rpm engine speed with different intake temperatures and test fuels

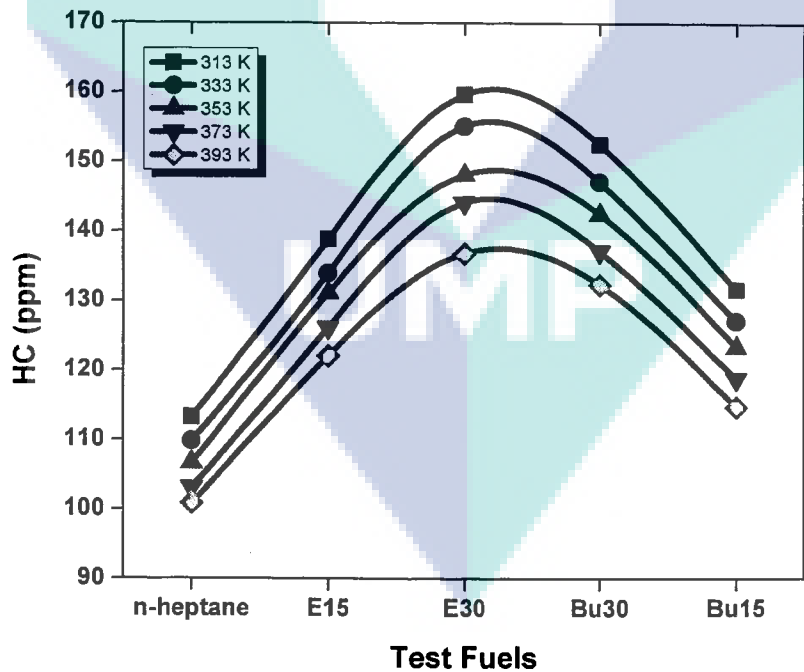


Figure 4.36 The variation of HC emissions on HCCI combustion at constant lambda, $\lambda = 2$ and 900 rpm engine speed with different intake temperatures and test fuels

Large parts of the HC emissions originate from the wall regions (Christensen et al., 1999b). Figure 4.36 presents that HC emissions decrease with the increase of intake temperature. The reason for this reduction is that chemical reactions improve and rapid combustion occurs at high intake temperatures. The productions of radicals accelerate with the increase of intake temperature and combustion reactions (Abd-Alla et al., 2001). Moreover, higher intake temperature decreases the cooling effects of homogeneous leaner charge mixture (Gan et al., 2011). It can be mentioned that minimum HC emissions were measured with n-heptane and Bu15 compared to other test fuels. It can be said that autoignition properties are deteriorated and HC emissions are generated when each test fuel is obtained by blending with ethanol and butanol. Maximum HC emissions were measured as 159.664 ppm with E30 test fuel at 313 K intake temperature.

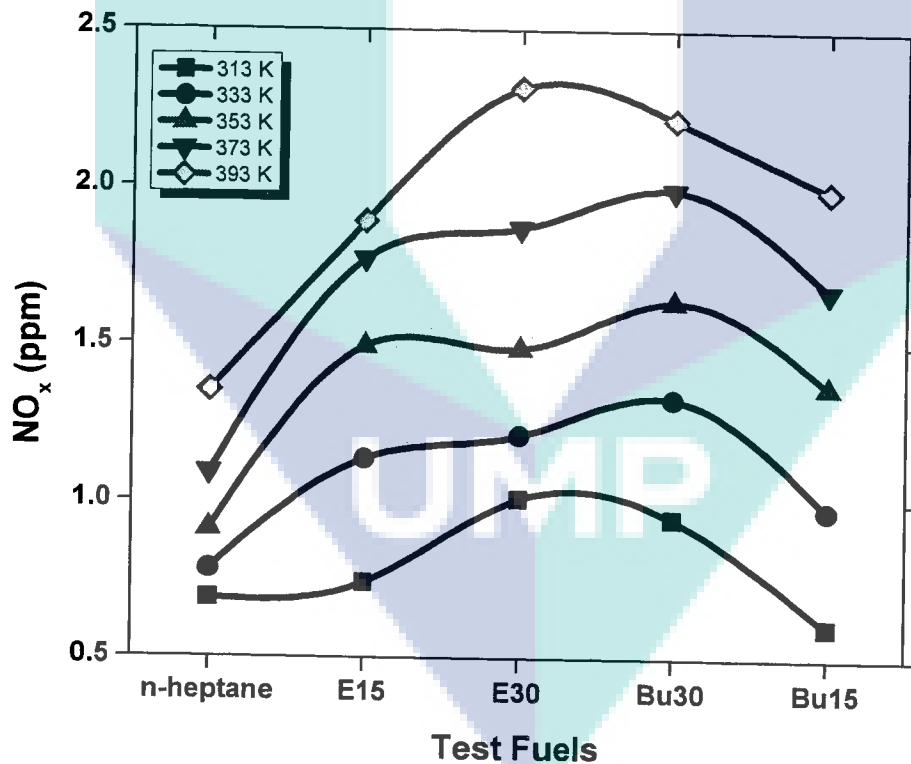


Figure 4.37 The variation of NO_x emissions on HCCI combustion at constant lambda, $\lambda = 2$ and 900 rpm engine speed with different intake temperatures and test fuels

The variation of NO_x emissions is presented in Figure 4.37. In the present study, NO_x emissions were found very low which is less than 2.5 ppm with all test fuels at each intake temperature. NO_x emissions can be simultaneously reduced in HCCI combustion because HCCI engines operate with leaner homogenous charge mixtures. NO_x emissions are produced at high combustion temperatures. Thus NO formation mechanisms cannot occur due to the lower end of combustion temperature. This is one of the most important advantages of HCCI combustion. Figure 4.37 presents that NO_x emissions increase with the increase of intake temperature. This is because of the higher in-cylinder temperature with increasing intake temperature. Minimum NO_x emissions were measured with Bu15 and Bu30 test fuel at all intake temperatures.

4.7 Summary

The Chapter has presented the validation of the model against experimental results. The validation results show good agreement with the experimental data and capture important combustion phase trends as engine parameters are varied with maximum percentage of error which is less than 6% for diesel HCCI and 4% for gasoline HCCI. This Chapter has also presented the performance and emissions of the HCCI engine and compared it side-by-side with the CI and SI engine. When comparing the CI and SI with HCCI engines at the same engine speed and load condition, both CI and SI engines have the advantage over the HCCI engine. This is consistent with the literature, where the HCCI engine has the limitation of operating in a full load condition. The effects of different engine parameters on combustion and performance of both diesel and gasoline HCCI engines have also presented in this Chapter. The intake temperature has the most significant effect on HCCI combustion and performance characteristics. The proper controlling of engine parameters can extend the operating range of HCCI engines. This Chapter has also presented the effects of fuel blends on combustion, performance and emissions characteristics of HCCI engines. Both ethanol and butanol has ability to delay the ignition timing which may save HCCI engine from excessive pressure and temperature rise. The engine efficiency and emissions levels can be improved further by utilizing different control parameters such as compression ratio, leaner mixture, exhaust gas recirculation, etc. Therefore, the HCCI engine could be a viable option in the near future.

CHAPTER 5

CONCLUSIONS AND RECOMMENDATIONS

5.1 Introduction

The importance of developing IC engines which increase efficiency while decreasing harmful emissions is steadily increasing. An emergence of alternative energy-providing technologies such as fuel cells and solar power is also changing the landscape of the world's energy economy. However, the reliability and effectiveness of the IC engine make sure that it will be a key player in our future. One way to further improve upon IC engines is to implement a combustion cycle known as Homogeneous Charge Compression Ignition which has the potential to reduce fuel consumption while simultaneously drastically reducing emissions of NO_x and PM, two results of combustion known to be harmful to human health and the environment. HCCI is premixed, like gasoline engines, and compression ignited, like a diesel engine. This allows for high compression ratios and therefore higher engine efficiencies. The fuel and air mixtures are unusually lean (stoichiometric ratios around 0.3) which results in low peak temperatures thus limiting the production of NO_x . The lean nature of the combustion process also leads to less PM since excess HC are not present.

5.2 Summary of Findings

In this study, a zero-dimensional single zone model was established to investigate HCCI combustion, performance and emissions characteristics over a wide range of operating conditions. Various chemical reaction mechanisms of various fuels and fuel blends were used to solve the chemical reactions during combustion. The model was validated against previously published experimental results. The simulations show good agreement with the experimental results and capture important combustion

phase trends as engine parameters are varied with a maximum percentage of error which is less than 6% for diesel HCCI and 4% for gasoline HCCI. The validated numerical simulation was able to capture trends in combustion phasing variation with critical engine parameters, particularly the low-temperature reaction (LTR). The main combustion stage predicted by the numerical simulation is advanced compared to the experimental results because of the assumption of uniform mixture temperature and mixture composition.

This study reports the results of a modeling study of HCCI combustion using diesel fuel and compared the results with diesel engine experimental results using diesel fuel. When comparing the CI engines with HCCI engines at the same engine speed and load condition, CI engines have the advantage over the HCCI engine. This is consistent with the literature, where the HCCI engine has the limitation of operating in a low load condition. As for the emissions levels, the HCCI engine in this study recorded a very low level of NO_x due to nature of this type of combustion. Unburned HC is higher than in the CI engines at full load condition. The same applies for CO emissions levels, where the HCCI engine returns higher CO than the CI engines at the same speed and load condition. This is also consistent with the literature where the HCCI engine has the disadvantage of producing more unburned HC and CO than the CI engines. Increasing the engine speed peak pressure location is retarded due to retarded MCS. IMEP, IT, and IP were increased up to a certain limit then decreased with increasing speed. This is because of with the increase of engine speed; the combustion duration is shortened with respect to time. Increasing the intake temperature advances the phasing of both the low-temperature reaction and main combustion stage and IMEP, IT and IP decreases with increasing intake temperature. This is due to the chemical reactions in the low-temperature phase which is retarded for increasing intake air temperature. The effects of turbocharging on the phasing of low-temperature reaction are relatively weak, but they significantly affect the phasing of the main combustion stage. The effect of compression ratio advances the phasing of the low-temperature reaction and main combustion stage and IMEP, IT and IP increases with increasing compression ratio.

This study also reports the results of a modeling study of HCCI combustion using gasoline surrogate fuel and compared the results with gasoline engine experimental results using gasoline surrogate fuel. When comparing the SI engines with

HCCI engines at the same engine speed and load condition, SI engines have the advantage over the HCCI engine. This is consistent with the literature, where the HCCI engine has the limitation of operating in a low load condition. As for the emissions levels, the HCCI engine in this study recorded a very low level of NO_x due to nature of this type of combustion. Unburned HC is higher than in the SI engines at full load condition. The same applies for CO emissions levels, where the HCCI engine returns higher CO than the SI engines at the same speed and load condition. This is also consistent with the literature where the HCCI engine has the disadvantage of producing more unburned HC and CO than the SI engines. Increasing the engine speed peak pressure location is retarded due to retarded MCS. IMEP, IT, and IP were increased up to a certain limit then decreased with increasing speed. This is because of with the increase in engine speed, the combustion duration is shortened with respect to time. Increasing the intake temperature advances the phasing of both the low-temperature reaction and main combustion stage and IMEP, IT and IP decreases with increasing intake temperature. This is due to the chemical reactions in the low-temperature phase which is retarded for increasing intake air temperature. The effects of turbocharging on the phasing of low-temperature reaction are relatively weak, but they significantly affect the phasing of the main combustion stage. The effect of compression ratio advances the phasing of the low-temperature reaction and main combustion stage and IMEP, IT and IP increases with increasing compression ratio.

HCCI combustion with different test fuels was also investigated numerically at different intake temperatures in this study. Simulation results showed that combustion was delayed slightly with the increase of the amount of ethanol and butanol in the test fuels. It was also seen that HCCI combustion was advanced with the increase of intake temperature. It can be also said that ethanol is more suitable as fuel for controlling the HCCI combustion phasing compared to butanol due to higher octane number. When thermal efficiency is examined, butanol has advantage according to ethanol. Thermal efficiency increased by about 17.71% with Bu30 compared to n-heptane at 393 K intake temperature. IMEP decreased at all intake temperatures with n-heptane. Very low amount of NO_x emissions were found with test fuels. It can be said that CO emissions increased with the increase of ethanol in the test fuels. Higher HC emissions were obtained especially at lower inlet air temperatures when ethanol was used as an additive fuel in the simulations. It is hoped that this numerical investigation contributes to the

determination of proper fuel mixture and intake temperature for the problems such as extending the HCCI operation range, controlling the combustion, preventing knocking combustion and reduction of CO and HC emissions in HCCI combustion.

5.3 Recommendations for Future Research

1. The purpose of this thesis was to model HCCI combustion numerically. For this reason, a zero-dimensional single zone model was prepared and validated. The model produced good agreement with the experiment but requires high computational resources. A zero-dimensional single-zone model has the advantage of faster computing time. However, it has the limitation of short burn duration which causes higher in-cylinder peak pressure. To mitigate this problem, zero-dimensional single zone model can be developed to a one-dimensional single zone model.
2. The use of a zero-dimensional single-zone model assumes that the combustion chamber is fully homogeneous without any turbulence effect. To mitigate this problem a conditional momentum closure model can be added to zero-dimensional single zone model.
3. To validate the model perfectly an experimental investigation can be done in the future.
4. In addition, the ignition control methods for HCCI combustion can be used in future work to improve the operation of the HCCI engine.

REFERENCES

- Abd-Alla, G., Soliman, H., Badr, O., and Abd-Rabbo, M. (2001). Effects of diluent admissions and intake air temperature in exhaust gas recirculation on the emissions of an indirect injection dual fuel engine. *Energy Conversion and Management*, 42(8), 1033-1045.
- Aceves, S., and Flowers, D. (2004). Engine shows diesel efficiency without the emissions. *Lawrence Livermore National Laboratory*.
- Aceves, S. M., Flowers, D. L., Martinez-Frias, J., Smith, J. R., Dibble, R., Au, M., and Girard, J. (2001). HCCI combustion: analysis and experiments. *SAE Technical Paper*, 2001-01-2077.
- Aceves, S. M., Flowers, D. L., Martinez-Frias, J., Smith, J. R., Westbrook, C. K., Pitz, W. J., Hessel, R. P. (2001). A sequential fluid-mechanic chemical-kinetic model of propane HCCI combustion. *SAE Transactions*, 110(3), 1019-1029.
- Aceves, S. M., Flowers, D. L., Westbrook, C. K., Smith, J. R., Pitz, W., Dibble, R., Johansson, B. (2000). A multi-zone model for prediction of HCCI combustion and emissions. *SAE Technical Paper*, 2000-01-0327.
- Agarwal, A. K. (2007). Biofuels (alcohols and biodiesel) applications as fuels for internal combustion engines. *Progress in Energy and Combustion Science*, 33(3), 233-271.
- Akagawa, H., Miyamoto, T., Harada, A., Sasaki, S., Shimazaki, N., Hashizume, T., and Tsujimura, K. (1999). Approaches to solve problems of the premixed lean diesel combustion. *SAE Technical Paper*, 1999-01-0183.
- Al-Khairi, N. N., Naveenchandran, P., and Aziz, A. R. A. (2011). Comparison of HCCI and SI Characteristics on Low Load CNG-DI Combustion. *Applied Science*, 11, 1827-1832.
- Amnéus, P., Mauss, F., Kraft, M., Vressner, A., and Johansson, B. (2005). NO_x and N₂O formation in HCCI engines. *SAE Technical Paper*, 2005-01-0126.
- An, H., Yang, W., Chou, S., and Chua, K. (2012). Combustion and emissions characteristics of diesel engine fueled by biodiesel at partial load conditions. *Applied Energy*, 99, 363-371.
- Andrae, J. (2011). A kinetic modeling study of self-ignition of low alkylbenzenes at engine-relevant conditions. *Fuel Processing Technology*, 92(10), 2030-2040.
- Assanis, D., and Polishak, M. (1990). Valve event optimization in a spark-ignition engine. *Journal of Engineering for Gas Turbines and Power*, 112(3), 341-347.

- Assanis, D. N., and Heywood, J. B. (1986). Development and use of a computer simulation of the turbocompounded diesel system for engine performance and component heat transfer studies. *SAE Technical Paper*, 1986-01-0329.
- Au, M. Y., Girard, J. W., Dibble, R., Flowers, D., Aceves, S. M., Martinez-Frias, J., Maas, U. (2001). 1.9-liter four-cylinder HCCI engine operation with exhaust gas recirculation. *SAE Technical Paper*. 2001-01-1894.
- Ball, M., and Wietschel, M. (2009). The future of hydrogen—opportunities and challenges. *International Journal of Hydrogen Energy*, 34(2), 615-627.
- Barroso, G., Escher, A., and Boulouchos, K. (2005). Experimental and numerical investigations on HCCI-combustion. *SAE Technical Paper*, 2005-24-038.
- Bendu, H., and Murugan, S. (2014). Homogeneous charge compression ignition (HCCI) combustion: Mixture preparation and control strategies in diesel engines. *Renewable and Sustainable Energy Reviews*, 38, 732-746.
- Bengtsson, J., Gäfvert, M., and Strandh, P. (2004). Modeling of HCCI engine combustion for control analysis. *43rd IEEE Conference on Decision and Control*, pp. 1682-1687.
- Bression, G., Soleri, D., Savy, S., Dehoux, S., Azoulay, D., Hamouda, H. B.-H., Lawrence, N. (2008). A study of methods to lower HC and CO emissions in diesel HCCI. *SAE Technical Paper*, 2008-01-0034.
- Bunting, B. G., Eaton, S., Naik, C. V., Puduppakkam, K. V., Chou, C. P., and Meeks, E. (2008). A Comparison of HCCI Ignition Characteristics of Gasoline Fuels Using a Single-Zone Kinetic Model with a Five Component Surrogate Fuel. *SAE Technical Paper*, 2008-01-2399.
- Campbell, M., Wyszynski, L. P., and Stone, R. (2004). Combustion of LPG in a spark-ignition engine. *SAE Technical Paper*, 2004-01-0974.
- Canakci, M. (2008). An experimental study for the effects of boost pressure on the performance and exhaust emissions of a DI-HCCI gasoline engine. *Fuel*, 87(8), 1503-1514.
- Canakci, M. (2012). Combustion characteristics of a DI-HCCI gasoline engine running at different boost pressures. *Fuel*, 96, 546-555.
- Canova, M., Garcin, R., Midlam-Mohler, S., Guezennec, Y., and Rizzoni, G. (2005). A control-oriented model of combustion process in a HCCI diesel engine. *Proceedings of the American Control Conference*, pp. 4446-4451.
- Cedrone, K., Cheng, W. K., Chahine, S., Williams, J., and VanDerWege, B. (2011). Fuel effects on HCCI operation in a spark assisted direct injection gasoline engine. *SAE Technical Paper*, 2011-01-1763.

- Celik, M. B. (2008). Experimental determination of suitable ethanol–gasoline blend rate at high compression ratio for gasoline engine. *Applied Thermal Engineering*, 28(5), 396-404.
- Chen, Z., Konno, M., Oguma, M., and Yanai, T. (2000). Experimental study of CI natural-gas/DME homogeneous charge engine. *SAE Technical Paper*, 2000-01-0329.
- Cho, H. M., and He, B.-Q. (2007). Spark ignition natural gas engines—A review. *Energy Conversion and Management*, 48(2), 608-618.
- Choi, D., Miles, P. C., Yun, H., and Reitz, R. D. (2005). A parametric study of low-temperature, late-injection combustion in a HSDI diesel engine. *JSME International Journal Series B Fluids and Thermal Engineering*, 48(4), 656-664.
- Christensen, M., Hultqvist, A., and Johansson, B. (1999). Demonstrating the multi fuel capability of a homogeneous charge compression ignition engine with variable compression ratio. *SAE Technical Paper*, 1999-01-3679.
- Christensen, M., and Johansson, B. (1999). Homogeneous charge compression ignition with water injection. *SAE Technical Paper*, 1999-01-1444.
- Christensen, M., and Johansson, B. (2000). Supercharged homogeneous charge compression ignition (HCCI) with exhaust gas recirculation and pilot fuel. *SAE Technical Paper*, 2000-01-1835.
- Christensen, M., Johansson, B., Amnéus, P., and Mauss, F. (1998a). Supercharged homogeneous charge compression ignition. *Journal of Engines*, 107, 728-739.
- Christensen, M., Johansson, B., Amnéus, P., and Mauss, F. (1998b). Supercharged homogeneous charge compression ignition. *SAE Technical paper*, 1998-01-0787.
- Christensen, M., Johansson, B., and Einewall, P. (1997). Homogeneous charge compression ignition (HCCI) using isooctane, ethanol and natural gas—a comparison with spark ignition operation. *SAE Technical Paper*, 1997-01-2874.
- Cinar, C., Uyumaz, A., Solmaz, H., Sahin, F., Polat, S., and Yilmaz, E. (2015). Effects of intake air temperature on combustion, performance and emission characteristics of a HCCI engine fueled with the blends of 20% n-heptane and 80% isooctane fuels. *Fuel Processing Technology*, 130, 275-281.
- Curran, H. J., Gaffuri, P., Pitz, W., and Westbrook, C. (2002). A comprehensive modeling study of iso-octane oxidation. *Combustion and Flame*, 129(3), 253-280.
- Curran, H. J., Gaffuri, P., Pitz, W. J., and Westbrook, C. K. (1998). A comprehensive modeling study of n-heptane oxidation. *Combustion and Flame*, 114(1), 149-177.

- Dagaut, P., and Togbé, C. (2009). Experimental and modeling study of the kinetics of oxidation of butanol– n-heptane mixtures in a jet-stirred reactor. *Energy & Fuels*, 23(7), 3527-3535.
- Dagaut, P., and Togbé, C. (2010). Experimental and modeling study of the kinetics of oxidation of ethanol-n-heptane mixtures in a jet-stirred reactor. *Fuel*, 89(2), 280-286.
- Dang, T., and Teng, J.-t. (2011). The effects of configurations on the performance of microchannel counter-flow heat exchangers—An experimental study. *Applied Thermal Engineering*, 31(17), 3946-3955.
- Dec, J. E. (2002). A computational study of the effects of low fuel loading and EGR on heat release rates and combustion limits in HCCI engines. *SAE Technical paper*, 2002-01-1309.
- Dec, J. E. (2009). Advanced compression-ignition engines—understanding the in-cylinder processes. *Proceedings of the Combustion Institute*, 32(2), 2727-2742.
- Dec, J. E., and Sjöberg, M. (2004). Isolating the effects of fuel chemistry on combustion phasing in an HCCI engine and the potential of fuel stratification for ignition control. *SAE Technical Paper*, 2004-01-0557.
- Dec, J. E., and Yang, Y. (2010). Boosted HCCI for high power without engine knock and with ultra-low NO_x emissions-using conventional gasoline. *SAE International Journal of Engines*, 3(1), 750-767.
- Duc, P. M., and Wattanavichien, K. (2007). Study on biogas premixed charge diesel dual fuelled engine. *Energy Conversion and Management*, 48(8), 2286-2308.
- Elghawi, U., Mayouf, A., Tsolakis, A., and Wyszynski, M. (2010). Vapour-phase and particulate-bound PAHs profile generated by a (SI/HCCI) engine from a winter grade commercial gasoline fuel. *Fuel*, 89(8), 2019-2025.
- Eng, J. A., Leppard, W. R., and Sloane, T. (2003). The effect of di-tertiary butyl peroxide (DTBP) addition to gasoline on HCCI combustion. *SAE Technical Paper*, 2003-01-3170.
- EPA-Gasoline, R. (1999). Regulatory Impact Analysis—Control of Air Pollution from New Motor Vehicles: Tier 2 Motor Vehicle Emissions Standards and Gasoline Sulfur Control Requirements, US Environmental Protection Agency, Air and Radiation. *US Environmental Protection Agency, Air and Radiation EPA420*.
- Epping, K., Aceves, S., Bechtold, R., and Dec, J. E. (2002). The potential of HCCI combustion for high efficiency and low emissions. *SAE Technical Paper*, 2002-01-1923.
- Ericson, C., Andersson, M., Egnell, R., and Westerberg, B. (2006). Modelling diesel engine combustion and NO_x formation for model based control and simulation

of engine and exhaust aftertreatment systems. *SAE Technical Paper*, 2006-01-0687.

Fiveland, S. B., and Assanis, D. N. (2000). A four-stroke homogeneous charge compression ignition engine simulation for combustion and performance studies. *SAE Technical Paper*, 2000-01-0332.

Fiveland, S. B., and Assanis, D. N. (2001). Development of a two-zone HCCI combustion model accounting for boundary layer effects. *SAE Transactions*, 110(3), 1030-1044.

Fiveland, S. B., and Assanis, D. N. (2002). Development and validation of a quasi-dimensional model for HCCI engine performance and emissions studies under turbocharged conditions. *SAE Technical Paper*, 2002-01-1757.

Flowers, D., Aceves, S., Westbrook, C., Smith, J., and Dibble, R. (2001). Detailed chemical kinetic simulation of natural gas HCCI combustion: gas composition effects and investigation of control strategies. *Journal of engineering for gas turbines and power*, 123(2), 433-439.

Flowers, D., Aceves, S. M., Martinez-Frias, J., Smith, J. R., Au, M., Girard, J., and Dibble, R. (2001). Operation of a four-cylinder 1.9 L propane fueled homogeneous charge compression ignition engine: basic operating characteristics and cylinder-to-cylinder effects. *SAE Technical Paper*, 2001-01-1895.

Gan, S., Ng, H. K., and Pang, K. M. (2011). Homogeneous charge compression ignition (HCCI) combustion: implementation and effects on pollutants in direct injection diesel engines. *Applied Energy*, 88(3), 559-567.

Ganesan, V. (2012). *Internal combustion engines*: McGraw Hill Education (India) Pvt Ltd.

Ganesh, D., and Nagarajan, G. (2010). Homogeneous charge compression ignition (HCCI) combustion of diesel fuel with external mixture formation. *Energy*, 35(1), 148-157.

Ganesh, D., Nagarajan, G., and Ganesan, S. (2014). Experimental Investigation of Homogeneous Charge Compression Ignition Combustion of Biodiesel Fuel with External Mixture Formation in a CI engine. *Environmental Science & Technology*, 48(5), 3039-3046.

Ganesh, D., Nagarajan, G., and Mohamed Ibrahim, M. (2008). Study of performance, combustion and emission characteristics of diesel homogeneous charge compression ignition (HCCI) combustion with external mixture formation. *Fuel*, 87(17), 3497-3503.

García, M. T., Aguilar, F. J. J.-E., and Lencero, T. S. (2009). Experimental study of the performances of a modified diesel engine operating in homogeneous charge

- compression ignition (HCCI) combustion mode versus the original diesel combustion mode. *Energy*, 34(2), 159-171.
- García, M. T., Aguilar, F. J. J.-E., Lencero, T. S., and Villanueva, J. A. B. (2009). A new heat release rate (HRR) law for homogeneous charge compression ignition (HCCI) combustion mode. *Applied Thermal Engineering*, 29(17), 3654-3662.
- Garcia, M. T., Jiménez-Espadafor Aguilar, F. J., Becerra Villanueva, J. A., and Trujillo, E. C. (2011). Analysis of a new analytical law of heat release rate (HRR) for homogenous charge compression ignition (HCCI) combustion mode versus analytical parameters. *Applied Thermal Engineering*, 31(4), 458-466.
- Ghazikhani, M., Feyz, M. E., and Joharchi, A. (2010). Experimental investigation of the Exhaust Gas Recirculation effects on irreversibility and Brake Specific Fuel Consumption of indirect injection diesel engines. *Applied Thermal Engineering*, 30(13), 1711-1718.
- Golub, A., and Ghoniem, A. (1999). Modeling NO_x formation in a small bore, lean natural gas, spark ignition engine. *SAE Technical Paper*, 1999-01-3480.
- Gomes Antunes, J., Mikalsen, R., and Roskilly, A. (2008). An investigation of hydrogen-fuelled HCCI engine performance and operation. *International Journal of Hydrogen Energy*, 33(20), 5823-5828.
- Gotoh, S., Kuboyama, T., Moriyoshi, Y., Hatamura, K., Yamada, T., Takanashi, J., and Urata, Y. (2013). Evaluation of the Performance of a Boosted HCCI Gasoline Engine with Blowdown Supercharge System. *SAE Technical Paper*, 2013-32-9172.
- Gray, A. W. B., and Ryan, T. W. (1997). Homogeneous charge compression ignition (HCCI) of diesel fuel. *SAE Technical Paper*, 1997-01-1676.
- Guo, H., Hosseini, V., Neill, W. S., Chippior, W. L., and Dumitrescu, C. E. (2011). An experimental study on the effect of hydrogen enrichment on diesel fueled HCCI combustion. *International Journal of Hydrogen Energy*, 36(21), 13820-13830.
- Guo, H., Neill, W. S., Chippior, W., Li, H., and Taylor, J. D. (2010). An experimental and modeling study of HCCI combustion using n-heptane. *Journal of Engineering for Gas Turbines and Power*, 132(2), 022801.
- Hakansson, A. (2007). *CA50 estimation on HCCI engine using engine speed variations*. MSc Thesis. Lund University, Sweden.
- Hasan, M., and Rahman, M. (2016). Homogeneous charge compression ignition combustion: Advantages over compression ignition combustion, challenges and solutions. *Renewable and Sustainable Energy Reviews*, 57, 282-291.
- He, B.-Q., Liu, M.-B., Yuan, J., and Zhao, H. (2013). Combustion and emission characteristics of a HCCI engine fuelled with n-butanol–gasoline blends. *Fuel*, 108, 668-674.

- He, B.-Q., Yuan, J., Liu, M.-B., and Zhao, H. (2014a). Combustion and emission characteristics of a n-butanol HCCI engine. *Fuel*, 115, 758-764.
- He, B.-Q., Yuan, J., Liu, M.-B., and Zhao, H. (2014b). Low-Temperature Combustion Characteristics of an-Butanol/Isooctane HCCI Engine. *Energy & Fuels*, 28(6), 4183-4192.
- Hernandez, J., Sanz-Argent, J., Benajes, J., and Molina, S. (2008). Selection of a diesel fuel surrogate for the prediction of auto-ignition under HCCI engine conditions. *Fuel*, 87(6), 655-665.
- Heywood, J. B. (1988). *Internal combustion engine fundamentals* (Vol. 930): McGraw-Hill New York.
- Hiltner, J., Agama, R., Mauss, F., Johansson, B., and Christensen, M. (2000). Homogeneous charge compression ignition operation with natural gas: Fuel composition implications. *Journal of Engineering for Gas Turbines and Power*, 125(3), 837-844.
- Holtzapple, M. T., Davison, R. R., Ross, M. K., Aldrett-Lee, S., Nagwani, M., Lee, C.-M., Gaskin, D. (1999). Biomass conversion to mixed alcohol fuels using the MixAlco process. *Twentieth Symposium on Biotechnology for Fuels and Chemicals*, pp. 609-631.
- Hosseini, V., and Checkel, M. D. (2007). Intake pressure effects on HCCI combustion in a CFR engine. *Proceedings of the Combustion Institute, Canadian Section, Spring Technical Meeting*, pp. 1-6.
- Hyvönen, J., Haraldsson, G., and Johansson, B. (2003). Supercharging HCCI to extend the operating range in a multi-cylinder VCR-HCCI engine. *SAE Technical Paper, 2003-01-3214*.
- Hyvönen, J., Haraldsson, G., and Johansson, B. (2005). Operating conditions using spark assisted HCCI combustion during combustion mode transfer to SI in a multi-cylinder VCR-HCCI engine. *SAE Technical Paper, 2003-01-3214*.
- Ibrahim, M. M., and Ramesh, A. (2014). Investigations on the effects of intake temperature and charge dilution in a hydrogen fueled HCCI engine. *International Journal of Hydrogen Energy*, 39(26), 14097-14108.
- Iida, M., Aroonsrisopon, T., Hayashi, M., Foster, D. E., and Martin, J. (2001). The effect of intake air temperature, compression ratio and coolant temperature on the start of heat release in an HCCI (homogeneous charge compression ignition) engine: *SAE Technical Paper, 2001-01-1880*.
- Iida, N. (1994). Combustion analysis of methanol-fueled active thermo-atmosphere combustion (ATAC) engine using a spectroscopic observation. *SAE Technical Paper, 1994-01-0684*.

- Iida, N., and Igarashi, T. (2000). Auto-ignition and combustion of n-butane and DME/air mixtures in a homogeneous charge compression ignition engine. *SAE Technical Paper*, 2000-01-1832.
- Ishii, H., Koike, N., Suzuki, H., and Odaka, M. (1997). Exhaust purification of diesel engines by homogeneous charge with compression ignition Part 2: Analysis of combustion phenomena and NO_x formation by numerical simulation with experiment. *SAE Technical Paper*, 1997-01-0315.
- Iwabuchi, Y., Kawai, K., Shoji, T., and Takeda, Y. (1999). Trial of new concept diesel combustion system-premixed compression-ignited combustion. *SAE Technical Paper*, 1999-01-0185.
- Izadi Najafabadi, M., and Abdul Aziz, N. (2013). Homogeneous charge compression ignition combustion: challenges and proposed solutions. *Journal of Combustion*, 2013.
- Ji, C., Dec, J. E., Dernotte, J., and Cannella, W. (2014). Effect of Ignition Improvers on the Combustion Performance of Regular-Grade E10 Gasoline in an HCCI Engine. *SAE Technical Paper*, 2014-01-1282.
- Jiménez-Espadafor, F. J., Torres, M., Velez, J. A., Carvajal, E., and Becerra, J. A. (2012). Experimental analysis of low temperature combustion mode with diesel and biodiesel fuels: A method for reducing NO_x and soot emissions. *Fuel Processing Technology*, 103, 57-63.
- Kaneko, N., Ando, H., Ogawa, H., and Miyamoto, N. (2002). Expansion of the operating range with in-cylinder water injection in a premixed charge compression ignition engine. *SAE Technical Paper*, 2002-01-1743.
- Kelly-Zion, P. L., and Dec, J. E. (2000). A computational study of the effect of fuel type on ignition time in homogenous charge compression ignition engines. *Proceedings of the Combustion Institute*, 28(1), 1187-1194.
- Killingsworth, N. J., Aceves, S. M., Flowers, D. L., and Krstić, M. (2006). A simple HCCI engine model for control. *IEEE International Conference on Control Applications*, pp. 2424-2429.
- Kim, M. Y., and Lee, C. S. (2007). Effect of a narrow fuel spray angle and a dual injection configuration on the improvement of exhaust emissions in a HCCI diesel engine. *Fuel*, 86(17), 2871-2880.
- Kimura, S., Aoki, O., Ogawa, H., Muranaka, S., and Enomoto, Y. (1999). New combustion concept for ultra-clean and high-efficiency small DI diesel engines. *SAE Technical Paper*, 1999-01-3681.
- Kobayashi, K., Sako, T., Sakaguchi, Y., Morimoto, S., Kanematsu, S., Suzuki, K., Ohtsubo, H. (2011). Development of HCCI natural gas engines. *Journal of Natural Gas Science and Engineering*, 3(5), 651-656.

- Komninos, N., and Rakopoulos, C. (2012). Modeling HCCI combustion of biofuels: A review. *Renewable and Sustainable Energy Reviews*, 16(3), 1588-1610.
- Komninos, N. P. (2009). Investigating the importance of mass transfer on the formation of HCCI engine emissions using a multi-zone model. *Applied Energy*, 86(7–8), 1335-1343.
- Kong, S.-C., and Reitz, R. D. (2002). Use of detailed chemical kinetics to study HCCI engine combustion with consideration of turbulent mixing effects. *Journal of Engineering for Gas Turbines and Power*, 124(3), 702-707.
- Kong, S.-C., and Reitz, R. D. (2003). Numerical study of premixed HCCI engine combustion and its sensitivity to computational mesh and model uncertainties. *Combustion Theory and Modelling*, 7(2), 417-433.
- Kong, S.-C., Reitz, R. D., Christensen, M., and Johansson, B. (2003). Modeling the effects of geometry generated turbulence on HCCI engine combustion. *SAE Technical Paper*, 2003-01-1088.
- Kook, S., Bae, C., and Kim, J. (2007). Diesel-fuelled homogeneous charge compression ignition engine with optimized premixing strategies. *International Journal of Engine Research*, 8(1), 127-137.
- Kuboyama, T., Moriyoshi, Y., Hatamura, K., Takanashi, J., and Urata, Y. (2011). Extension of operating range of a multi-cylinder gasoline HCCI engine using the blowdown supercharging system. *SAE Technical Paper*, 2011-01-0896.
- Kuboyama, T., Moriyoshi, Y., Hatamura, K., Takanashi, J., Urata, Y., and Yamada, T. (2011). A Study of Newly Developed HCCI Engine With Wide Operating Range Equipped With Blowdown Supercharging System. *SAE Technical Paper*, 2011-01-1766.
- Kulzer, A., Lejsek, D., and Nier, T. (2010). A thermodynamic study on boosted HCCI: motivation, analysis and potential. *SAE Technical Paper*, 2010-01-1082.
- Kuo, K. K. (1986). *Principles of combustion*, John Wiley and Sons, New York, USA.
- Kwon, J., Seo, J., Lee, D., and Huh, K. Y. (2011). Zero-dimensional simulation of diesel engine combustion and emissions based on CMC model and skeletal reaction mechanism. *SAE International Journal of Engines*, 4(1), 964-975.
- Laguitton, O., Crua, C., Cowell, T., Heikal, M., and Gold, M. (2007). The effect of compression ratio on exhaust emissions from a PCCI diesel engine. *Energy Conversion and Management*, 48(11), 2918-2924.
- Lawler, B., Ortiz-Soto, E., Gupta, R., Peng, H., and Filipi, Z. S. (2011). Hybrid electric vehicle powertrain and control strategy optimization to maximize the synergy with a gasoline HCCI engine. *SAE Technical Paper*, 2011-01-0888.

- Lee, K., Kim, Y., and Min, K. (2010). Development of a reduced chemical kinetic mechanism for a gasoline surrogate for gasoline HCCI combustion. *Combustion Theory and Modelling*, 15(1), 107-124.
- Lemberger, I., and Floweday, G. (2009). 25cc HCCI Engine Fuelled with DEE. *SAE Technical Paper*, 2009-01-1771.
- Li, H., Guo, H., Neill, W. S., Chippior, W., and Taylor, J. D. (2006). An experimental and modeling study of HCCI combustion using n-heptane. *Proceedings of the ASME International Combustion Engine Division*, pp. 1-11.
- Li, H., Neill, W. S., Chippior, W., Graham, L., Connolly, T., and Taylor, J. D. (2007). An experimental investigation on the emission characteristics of HCCI engine operation using n-heptane. *SAE Technical Paper*, 2007-01-1854.
- Lin, Y.-C., Hsu, K.-H., and Chen, C.-B. (2011). Experimental investigation of the performance and emissions of a heavy-duty diesel engine fueled with waste cooking oil biodiesel/ultra-low sulfur diesel blends. *Energy*, 36(1), 241-248.
- Liu, H., Yao, M., Zhang, B., and Zheng, Z. (2008). Effects of inlet pressure and octane numbers on combustion and emissions of a homogeneous charge compression ignition (HCCI) engine. *Energy & Fuels*, 22(4), 2207-2215.
- Lu, T., Plomer, M., Luo, Z., Sarathy, S., Pitz, W., Som, S., and Longman, D. (2011). Directed relation graph with expert knowledge for skeletal mechanism reduction. *7th US National Combustion Meeting*, pp. 1-10.
- Lu, X.-C., Chen, W., and Huang, Z. (2005). A fundamental study on the control of the HCCI combustion and emissions by fuel design concept combined with controllable EGR. Part 2. Effect of operating conditions and EGR on HCCI combustion. *Fuel*, 84(9), 1084-1092.
- Lü, X., Hou, Y., Zu, L., and Huang, Z. (2006). Experimental study on the auto-ignition and combustion characteristics in the homogeneous charge compression ignition (HCCI) combustion operation with ethanol/n-heptane blend fuels by port injection. *Fuel*, 85(17), 2622-2631.
- Lu, X., Ji, L., Ma, J., Zhou, X., and Huang, Z. (2011). Combustion characteristics and influential factors of isooctane active-thermal atmosphere combustion assisted by two-stage reaction of n-heptane. *Combustion and Flame*, 158(2), 203-216.
- Ma, J., Lü, X., Ji, L., and Huang, Z. (2008). An experimental study of HCCI-DI combustion and emissions in a diesel engine with dual fuel. *International Journal of Thermal Sciences*, 47(9), 1235-1242.
- Machrafi, H., Cavadias, S., and Amouroux, J. (2008). A parametric study on the emissions from an HCCI alternative combustion engine resulting from the auto-ignition of primary reference fuels. *Applied Energy*, 85(8), 755-764.

- Machrafi, H., Cavadias, S., and Amouroux, J. (2010). Influence of fuel type, dilution and equivalence ratio on the emission reduction from the auto-ignition in an Homogeneous Charge Compression Ignition engine. *Energy*, 35(4), 1829-1838.
- Mack, J. H. (2007a). *Investigation of Homogeneous Charge Compression Ignition (HCCI) engines fuelled with ethanol blends using experiments and numerical simulations*. PhD thesis. University of California, USA.
- Mack, J. H. (2007b). *Investigation of homogeneous charge compression ignition engines fuelled with ethanol blends using experiments and numerical simulations*: University of California, Berkeley, USA.
- Mack, J. H., Aceves, S. M., and Dibble, R. W. (2009). Demonstrating direct use of wet ethanol in a homogeneous charge compression ignition (HCCI) engine. *Energy*, 34(6), 782-787.
- Mancaruso, E., and Vaglieco, B. (2010). Optical investigation of the combustion behaviour inside the engine operating in HCCI mode and using alternative diesel fuel. *Experimental Thermal and Fluid Science*, 34(3), 346-351.
- Mangus, M., Kiani, F., Mattson, J., Depcik, C., Peltier, E., and Stagg-Williams, S. (2014). Comparison of neat biodiesels and ULSD in an optimized single-cylinder diesel engine with electronically-controlled fuel injection. *Energy & Fuels*, 28(6), 3849-3862.
- Mase, Y., Kawashima, J.-i., Sato, T., and Eguchi, M. (1998). Nissan's new multivalve DI diesel engine series. *SAE Technical Paper*, 1998-01-1039.
- Maurya, R. K., and Agarwal, A. K. (2011). Experimental study of combustion and emission characteristics of ethanol fuelled port injected homogeneous charge compression ignition (HCCI) combustion engine. *Applied Energy*, 88(4), 1169-1180.
- Maurya, R. K., and Akhil, N. (2016). Numerical investigation of ethanol fuelled HCCI engine using stochastic reactor model. Part 2: Parametric study of performance and emissions characteristics using new reduced ethanol oxidation mechanism. *Energy Conversion and Management*, 121, 55-70.
- Mehl, M., Chen, J.-Y., Pitz, W. J., Sarathy, S., and Westbrook, C. K. (2011). An approach for formulating surrogates for gasoline with application toward a reduced surrogate mechanism for CFD engine modeling. *Energy & Fuels*, 25(11), 5215-5223.
- Mehl, M., Pitz, W., Sarathy, M., Yang, Y., and Dec, J. E. (2012). Detailed kinetic modeling of conventional gasoline at highly boosted conditions and the associated intermediate temperature heat release. *SAE Technical Paper*, 2012-01-1109.

- Mehl, M., Pitz, W. J., Westbrook, C. K., and Curran, H. J. (2011). Kinetic modeling of gasoline surrogate components and mixtures under engine conditions. *Proceedings of the Combustion Institute*, 33(1), 193-200.
- Miller, J. A., and Bowman, C. T. (1989). Mechanism and modeling of nitrogen chemistry in combustion. *Progress in Energy and Combustion Science*, 15(4), 287-338.
- Miller, J. A., Pilling, M. J., and Troe, J. (2005). Unravelling combustion mechanisms through a quantitative understanding of elementary reactions. *Proceedings of the Combustion Institute*, 30(1), 43-88.
- Milovanovic, N., Blundell, D., Pearson, R., Turner, J., and Chen, R. (2005). Enlarging the operational range of a gasoline HCCI engine by controlling the coolant temperature. *SAE Technical Paper*, 2005-01-0157.
- Mo, Y. (2008). *HCCI Heat Release Rate and Combustion Efficiency: A Couple KIVA Multi-Zone Modeling Study*. PhD Thesis. University of Michigan, USA.
- Mohanamurugan, S., and Sendilvelan, S. (2011). Emission and combustion characteristics of different fuel in HCCI engine. *International Journal of Automotive and Mechanical Engineering*, 3, 279-292.
- Mueller, M. A., Yetter, R. A., and Dryer, F. L. (2000). Kinetic modeling of the CO/H₂O/O₂/NO/SO₂ system: Implications for high-pressure fall-off in the SO₂ + O(+M) = SO₃(+M) reaction. *International Journal of Chemical Kinetics*, 32(6), 317-339.
- Najt, P. M., and Foster, D. E. (1983). Compression-ignited homogeneous charge combustion. *SAE Technical Paper*, 1983-01-0264.
- Nakagome, K., Shimazaki, N., Niimura, K., and Kobayashi, S. (1997). Combustion and emission characteristics of premixed lean diesel combustion engine. *SAE Technical Paper*, 1997-01-0898.
- Nishi, M., Kanehara, M., and Iida, N. (2016). Assessment for innovative combustion on HCCI engine by controlling EGR ratio and engine speed. *Applied Thermal Engineering*, 99, 42-60.
- Oakley, A., Zhao, H., Ma, T., and Ladommatos, N. (2001). Dilution effects on the controlled auto-ignition (CAI) combustion of hydrocarbon and alcohol fuels. *SAE Technical Paper*, 2001-01-3606.
- Ogink, R., and Golovitchev, V. (2001). Gasoline HCCI modeling: computer program combining detailed chemistry and gas exchange processes. *SAE Technical Paper*, 2001-01-3664.
- Ogink, R., and Golovitchev, V. (2002). Gasoline HCCI modeling: an engine cycle simulation code with a multi-zone combustion model. *SAE Technical Paper*, 2002-01-1745.

- Olsson, J.-O., Tunestål, P., Haraldsson, G., and Johansson, B. (2001). A turbocharged dual-fuel HCCI engine. *SAE Technical Paper*, 2001-01-1627.
- Olsson, J.-O., Tunestål, P., and Johansson, B. (2004). Boosting for high load HCCI. *SAE Technical Paper*, 2004-01-0940.
- Olsson, J.-O., Tunestål, P., Johansson, B., Fiveland, S., Agama, J. R., and Assanis, D. N. (2002). Compression ratio influence on maximum load of a natural gas fueled HCCI engine. *SAE Transactions, Journal of Engines*, 111(3), 442-458.
- Olsson, J.-O., Tunestål, P., Johansson, B., Fiveland, S., Agama, R., Willi, M., and Assanis, D. N. (2002). Compression ratio influence on maximum load of a natural gas fueled HCCI engine. *SAE Technical Paper*, 2002-01-0111.
- Padala, S., Woo, C., Kook, S., and Hawkes, E. R. (2013). Ethanol utilisation in a diesel engine using dual-fuelling technology. *Fuel*, 109, 597-607.
- Patel, A., Kong, S.-C., and Reitz, R. D. (2004). Development and validation of a reduced reaction mechanism for HCCI engine simulations. *SAE Technical Paper*, 2004-01-0558.
- Payri, F., Lujan, J., Martin, J., and Abbad, A. (2010). Digital signal processing of in-cylinder pressure for combustion diagnosis of internal combustion engines. *Mechanical Systems and Signal Processing*, 24(6), 1767-1784.
- Pei, Y., Mehl, M., Liu, W., Lu, T., Pitz, W. J., and Som, S. (2015). A Multicomponent Blend as a Diesel Fuel Surrogate for Compression Ignition Engine Applications. *Journal of Engineering for Gas Turbines and Power*, 137(11), 111502.
- Peng, Z., Zhao, H., Ma, T., and Ladommatos, N. (2005). Characteristics of homogeneous charge compression ignition (HCCI) combustion and emissions of n-heptane. *Combustion Science and Technology*, 177(11), 2113-2150.
- Pitz, W. J., and Mueller, C. J. (2011). Recent progress in the development of diesel surrogate fuels. *Progress in Energy and Combustion Science*, 37(3), 330-350.
- Polovina, D., McKenna, D., Wheeler, J., Sterniak, J., Miersch-Wiemers, O., Mond, A., and Yilmaz, H. (2013). Steady-state combustion development of a downsized multi-cylinder engine with range extended HCCI/SACI capability. *SAE Technical Paper*, 2013-01-1655.
- Popp, D. (2006). International innovation and diffusion of air pollution control technologies: the effects of NO_x and SO₂ regulation in the US, Japan, and Germany. *Journal of Environmental Economics and Management*, 51(1), 46-71.
- Pucher, G. R., Gardiner, D. P., Bardon, M. F., and Battista, V. (1996). Alternative combustion systems for piston engines involving homogeneous charge compression ignition concepts-a review of studies using methanol, gasoline and diesel fuel. *SAE Technical Paper*, 1996-01-2063.

- Pulkrabek, W. W. (1997). *Engineering fundamentals of the internal combustion engine* (Vol. 478): Prentice Hall Upper Saddle River, NJ.
- Ra, Y., and Reitz, R. D. (2008). A reduced chemical kinetic model for IC engine combustion simulations with primary reference fuels. *Combustion and Flame*, 155(4), 713-738.
- Raheman, H., and Phadatare, A. (2004). Diesel engine emissions and performance from blends of karanja methyl ester and diesel. *Biomass and Bioenergy*, 27(4), 393-397.
- Raitanapaibule, K., and Aung, K. (2005). Performance predictions of a hydrogen-enhanced natural gas HCCI engine. *ASME International Mechanical Engineering Congress and Exposition*, pp. 289-294.
- Ricklin, P., Kazakov, A., Dryer, F., Kong, S., and Reitz, R. D. (2002). The effects of NO_x addition on the auto ignition behavior of natural gas under HCCI conditions. *SAE Technical Paper*, 2002-01-1746.
- Rizvi, S. Q. (2009). *Lubricant Chemistry, Technology, Selection, and Design*: West Conshohocken: ASTM International.
- Ryan, T. W., and Callahan, T. J. (1996). Homogeneous charge compression ignition of diesel fuel. *SAE Technical Paper*, 1996-01-1160.
- Saisirirat, P., Togbé, C., Chanchaona, S., Foucher, F., Mounaim-Rousselle, C., and Dagaut, P. (2011). Auto-ignition and combustion characteristics in HCCI and JSR using 1-butanol/n-heptane and ethanol/n-heptane blends. *Proceedings of the Combustion Institute*, 33(2), 3007-3014.
- Sanjid, A., Masjuki, H., Kalam, M., Rahman, S., Abedin, M., and Palash, S. (2013). Impact of palm, mustard, waste cooking oil and Calophyllum inophyllum biofuels on performance and emission of CI engine. *Renewable and Sustainable Energy Reviews*, 27, 664-682.
- Sarathy, S. M., Westbrook, C. K., Mehl, M., Pitz, W. J., Togbe, C., Dagaut, P., Seshadri, K. (2011). Comprehensive chemical kinetic modeling of the oxidation of 2-methylalkanes from C 7 to C 20. *Combustion and Flame*, 158(12), 2338-2357.
- Saxena, S., and Bedoya, I. D. (2013). Fundamental phenomena affecting low temperature combustion and HCCI engines, high load limits and strategies for extending these limits. *Progress in Energy and Combustion Science*, 39(5), 457-488.
- Seiser, R., Pitsch, H., Seshadri, K., Pitz, W., and Gurran, H. (2000). Extinction and autoignition of n-heptane in counterflow configuration. *Proceedings of the Combustion Institute*, 28(2), 2029-2037.

- Shahbakhti, M., and Koch, C. (2008). Characterizing the cyclic variability of ignition timing in a homogeneous charge compression ignition engine fuelled with n-heptane/iso-octane blend fuels. *International Journal of Engine Research*, 9(5), 361-397.
- Shaver, G. M., Gerdes, J. C., Jain, P., Caton, P., and Edwards, C. (2003). Modeling for control of HCCI engines. *Proceedings of the American Control Conference*, pp. 749-754.
- Shi, L., Cui, Y., Deng, K., Peng, H., and Chen, Y. (2006). Study of low emission homogeneous charge compression ignition (HCCI) engine using combined internal and external exhaust gas recirculation (EGR). *Energy*, 31(14), 2665-2676.
- Shudo, T., and Ono, Y. (2002). HCCI combustion of hydrogen, carbon monoxide and dimethyl ether. *SAE Technical Paper*, 2002-01-0112.
- Singh, A. P., and Agarwal, A. K. (2012). Combustion characteristics of diesel HCCI engine: an experimental investigation using external mixture formation technique. *Applied Energy*, 99, 116-125.
- Singh, G., Singh, A. P., and Agarwal, A. K. (2014). Experimental investigations of combustion, performance and emission characterization of biodiesel fuelled HCCI engine using external mixture formation technique. *Sustainable Energy Technologies and Assessments*, 6, 116-128.
- Sjöberg, M., and Dec, J. E. (2006). Smoothing HCCI heat-release rates using partial fuel stratification with two-stage ignition fuels. *SAE Technical Paper*, 2006-01-0629.
- Soloiu, V., Duggan, M., Ochieng, H., Williams, D., Molina, G., and Vlcek, B. (2013). Investigation of Low Temperature Combustion Regimes of Biodiesel With n-Butanol Injected in the Intake Manifold of a Compression Ignition Engine. *Journal of Energy Resources Technology*, 135(4), 041101.
- Soyhan, H., Yasar, H., Walmsley, H., Head, B., Kalghatgi, G., and Sorousbay, C. (2009). Evaluation of heat transfer correlations for HCCI engine modeling. *Applied Thermal Engineering*, 29(2), 541-549.
- Stanglmaier, R. H., Ryan, T. W., and Souder, J. S. (2001). HCCI operation of a dual-fuel natural gas engine for improved fuel efficiency and ultra-low NOx emissions at low to moderate engine loads. *SAE Technical Paper*, 2001-01-1897.
- Stiesch, G. (2013). *Modeling engine spray and combustion processes*: Springer Science & Business Media.
- Stone, R. (2012). *Introduction to internal combustion engines*: Palgrave Macmillan.

- Su, H. (2010). *Stochastic Reactor Models for Simulating Direct Injection Homogeneous Charge Compression Ignition Engines*. PhD Thesis. University of Cambridge, UK.
- Su, H., Mosbach, S., Kraft, M., Bhave, A., Kook, S., and Bae, C. (2007). Two-stage fuel direct injection in a diesel fuelled HCCI engine. *SAE Technical Paper*, 2007-01-1880.
- Suzuki, T., Kakegawa, T., Hikino, K., and Obata, A. (1997). Development of diesel combustion for commercial vehicles. *SAE Technical Paper*, 1997-01-2685.
- Swami Nathan, S., Mallikarjuna, J., and Ramesh, A. (2010a). Effects of charge temperature and exhaust gas re-circulation on combustion and emission characteristics of an acetylene fuelled HCCI engine. *Fuel*, 89(2), 515-521.
- Swami Nathan, S., Mallikarjuna, J., and Ramesh, A. (2010b). An experimental study of the biogas–diesel HCCI mode of engine operation. *Energy Conversion and Management*, 51(7), 1347-1353.
- Szwaja, S., and Grab-Rogalinski, K. (2009). Hydrogen combustion in a compression ignition diesel engine. *International Journal of Hydrogen Energy*, 34(10), 4413-4421.
- Szybist, J. P., Edwards, K. D., Foster, M., Confer, K., and Moore, W. (2013). Characterization of engine control authority on HCCI combustion as the high load limit is approached. *SAE Technical Paper*, 2013-01-1665.
- Takeda, Y., Keiichi, N., and Keiichi, N. (1996). Emission characteristics of premixed lean diesel combustion with extremely early staged fuel injection. *SAE Technical Paper*, 1996-01-1163.
- Tanaka, S., Ayala, F., and Keck, J. C. (2003). A reduced chemical kinetic model for HCCI combustion of primary reference fuels in a rapid compression machine. *Combustion and Flame*, 133(4), 467-481.
- Tomita, E. (2004). Dual fuel HCCI combustion-High octane and high cetane number fuels. *HCCI Symposium*, pp. 1-10.
- Topgül, T. (2015). The effects of MTBE blends on engine performance and exhaust emissions in a spark ignition engine. *Fuel Processing Technology*, 138, 483-489.
- Tree, D. R., and Svensson, K. I. (2007). Soot processes in compression ignition engines. *Progress in Energy and Combustion Science*, 33(3), 272-309.
- Tsolakis, A., and Megaritis, A. (2005). Partially premixed charge compression ignition engine with on-board production by exhaust gas fuel reforming of diesel and biodiesel. *International Journal of Hydrogen Energy*, 30(7), 731-745.

- Turkcan, A., Ozsezen, A. N., and Canakci, M. (2013). Effects of second injection timing on combustion characteristics of a two stage direct injection gasoline-alcohol HCCI engine. *Fuel*, 111, 30-39.
- Uyumaz, A. (2015). An experimental investigation into combustion and performance characteristics of an HCCI gasoline engine fueled with n-heptane, isopropanol and n-butanol fuel blends at different inlet air temperatures. *Energy Conversion and Management*, 98, 199-207.
- Valentino, G., Corcione, F. E., Iannuzzi, S. E., and Serra, S. (2012). Experimental study on performance and emissions of a high speed diesel engine fuelled with n-butanol diesel blends under premixed low temperature combustion. *Fuel*, 92(1), 295-307.
- Verhelst, S., and Wallner, T. (2009). Hydrogen-fueled internal combustion engines. *Progress in Energy and Combustion Science*, 35(6), 490-527.
- Walter, B., and Gatellier, B. (2002). Development of the high power NADI™ concept using dual mode diesel combustion to achieve zero NOx and particulate emissions. *SAE Technical Paper*, 2002-01-1744.
- Wang, H., Jiao, Q., Yao, M., and Reitz, R. D. (2013). Development of an n-heptane/toluene/PAH Mechanism and its Application for Soot Prediction. *International Journal of Engine Research*, 14(5), 434-451.
- Wang, Z., Shuai, S.-J., Wang, J.-X., Tian, G.-H., and An, X.-L. (2006). Modeling of HCCI combustion: From 0D to 3D. *SAE Technical Paper*, 2006-01-1364.
- Warnatz, J., Maas, U., and Dibble, R. W. (2006). *Combustion: physical and chemical fundamentals, modeling and simulation, experiments, pollutant formation*: Springer, New York, USA.
- Weall, A., Szybist, J. P., Edwards, K. D., Foster, M., Confer, K., and Moore, W. (2012). HCCI load expansion opportunities using a fully variable HVA research engine to guide development of a production intent cam-based VVA engine: the low load limit. *SAE Technical Paper*, 2012-01-1134.
- Wesselink, L., Buijsman, E., and Annema, J. (2006). The impact of Euro 5: facts and figures. *Netherlands Environmental Assessment Agency Report*, 500043002.
- Westbrook, C. K., Pitz, W. J., and Curran, H. J. (2006). Chemical kinetic modeling study of the effects of oxygenated hydrocarbons on soot emissions from diesel engines. *The Journal of Physical Chemistry A*, 110(21), 6912-6922.
- Yang, F., Gao, G., Ouyang, M., Chen, L., and Yang, Y. (2013). Research on a diesel HCCI engine assisted by an ISG motor. *Applied Energy*, 101, 718-729.
- Yang, Y., Dec, J. E., Dronniou, N., and Sjöberg, M. (2011). Tailoring HCCI heat-release rates with partial fuel stratification: Comparison of two-stage and single-stage-ignition fuels. *Proceedings of the Combustion Institute*, 33(2), 3047-3055.

- Yao, M., Zheng, Z., and Liu, H. (2009). Progress and recent trends in homogeneous charge compression ignition (HCCI) engines. *Progress in Energy and Combustion Science*, 35(5), 398-437.
- Yap, D., Karlovsky, J., Megaritis, A., Wyszynski, M., and Xu, H. (2005). An investigation into propane homogeneous charge compression ignition (HCCI) engine operation with residual gas trapping. *Fuel*, 84(18), 2372-2379.
- Yeom, K., Jang, J., and Bae, C. (2007). Homogeneous charge compression ignition of LPG and gasoline using variable valve timing in an engine. *Fuel*, 86(4), 494-503.
- Yokota, H., Kudo, Y., Nakajima, H., Kakegawa, T., and Suzuki, T. (1997). A new concept for low emission diesel combustion. *SAE Technical Paper*, 1997-01-0891.
- Yu, C., Bari, S., and Ameen, A. (2002). A comparison of combustion characteristics of waste cooking oil with diesel as fuel in a direct injection diesel engine. *Proceedings of the Institution of Mechanical Engineers, Part D: Journal of Automobile Engineering*, 216(3), 237-243.
- Yun, H., Wermuth, N., and Najt, P. (2010). Extending the high load operating limit of a naturally-aspirated gasoline HCCI combustion engine. *SAE Technical Paper*, 2010-01-0847.
- Zhang, C., and Wu, H. (2015). Combustion characteristics and performance of a methanol fueled homogenous charge compression ignition (HCCI) engine. *Journal of the Energy Institute*, 89(3), 346-353.
- Zhang, C. H., Xue, L., and Wang, J. (2014). Experimental study of the influence of λ and intake temperature on combustion characteristics in an HCCI engine fueled with n-heptane. *Journal of the Energy Institute*, 87(2), 175-182.
- Zhang, S., Broadbelt, L. J., Androulakis, I. P., and Ierapetritou, M. G. (2012). Comparison of biodiesel performance based on HCCI engine simulation using detailed mechanism with on-the-fly reduction. *Energy & Fuels*, 26(2), 976-983.
- Zhang, Y., and Zhao, H. (2014). Investigation of combustion, performance and emission characteristics of 2-stroke and 4-stroke spark ignition and CAI/HCCI operations in a DI gasoline. *Applied Energy*, 130, 244-255.
- Zhao, F. (2003). *Homogeneous charge compression ignition (HCCI) engines: key research and development issues*: SAE International.
- Zhao, H. (2007). *HCCI and CAI Engines for the Automotive Industry*: Elsevier.
- Zhen, X., Wang, Y., Xu, S., Zhu, Y., Tao, C., Xu, T., and Song, M. (2012). The engine knock analysis—An overview. *Applied Energy*, 92, 628-636.

- Zheng, J., Yang, W., Miller, D. L., and Cernansky, N. P. (2001). Prediction of pre-ignition reactivity and ignition delay for HCCI using a reduced chemical kinetic model. *SAE Technical Paper*, 2001-01-1025.
- Zheng, J., Yang, W., Miller, D. L., and Cernansky, N. P. (2002). A skeletal chemical kinetic model for the HCCI combustion process. *SAE Transactions*, 111(3), 898-912.
- Zheng, Q. P., and Zhang, H. M. (2005). A computational study of combustion in compression ignition natural gas engine with separated chamber. *Fuel*, 84(12), 1515-1523.
- Zhou, P., Zhou, S., and Clelland, D. (2006). A modified quasi-dimensional multi-zone combustion model for direct injection diesels. *International Journal of Engine Research*, 7(4), 335-345.
- Zhuang, Y., and Hong, G. (2013). Primary investigation to leveraging effect of using ethanol fuel on reducing gasoline fuel consumption. *Fuel*, 105, 425-431.

APPENDIX A

DERIVATION OF TEMPERATURE EQUATION

This appendix contains the derivation of temperature changes in a zero-dimensional single-zone model from the first law of thermodynamics equation. The first law of thermodynamics equation is

$$U = -W + Q_h + \sum_j m_j h_j \quad (\text{A.1})$$

where j represents each flow entering or leaving the system. For a quasi-static process, where work can be expressed as $W = pdV$, the first law equation in its differential form is given by

$$\frac{d(mu)}{dt} = \frac{dQ_h}{dt} - \frac{pdV}{dt} + \sum_j \dot{m}_j h_j \quad (\text{A.2})$$

The enthalpy for a homogeneous system is defined as

$$h = u + pv \quad (\text{A.3})$$

and can be substituted into equation (A.2) to yield

$$\frac{d(mh)}{dt} - \frac{d(pV)}{dt} = \frac{dQ_h}{dt} - \frac{pdV}{dt} + \sum_j \dot{m}_j h_j \quad (\text{A.4})$$

Equation (A.4) is manipulated and becomes

$$m \frac{dh}{dt} + h \frac{dm}{dt} - p \frac{dV}{dt} - V \frac{dp}{dt} = \frac{dQ_h}{dt} - \frac{pdV}{dt} + \sum_j \dot{m}_j h_j \quad (\text{A.5})$$

$$m \frac{dh}{dt} = \frac{dQ_h}{dt} - h \frac{dm}{dt} + V \frac{dp}{dt} + \sum_j \dot{m}_j h_j \quad (\text{A.6})$$

In equation (A.6), dh/dt needs to be expressed in terms of change in temperature. For a multi-component mixture of ideal gasses in a single phase,

$$h = \sum_i Y_i h_i \quad \text{and} \quad h = h(T, p, Y_i) \quad (\text{A.7})$$

where i is the component species in the mixture. Applying the chain rule to the derivative of enthalpy produces

$$\frac{dh}{dt} = \left. \frac{\partial h}{\partial T} \right|_{p, Y_i} \frac{dT}{dt} + \left. \frac{\partial h}{\partial p} \right|_{T, Y_i} \frac{dp}{dt} + \sum_i \left. \frac{\partial h}{\partial Y_i} \right|_{p, T, Y_{i \neq j}} \frac{dY_i}{dt} \quad (\text{A.8})$$

The change of enthalpy with respect to pressure at constant temperature and composition is zero, hence equation (A.8) becomes

$$\frac{dh}{dt} = C_p \frac{dT}{dt} + \sum_i h_i \frac{dY_i}{dt} \quad (\text{A.9})$$

The pressure change in equation (A.6) can be obtained by manipulating the equation of state for an ideal gas

$$pv = mRT$$

$$p \frac{dV}{dt} + V \frac{dp}{dt} = mR \frac{dT}{dt} + T \frac{d(mR)}{dt}$$

$$p \frac{dV}{dt} + V \frac{dp}{dt} = mR \frac{dT}{dt} + mT \frac{dR}{dt} + RT \frac{dm}{dt}$$

$$mT \frac{dR}{dt} = p \frac{dV}{dt} + V \frac{dp}{dt} - mR \frac{dT}{dt} - RT \frac{dm}{dt} \quad (\text{A.10})$$

The ideal gas law is used to substitute for the coefficients of each derivative so that the quantity being differentiated appears in the coefficient

$$\frac{pV}{R} \frac{dR}{dt} = \frac{mRT}{V} \frac{dV}{dt} + \frac{mRT}{p} \frac{dp}{dt} - \frac{pV}{T} \frac{dT}{dt} - \frac{pV}{m} \frac{dm}{dt} \quad (\text{A.11})$$

Dividing both sides of equation (A.11) with pV gives

$$\begin{aligned} \frac{1}{R} \frac{dR}{dt} &= \frac{mRT}{pV^2} \frac{dV}{dt} + \frac{mRT}{Vp^2} \frac{dp}{dt} - \frac{1}{T} \frac{dT}{dt} - \frac{1}{m} \frac{dm}{dt} \\ \frac{1}{R} \frac{dR}{dt} &= \frac{mRT}{mRTV} \frac{dV}{dt} + \frac{mRT}{mRTp} \frac{dp}{dt} - \frac{1}{T} \frac{dT}{dt} - \frac{1}{m} \frac{dm}{dt} \\ \frac{1}{R} \frac{dR}{dt} &= \frac{1}{V} \frac{dV}{dt} + \frac{1}{p} \frac{dp}{dt} - \frac{1}{T} \frac{dT}{dt} - \frac{1}{m} \frac{dm}{dt} \end{aligned} \quad (\text{A.12})$$

The relationship

$$\frac{dR}{dt} = \sum_i R_i \frac{dY_i}{dt} \quad (\text{A.13})$$

can be substituted into equation (A.12), and rearranging gives

$$\frac{dp}{dt} = p \left[\frac{1}{R} \sum_i R_i \frac{dY_i}{dt} + \frac{1}{m} \frac{dm}{dt} + \frac{1}{T} \frac{dT}{dt} - \frac{1}{V} \frac{dV}{dt} \right] \quad (\text{A.14})$$

Hence, substituting equation (A.14) to (A.6)

$$m \frac{dh}{dt} = \frac{dQ_h}{dt} - h \frac{dm}{dt} + pV \left[\frac{1}{R} \sum_i R_i \frac{dY_i}{dt} + \frac{1}{m} \frac{dm}{dt} + \frac{1}{T} \frac{dT}{dt} - \frac{1}{V} \frac{dV}{dt} \right] + \sum_j m_j h_j$$

and now substituting equation (A.9) and rearranging yields

$$m \left(C_p \frac{dT}{dt} + \sum_i h_i \frac{dY_i}{dt} \right) = \frac{dQ_h}{dt} - h \frac{dm}{dt} + pV \left[\frac{1}{R} \sum_i R_i \frac{dY_i}{dt} + \frac{1}{m} \frac{dm}{dt} + \frac{1}{T} \frac{dT}{dt} - \frac{1}{V} \frac{dV}{dt} \right] + \sum_j m_j h_j$$

$$m C_p \frac{dT}{dt} - pV \frac{1}{T} \frac{dT}{dt} = \frac{dQ_h}{dt} - h \frac{dm}{dt} + \frac{pV}{R} \sum_i R_i \frac{dY_i}{dt} + \frac{pV}{m} \frac{dm}{dt} - p \frac{dV}{dt} - \sum_i h_i \frac{dY_i}{dt} + \sum_j m_j h_j$$

$$\frac{dT}{dt} \left(m C_p - \frac{pV}{T} \right) = \frac{dQ_h}{dt} - h \frac{dm}{dt} + \frac{pV}{R} \sum_i R_i \frac{dY_i}{dt} + \frac{pV}{m} \frac{dm}{dt} - p \frac{dV}{dt} - \sum_i h_i \frac{dY_i}{dt} + \sum_j m_j h_j$$

$$\frac{dT}{dt} \left(\overline{C_p} - \frac{pV}{mT} \right) = \sum_i \left[\left(\frac{pv}{R} R_i - h_i \right) \frac{dY_i}{dt} \right] + \sum_j \frac{m_j h_j}{m} + \frac{1}{m} \frac{dQ_h}{dt} + pv \frac{1}{m} \frac{dm}{dt} - h \frac{1}{m} \frac{dm}{dt} - \frac{p}{m} \frac{dV}{dt}$$

The final equation is

$$\frac{dT}{dt} = \frac{1}{C_A} \left[\sum_i \left[\left(\frac{pv R_i}{R} - h_i \right) \frac{dY_i}{dt} \right] - \frac{C_B}{m} \frac{dm}{dt} + \frac{1}{m} \left(\frac{dQ_h}{dt} - \frac{pdV}{dt} + \sum_j \dot{m}_j h_j \right) \right] \quad (\text{A.15})$$

where

$$C_A = \overline{c_p} - \frac{\rho v}{T} \quad (\text{A.16})$$

$$C_B = h - \rho v \quad (\text{A.17})$$

APPENDIX B

COMPUTER SOFTWARE SUMMARY

Below is a list and discussion of the software used in the analysis and preparation of this dissertation.

B.1 MATLAB

MATLAB is a numerical computing environment and programming language created by The MathWorks. It allows easy matrix manipulation, plotting of functions and data, and implementation of algorithms. Many toolboxes exist which also allow integration with other computer codes and user interfaces. Parts of the control programming can be done using the Simulink toolbox which is a graphical block diagramming tool for modeling, simulating and analyzing multidomain dynamic systems. The Matlab version used was R2013a (8.1.0.604).

B.2 CANTERA

Cantera is an open-source, object-oriented software package for problems involving chemically-reacting flows. Capabilities include: multiphase chemical equilibrium, thermodynamic and transport properties, homogeneous and heterogeneous kinetics, reactor networks, one-dimensional flames, and reaction path diagrams. It has interfaces for MATLAB, Python, C ++, and FORTRAN. The simulations that use Cantera in this study were done using MATLAB and the appropriate interface.

B.3 EXCELL

Microsoft Excel (full name Microsoft Office Excel) is a spreadsheet program used in data analysis and the preparation of figures. The version used was Microsoft Excel 2010.

B.4 ORIGIN

Origin is a proprietary computer program for interactive scientific graphing and data analysis. It is produced by OriginLab Corporation, and runs on Microsoft Windows. It has inspired several platform-independent open source clones like QtiPlot or SciDAVis. Graphing support in Origin includes various 2D/3D plot types. Data analyses in Origin include statistics, signal processing, curve fitting and peak analysis. Origin's curve fitting is performed by the nonlinear least squares fitter which is based on the Levenberg–Marquardt algorithm. Origin imports data files in various formats such as ASCII text, Excel, NI TDM, DIADem, NetCDF, SPC, etc. It also exports the graph to various image file formats such as JPEG, GIF, EPS, TIFF, etc. There is also a built-in query tool for accessing database data via ADO. The version used was Origin pro 9.0.



UMP

APPENDIX C

ZERO-DIMENSIONAL SINGLE ZONE NUMERICAL MODEL CODE

This appendix includes the base code for a zero-dimensional single zone engine model written in MATLAB and using Cantera for the chemical kinetics calculations. Besides the primary script file there is an ODE function and some geometric calculations using slider crank relations, each of which is discussed below.

slidercrank.m - base program

slidercrankODE.m - ordinary differential equation

volume.m - volume of the combustion chamber

dvolumedt.m - change in volume with respect to time of the combustion chamber

asurf.m - surface area of the combustion chamber

This example single zone code uses a built-in GRI Mech 3.0 kinetics file inside Cantera. It models the combustion of methane in an HCCI engine running at an equivalence ratio of 0.3.

slidercrank.m

```
% slider crank (base program)
% mmhasan-ump
% updated september 2015
clear all
close all
% INPUTS:
Tin=380;
Pin=oneatm;
g=GRI30;
set(g,'T',Tin,'P',Pin,'X','CH4:1.0001,O2:3,N2:11.28');
% INITIAL FUEL PARAMETERS
CH4index=speciesIndex(g,'CH4'); % find CH4 mass fraction
massfrac=massFractions(g);
CH4massfracinit=massfrac(CH4index);
% ENGINE PARAMETERS:
bore=0.0875; % bore (m)
stroke=0.11 ; % stroke (m)
compress=17.5; % compression ratio (no units)
conrod=.254; % connecting rod length (m)
rpm=1500; % rpm
```

```

swirl=2.0 ; % swirl (no units)
twall=530; % wall temperature (K)
omega=2*pi*rpm /60.0;
enginedata= [bore,stroke,compress,conrod,rpm,swirl,twall]';
% TIMING PARAMETERS:
% simulation conducted for closed part of the cycle
% from intake valve close (ivc) to exhaust valve opening(evo)
ivc=-144; % degrees ATDC (negative means before TDC)
evo=140; % degress ATDC
dtheta= .5; % crank angle resolution for output
% simulation time parameters converted from degrees
t0=ivc*pi/180/omega; % start time
tf=evo*pi/180/omega; % stop time
dt= dtheta*pi/180/omega; % time interval
time= [t0:dt:tf]; % creating a time vector
v0=volume(t0,enginedata); % VOLUME at time=0
mass1=density(g)*v0; % mass
zO = [Tin;massFractions(g)]; % initial z vector
% differential equation solving
options=odeset('Reltol',1e-6,'Abstol',1e-
15,'Stats','on','OutputFcn',@odeplot,'OutputSel',[1]);
out=ode15s(@slidercrankODE,[time(1) time(end)],zO,options,g,enginedata,mass1);
x=deval(out,time); % evaluating solutions to ODE at TIMES
th=time*180/pi*omega; % creating CA array from time
ns=nSpecies(g); % total number of species
T1= x(1,:); %
Ru=gasconstant; % gas constant
for i=1:length(time);
v1=volume(time(i),enginedata); % find volume of chamber at time i
vol(i)= v1; % store volume d ata
dv1=volume(time(i),enginedata); % find volume of chamber at time i
y1= x(2:ns+ 1,i); % species at time i
setMassFractions(g,y1); % set mass fractions of cantera gas object g
wt1=meanMolecularWeight(g); % mean molecular weight of cantera gas object g
p1(i)= mass1*Ru*T1(i)/wt1/v1; % calculate pressure in pascals
p1atm(i)= p1(i)/oneatm ; % calculate pressure in atm
CH4index=speciesIndex(g,'CH4'); % find CH4 mass fraction
massfrac=massFractions (g);
CH4massfrac(i)=massfrac(CH4index);
end
for j=1:length(CH4massfrac)
if CH4massfrac(j)\0.5*CH4massfracinit
CA50=th(j);
break
end
end

CA50
figure(1)
plot(th ,p1atm),xlabel('CAD'),ylabel('Pressure'),legend('In-cylinder Pressure');

```



```

figure(2)
plot(th,CH4massfrac),xlabel('CAD'),ylabel('Mass Fraction'),legend('CH4');
figure (3)
plot(th,vol),xlabel('CAD'),ylabel('Volume'),legend('Volume');
figure (4)
plot(th,T1),xlabel('CAD'),ylabel('Temperature'),legend('In-cylinder Temperature');

```

slidercrankODE.m

```

function dzdt=slidercrankODE (t,z,g,enginedata,mass1)
%-----
%Engine Properties
bore=enginedata(1);
stroke=enginedata(2);
compress=enginedata(3);
conrod=enginedata(4);
rpm=enginedata(5);
swirl=enginedata(6 );
twall=enginedata(7);
omega=2*pi*rpm/60.0;
%Engine Properties
%-----
Ru=gasconstant;
kk=nSpecies(g);
T1=z(1);
y1=z(2:kk+1);
wt=molecularWeights(g);
%zone1 setup
v1=volume(t,enginedata);
dv1=dvolumedt(t,enginedata);
a1=asurf(t,enginedata);
setMassFractions(g,y1);
wtave1=meanMolecularWeight(g);
p1= mass1 *Ru*T1/v1/wtave1;
set(g,'T',T1,'P',p1,'Y',y1);
rho1=density(g);
cvave1=cv_mass(g);
uave1=intEnergy_mass(g);
have1=enthalpy_mass(g);
h1=enthalpies_RT(g)*Ru./wt*T1;
u1=(enthalpies_RT(g)-1)*Ru./wt*T1;
wdot1=netProdRates(g);
hheat1=0.0;
qdot1= hheat1*a1*(T1-twall);
dT1=(-v1*sum(wdot1.*wt.*u1)+qdot1-p1*dv1)/rho1/v1/cvave1;
dy1= +wdot1.*wt/rho1;
dzdt=[dT1;dy1];

```

volume.m

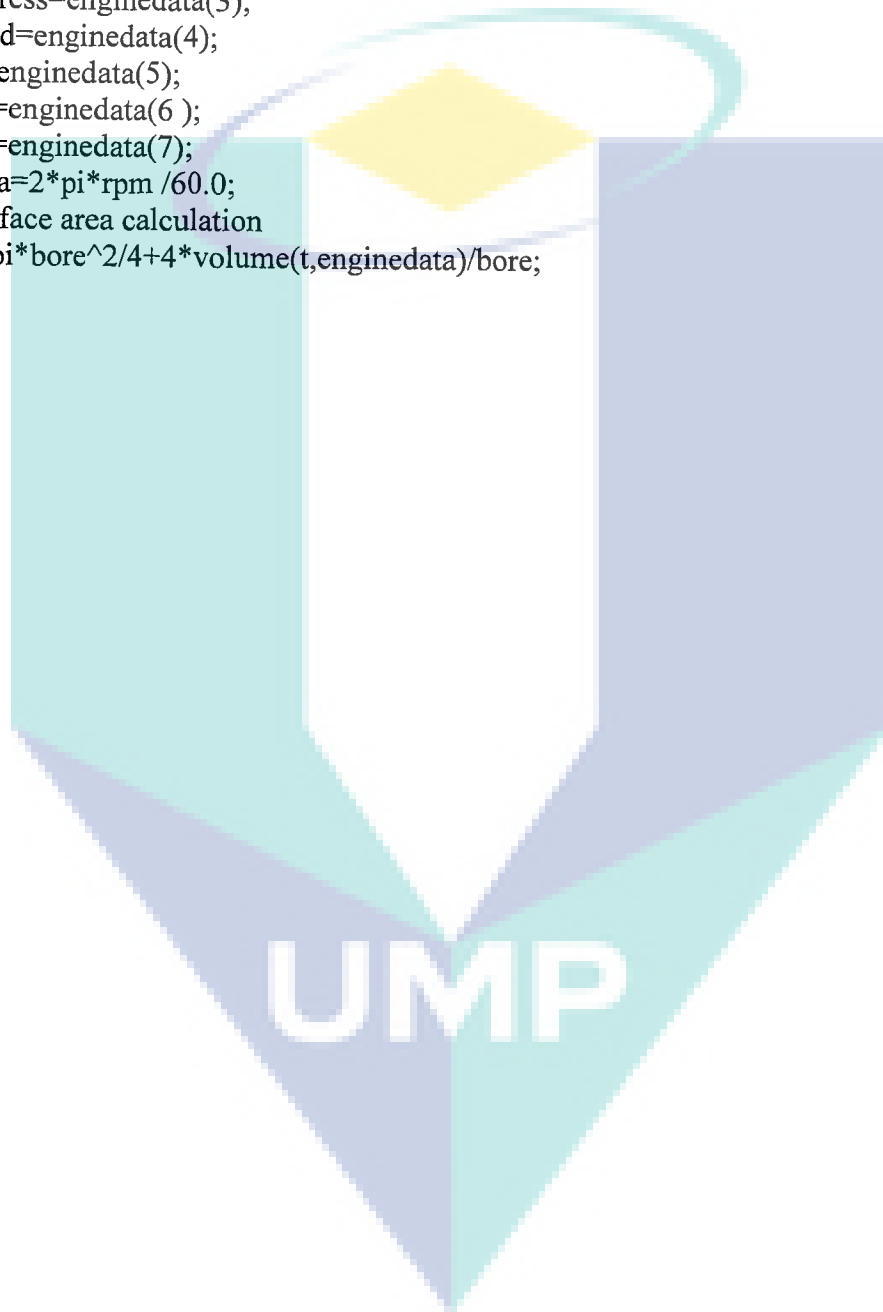
```
function vol=volume(time,enginedata)
% v=volume(time); %assumes time=0 at theta=0(TDC)
%
% v - m3
% theta-degrees
%-----
%Engine Properties
bore=enginedata(1);
stroke=enginedata(2);
compress=enginedata(3);
conrod=enginedata(4);
rpm=enginedata(5);
swirl=enginedata(6);
twall=enginedata(7);
omega=2*pi*rpm/60.0;
%Engine Properties
%-----
vc=pi*bore^2/4*stroke/(compress-1);
vtot=pi*bore^2/4.*stroke+vc;
a=stroke/2;
c=conrod;
thrad=time*omega; % convert time to crank angle (rad)
s=a*cos(thrad)+sqrt(c^2 -(a*sin(thrad)).^2);
vol=vc+pi*bore^2/4*(c+a-s);
```

dvolumedt.m

```
function dvdt=dvolumedt(time,enginedata)
% dvdt=dvolumedt(time); %in vol/time
% slider-crank formula, assumes t=0 at theta=0.0(BDC)
%
%-----
% Engine Properties
bore=enginedata(1);
stroke=enginedata(2);
compress=enginedata(3);
conrod=enginedata(4);
rpm=enginedata(5);
swirl=enginedata(6);
twall=enginedata(7);
omega=2*pi*rpm/60.0;
a=pi*bore^2/4;
r=stroke/2;
c=conrod;
thrad=time*omega; % convert time to crank angle(rad)
dvdth=a*(r*sin(thrad)+r.^2.*sin(thrad).*cos(thrad)./sqrt(c.^2-r.^2*sin(thrad).^2));
dvdt=dvdth*omega; % convert from vol/radian to vol/time
```

asurf.m

```
function a=asurf(t,enginedata)
% surface area calculator function
% Engine Properties
bore=enginedata(1);
stroke=enginedata(2);
compress=enginedata(3);
conrod=enginedata(4);
rpm=enginedata(5);
swirl=enginedata(6);
twall=enginedata(7);
omega=2*pi*rpm/60.0;
% surface area calculation
a=2*pi*bore^2/4+4*volume(t,enginedata)/bore;
```



APPENDIX D

LIST OF PUBLICATIONS

1. M.M. Hasan and M.M. Rahman, "Homogeneous charge compression ignition combustion: Advantages over compression ignition combustion, challenges and overcomes" *Renewable and Sustainable Energy Reviews*, 2016. 57: p.282-291. (SCI Indexed, Q1, IF=6.80)
2. M.M. Hasan, M.M. Rahman and K. Kadirgama, "A review on homogeneous charge compression ignition (HCCI) engine performance using diesel and biodiesel-diesel blend as fuel" *International Journal of Automotive and Mechanical Engineering*, 2015. 11: p. 2199-2211. (Scopus Indexed, Q2, SJR=0.43)
3. M.M. Hasan and M.M. Rahman, "A review on properties, combustion, performance, and emission characteristics of biodiesel-diesel blend in compression ignition engine" *Renewable and Sustainable Energy Reviews*, (SCI Indexed, Q1, IF=6.80) (Accepted with Correction)
4. M.M. Hasan and M.M. Rahman, "Homogeneous charge compression ignition combustion: Advantages over spark ignition combustion in terms of performance and emission as well as effects of fuels and additives" *Renewable and Sustainable Energy Reviews* (Under Review)
5. M.M. Hasan, M.M. Rahman, K. Kadirgama and D. Ramasamy, Combustion and performance characteristics in an HCCI engine fueled with diethyl ether and ethanol fuel blends, *Applied Energy* (Under Review)
6. M.M. Hasan and M.M. Rahman, "Numerical study on combustion, performance and emissions in an HCCI engine fueled with n-heptane, ethanol and butanol fuel blends at different intake temperatures" *International Journal of Automotive and Mechanical Engineering* (Under Review)
7. M.M. Hasan, M.M. Rahman and A.A. Abdullah, "Numerical study of engine parameters on combustion and performance characteristics in an n-Heptane fueled HCCI engine (To be submitted)